# Mathematical and Physical Modeling of Mixing and Flow Phenomena of Municipal Solid Waste Particles on a Reverse Acting Grate

Masato Nakamura

Submitted in partial fulfillment of the
requirements for the degree
of Doctor of Engineering Science
in the Fu Foundation School of
Engineering and Applied Science

COLUMBIA UNIVERSITY

2008

# Mathematical and Physical Modeling of Mixing and Flow Phenomena of Municipal Solid Waste Particles on a Reverse Acting Grate

Masato Nakamura

## ABSTRACT

The dominant process for the recovery of energy from municipal solid wastes (MSW) is mass burning on a moving grate. Also, the leading grate technology is the Martin reverse acting grate that was modeled in this study. The drying, volatilization, and combustion phenomena during the travel of the solid waste fuel over the grate depend on the physical and chemical properties of the diverse particles in MSW, the design of the grate and combustion chamber, and the distribution of air flowing through the bed of solids. On the average, it takes one hour for particles to traverse a 10-meter long grate. Therefore, the bed behaves essentially as a fixed bed moving downwards, by gravity because of the inclination of the grate. In the case of the Martin grate, the reverse action motion of the grate results in some upward flow and consequent mixing of the materials within the bed.

This study of the flow and mixing phenomena on a reverse acting grate included both theoretical and experimental research. In order to characterize the heterogeneous particle behavior, a two-dimensional stochastic model of particle mixing within the bed on the reciprocating grate was developed. The model was calibrated and validated by means of a full-scale physical model of the reverse acting grate, using tracer particles ranging from 6 – 22 cm in diameter. This size range was

based on a quantitative analysis of the size and shape factor distributions of MSW samples collected from different locations in New York City. It was found that different particle sizes result in different residence times because of the Brazil Nut Effect (BNE). In the BNE, larger particles rise to the surface while smaller particles migrate to lower depths of the bed where the reciprocating bars push them backward against the main direction of the MSW flow. The motion of the reverse acting grate (whose speed ranged from 15 to 90 reciprocations/hour) increases the mean residence time of small and medium particles by 69 % and 8%, respectively, while decreasing the mean residence time of large particles by 19%. Also, within this speed range, the mixing diffusion coefficient of each particle size was determined.

The ratio of particle diameter to the height of moving bar, *d/h*, was found to be a major parameter for affecting the mixing diffusion coefficient, $D_e$, and the residence time, *t*, at reciprocation speeds above 30/hr. When the ratio, *d/h*, increases from 0.46 to 1.69, the mixing diffusion coefficient, $D_e$ at 60/hr., decreases from 96 to 38.4. This indicates that the height of the moving bars should be grater than the diameter of targeted particles, usually the mean diameter of MSW particles. Accordingly, the traveling grate operation and moving bar height can be optimized in a more efficient way, based on these quantitative results and the local MSW particle size distribution.

In the future research, when the stochastic model is combined with particle size change due to combustion, the stochastic model simulation will become much

more complicated, because the Markov property will be applicable. In this case, the calculation should be carried out for each single time step (reciprocation), since the initial condition, instead of only the previous step.

## Table of Contents

## List of Tables

**List of Figures**

## Nomenclature

| | |
|---|---|
| $\boldsymbol{S}(0)$ | initial state vector (initial distribution of MSW) |
| $n$ | number of transition (number of the stroke of reciprocating bars) |
| $\boldsymbol{S}(n)$ | state vector after $n$ transitions (distribution of MSW after nth stroke of reciprocating bars) |
| $\boldsymbol{P}$ | transition matrix |
| $\boldsymbol{F}$ | flow matrix |
| $u_f$ | feed rate of MSW in the inlet of the mass-burn WTE chamber (cm/min) |
| $d$ | diameter of MSW particle (cm) |
| $D_e$ | mixing diffusion coefficient ($cm^2$/min) |
| $R_r$ | reciprocation speed of moving bars (recip./hour) |
| $n$ | number of transition (number of the reciprocation of moving bars) |
| $k$ | ratio between feed rate of MSW and frequency of reciprocating bars (cells / reciprocation) = $u_f/R_r$ (how many cells MSW travels during one reciprocation) |
| $t$ | residence time (min) |
| $\bar{t}$ | mean residence time (min) |
| $h$ | height of moving bars (cm) |
| $p_i$ | probability of remaining in state1 after one transition near the inlet |
| $p_r$ | probability of remaining in a state after one transition on the reciprocating bar |
| $r_r$ | probability of transiting to the adjacent state on the reciprocating bar |
| $p_f$ | probability of remaining in a state after one transition on the fixed bar |
| $r_f$ | probability of transiting to the adjacent state on the fixed bar |
| $p_o$ | probability of remaining in state16 after one transition near the outlet |
| $f_f$ | function of $R_f$ , S, ρ, Rr , L, α, H and θ to determine $p_f$ |
| $g_f$ | function of $R_f$ , S, ρ, Rr , L, α, H and θ to determine $r_f$ |
| $f_r$ | function of $R_f$ , S, ρ, Rr , L, α, H and θ to determine $p_r$ |
| $g_r$ | function of $R_f$ , S, ρ, Rr , L, α, H and θ to determine $r_r$ |
| $R_f$ | feed rate of MSW in the inlet of the mass-burn WTE chamber |

| | |
|---|---|
| S | particle size of MSW components |
| $\rho$ | particle density of MSW components |
| $R_r$ | frequency of reciprocating bars |
| L | the length of the reciprocating bars travel |
| H | height of the reciprocating bars |
| $\theta$ | angle of the reciprocating bars |
| $\alpha$ | angle of chamber bed decline |

**Acknowledgements**

First and foremost, I would like to express my deepest gratitude to Professors Nickolas J. Themelis and Marco J. Castaldi for their support and advice throughout this research and guiding me to the right direction.

Also, I would like to acknowledge Professors Upmanu Lall, Hoe I. Ling, and Vijay Modi for helping me as committee members of my dissertation defense.

The financial support of several organizations made this research possible: Columbia University's Department of Earth and Environmental Engineering (Henry Krumb School of Mines), the Earth Engineering Center (EEC), the Waste-to-Energy Research and Technology Council (WTERT), the Earth Institute (EI), and the Solid Waste Processing Division (SWPD) of the American Society of Mechanical Engineers (ASME). I am deeply indebted to these organizations.

Discussion with the engineers and researchers of Covanta Energy Corporation, especially Dr. Hanwei Zhang, Mark White, and Greg Epelbaum greatly helped me regarding experimental and modeling work. Dr. Ralf Koralewska from Martin GmbH introduced me useful theoretical research carried out by European WTE industry and academics.

I would also like to recognize Liliana Themelis, Peter J. Rennee, Gary S. Hill , as well as my research colleagues: Dr. Heidi C. Butterman, Dr. Karsten Millrath, Dionel Albina, Federico Barrai, Scott Kaufman, Eilhann Kwon, Shang-Hsiu Lee, Werner Sunk, and Yue Zhou. I have special appreciation for Anuta Belova, Dr. Fabiola Brusciotti, Dr. Joseph Di Dio III, and Dr. Frank S. Zeman, who organized a doctoral study group and encouraged me during my dissertation writing process.

Finally, thanks to my wife, Yoshie Tomozumi-Nakamura, my father Kazuo Ryuwa Nakamura, and my mother, Toyoko Nakamura for helping me along the whole way through.

# Chapter 1: Introduction

## 1-1. Background

### 1-1-1. Sustainable waste management and current WTE technologies

The United States generates approximately 1.31 short ton per capita of Municipal Solid Waste (MSW) annually (Kaufman et al. 2002) and the daily generation of MSW is estimated as 3.6 kg per capita. Sustainable Waste Management attempts to optimize the energy and resource recovery from collection, transport, and processing, while minimizing the environmental impact due to final deposition of residual MSW such as landfilling. Effective collection and transportation of MSW from residential areas to waste management facilities or landfills are required for reducing the transportation cost. Materials separation and processing technologies are used in the recovery of materials, by means of recycling of paper, plastics, metals and glass. Recovery of energy, known as waste-to-energy (WTE), is the conversion of post-recycling MSW into energy though the combustion or gasification processes. Landfilling is the disposal of MSW or the residuals from recycling and combustion processes. These technologies are utilized in Sustainable Waste Management.

Current WTE technologies are mainly used for the transformation of waste materials though combustion which reduces the volume and weight of residues for landfilling and recovers energy and metals. These advantages of WTE have increased WTE capacities throughout the world. For example, WTE capacities in Europe are

shown in Table 1-1. Total capacity in 1999 was more than 40 million tons annually and the generation of electrical and thermal energy were 41 million GJ and 110 GJ, respectively.

| Country | Tonnes/year (in 1999) | Kilograms /capita | Thermal energy (gigajoules) | Electric energy (gigajoules) |
|---|---|---|---|---|
| Austria | 450,000 | 56 | 3,053,000 | 131,000 |
| Denmark | 2,562,000 | 477 | 10,543,000 | 3,472,000 |
| France | 10,984,000 | 180 | 32,303,000 | 2,164,000 |
| Germany | 12,853,000 | 157 | 27,190,000 | 12,042,000 |
| Hungary | 352,000 | 6 | 2,000 | 399,000 |
| Italy | 2,169,000 | 137 | 3,354,000 | 2,338,000 |
| Netherlands | 4,818,000 | 482 | | 9,130,000 |
| Norway | 220,000 | 49 | 1,409,000 | 27,000 |
| Portugal | 322,000 | 32 | 1,000 | 558,000 |
| Spain | 1,039,000 | 26 | | 1,934,000 |
| Sweden | 2,005,000 | 225 | 22,996,000 | 4,360,000 |
| Switzerland | 1,636,000 | 164 | 8,698,000 | 2,311,000 |
| UK | 1,074,000 | 18 | 1,000 | 1,895,000 |
| Total reported | 40,484,000 | 154.5 (average) | 109,550,000 | 40,761,000 |

*Table 1-1 Reported WTE Capacity in Europe (IWSA 2003)*

Combustion of MSW is carried out using WTE units that are broadly divided into two classes: Those that combust bulk MSW as received (“mass burn”) and those that pre-process MSW, by magnetic separation, shredding, etc., to what is called refuse-derived fuel (RDF) units. See Section 1-2-2 for detail.

In recent years, WTE technologies have advanced rapidly. For example, the oxygen-enriched combustion system, which injects industrial oxygen in the primary air, has been developed by Martin GmbH and Mitsubishi Heavy Industry in order to generate a better grade of ash and reduce $NO_x$ and dioxin concentrations (Kira et al. 2001). This technology was tested at a demonstration plant in Germany and is combined with a flue gas recirculation system in the Martin Syncom process (Gohlke and Busch 2001). High temperature furnaces, like the thermal plasma torch ash melting system, have been developed to vitrify fly ashes and eliminate the chance of future contamination. A combustion improvement system with air injection tubes, called "Ecotube," has been developed by ECOMB company in order to reduce $NO_x$, CO, and Volatile Organic Compounds (VOCs). The "prism" system developed by IBB Engineering GmbH provides for additional secondary injection ports in the chamber with the objective of stabilizing stable temperature and gas velocity distributions in WTE units (Klasen et al. 2002). These advanced technologies have started to be applied to practical use in current WTE facilities.

### 1-1-2. Outline of the dissertation

This dissertation consists of six chapters. This chapter introduces a background of the WTE technologies and MSW properties, shortcomings of existing bed models, and objectives of this research. Chapter 2 gives mathematical models of WTE combustion including literature review of other related theoretical work. Chapter 3 is about experimental work of this study, using image analysis for a

measurement of MSW properties and a full-scale physical section model of the reverse acting grate system. Chapter 4 describes stochastic modeling of the flow and mixing of particles on the traveling grate. Chapter 5 is results and discussion of both experimental and mathematical work. The final chapter concludes this research with its major finding and limitation, including suggestions for future work. Abstract of this study is shown at the beginning of this dissertation.

## 1-2. Overview of WTE combustion systems (WTE units)

### 1-2-1. The mass-burn system

The mass-burn system is used by most existing WTE facilities in the world. A typical mass-burn WTE system is shown in Figure 1-1. It consists of the following

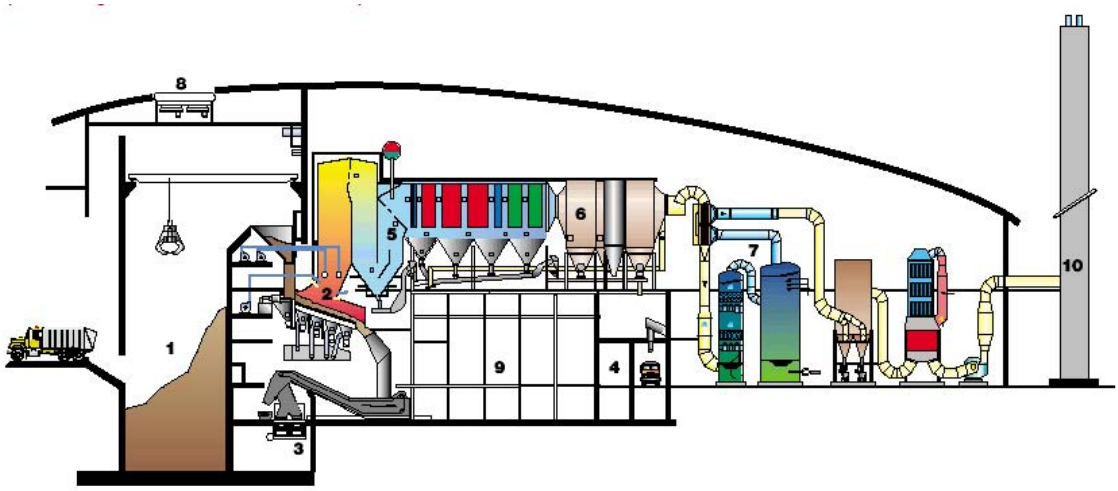


1 Waste pit
2 Grate combustion system (water-cooled)
3 Slag discharge
4 Fly ash loading station
5 Steam generation
6 Electrostatic precipitator
7 Flue gas purification
8 Heat exchanger
9 Electrical and Control Center
10 Stack

*Figure 1-1: Mass-burn grate combustion system (Von Roll, Brochure of Combustion System)*

sections: 1) combustion chamber, 2) energy recovery system (boiler), 3) air pollution control systems (APC). MSW is brought in by collection vehicles and is "tipped" on the unloading bay in an enclosed building. From there, it is loaded into the charging hopper by a crane, and is pushed by feeders into the combustion chamber. Each mass-burn combustion chamber is equipped with a traveling grate the motion of which slowly propels the MSW feed gradually down the grate. There are several types of traveling grates and will be described in Section 1-3.

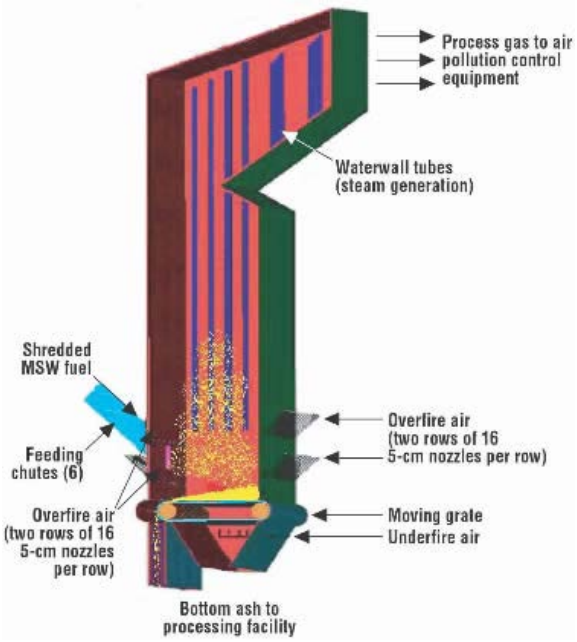


*Figure 1-2: Combustion Chamber in a RDF system (Themelis 2003)*

**1-2-2. The RDF combustion system**

Refuse-Derived Fuel (RDF) is produced from MSW by means of several processes, such as shredding, separation, and compaction before it is fed into the combustion chamber of a WTE facility. The RDF system has a combustion chamber that is physically smaller than a mass-burn chamber, because the heating value of RDF is higher than that of MSW as-collected. A typical combustion chamber of a

RDF system is shown in Figure 1-2. RDF is fed by a fuel distributor into the combustion chamber, which in this case is equipped with a horizontal traveling grate.

### 1-2-3. Other combustion systems

There are other combustion systems that are less common in WTE: Fluidized beds and rotary kiln. A fluidized bed system consists of a vertical steel cylinder and a sand bed shown in Figure 1-3. This system is operated on a variety of fuels such as MSW, coal, sludge, and chemical wastes. Rotary kiln systems are also versatile and can treat a range of materials, ranging from solid to liquid wastes. The rotary kiln, shown in Figure 1-4, is often used to process medical wastes as well as various industrial wastes.

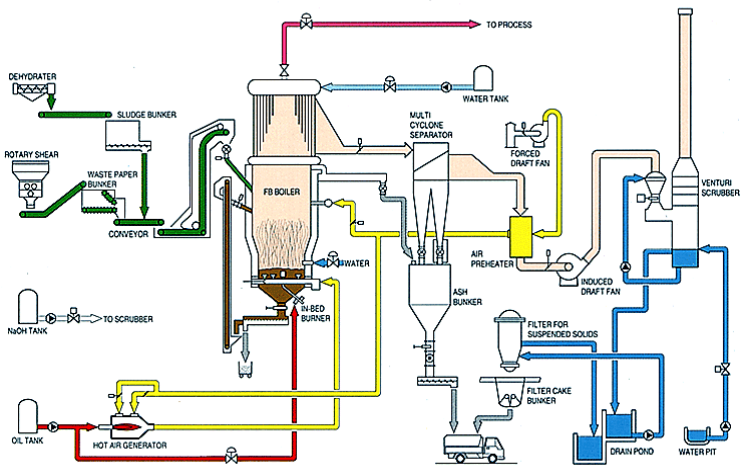


*Figure1- 3: Schematic diagram of fluidized bed system (ref. Takuma)*

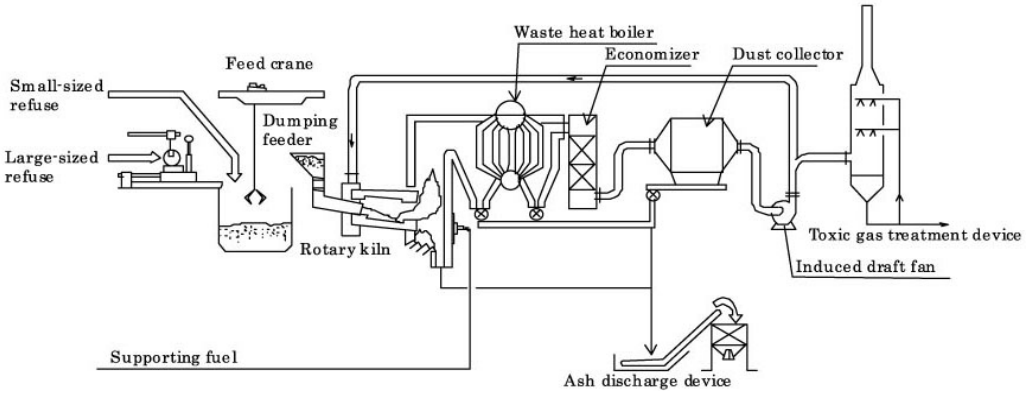


*Figure 1-4: Schematic diagram of rotary kiln system (ref. MHI)*

## 1-3. Traveling grate systems in WTE chambers

### 1-3-1. Reverse acting grate (Martin type)

A typical Martin reverse acting grate is 7 meters long, consists of a total of 15 bars and is inclined 26 degrees to the horizontal. The bars are positioned at an angle of 13 degrees from the traveling bed. In a common reverse acting grate configuration,

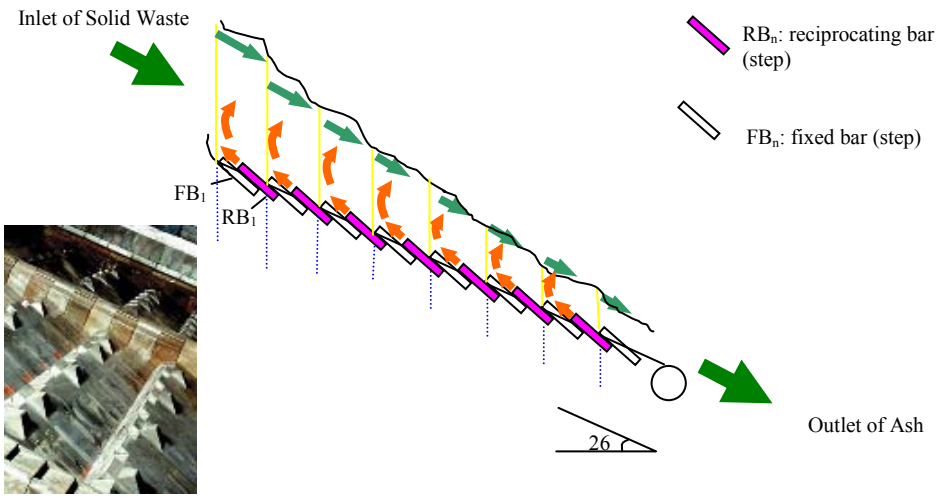


*Figure 1-5: Schematic Diagram of Reverse Acting Grate (Martin Grate)*

eight of the 15 bars are reciprocating and move a distance of 0.42 m (420 mm). The frequency of motion of the reciprocating bars can be adjusted from 10 to 60 double strokes per hour. A typical operating frequency in a WTE unit is 12 strokes per hour but the frequency used depends greatly on the composition of the MSW feed.

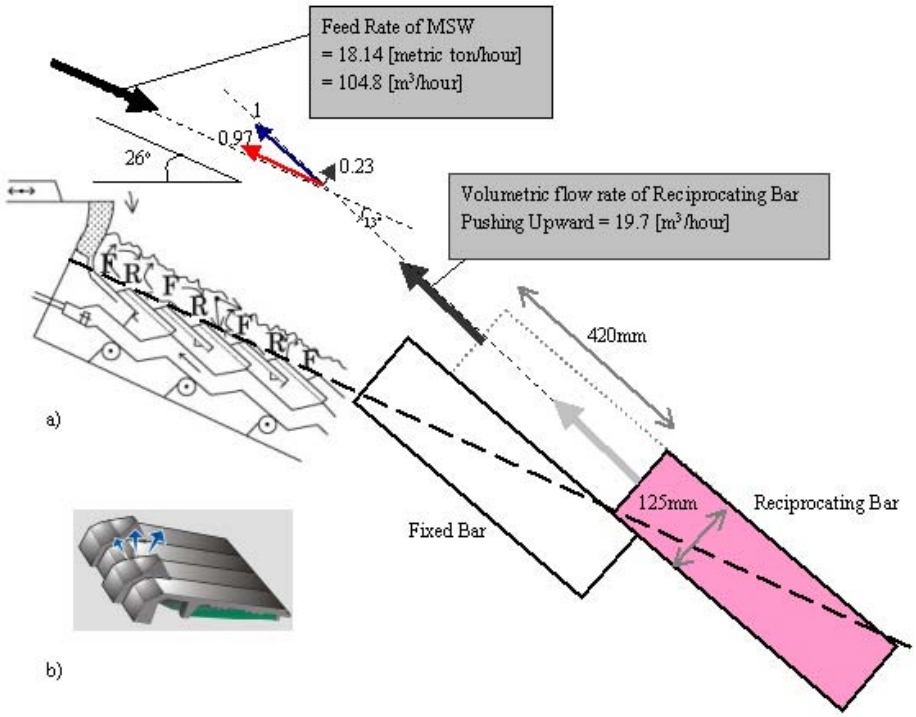


*Figure 1-6: Fixed and moving bars of Reverse acting grate (Martin): The reciprocating bars move against the direction of the feed by gravity: a) geometry of fixed and reciprocating bars, b) primary air (arrows) injected through the grate openings.*

A typical feed rate of MSW into the combustion chamber is 18.1 metric tons per hour (WTE of 480 short tons per day capacity). The average density of MSW is 500 lb per $yd^3$ or 173.2 kg per $m^3$ (Tchobanoglous *et al.* 1993) .Therefore, the corresponding volumetric feed rate of MSW is 104.8 $m^3$ per hour. A typical ratio of the downward volumetric flow rate of MSW feed to the upwards flow of waste due to the motion of the reciprocating bars (volume of material pushed upward by the bar motion) is approximately 5/1.

### 1-3-2. Forward acting grate (Von Roll type)

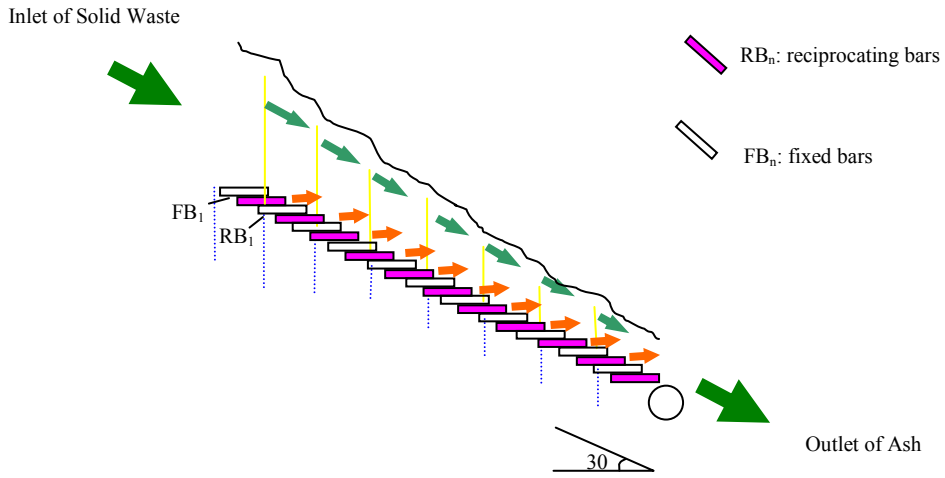


*Figure 1-7: Schematic Diagram of Forward Acting Grate (Von Roll type)*

Forward acting grate is made up of step grate type hearth as shown in Figure 1-7, in which the moving bars and fixed bars are arranged alternately. Moving bars reciprocate the same direction with the inlet flow of MSW.

### 1-3-3. Roller grate (Riley type)

The roller grate (also called the Duesseldorf/Babcock Grate) consists of 6 rollers of 2 m diameter that are inclined at $30^{o}$ to the horizontal as shown in Figure 1-8. As the rollers rotate slowly, the solid waste moves downward. Each roller "knead" and turn the solid waste. The rate of revolution for each roller can be varied from 0 to 6 rph.

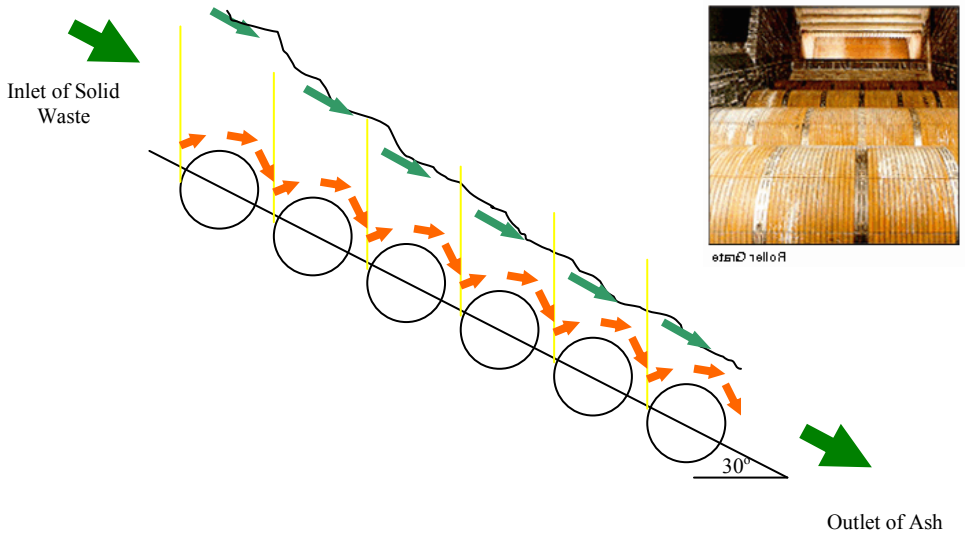


*Figure 1-8: Schematic Diagram of Roller Grate (Duesseldorf/Babcock Grate)*

Characteristics of these three types of traveling grates are summarized shown in Table 1-2. Forward and reverse acting grate systems are able to push MSW particles directly due to the motion of their reciprocating bars, whereas a roller grate conveys MSW particles because of the rotation of the rollers.

| Action on MSW bed | Grate Types | | |
|---|---|---|---|
| | Reverse acting grate | Forward acting grate | Roller grate |
| Mechanical Push | reverse | forward | ---- |
| Friction force (shear stress) | both directions | both directions | forward direction |

*Table 1-2: Comparison of reverse acting grate, forward acting grate, and roller grate systems*

## 1-4. Physical and chemical properties of Municipal Solid Waste (MSW) and combustion residues (ashes)

### 1-4-1. Physical properties

Physical properties of MSW and WTE combustion ashes include density, particle size, particle shape, and compressibility. These are dominant factors that determine how solid waste particles travel on the moving grate, transforming during the combustion process, and finally turning into ashes. The effect of sizes and shapes of solid waste particles, however, have been less studied, even though they govern movement and mixing on the grate as well as drying, volatilization, and, combustion rates. There is no study defining the shape factor of solid waste particles. The only comprehensive study of particle sizes (length, width and height) and size distributions was by Ruf, shown as Figure 1-9 (Ruf 1974), but it did not discuss the effect of shape or shape factor of MSW particles. In this study, physical properties of MSW particles were measured in order to develop more efficient mass-burn chambers (see Section 3-2). These are different from designs of coal chambers, since MSW, unlike coal, is a non-homogeneous fuel, of which combustion process is more complicated.

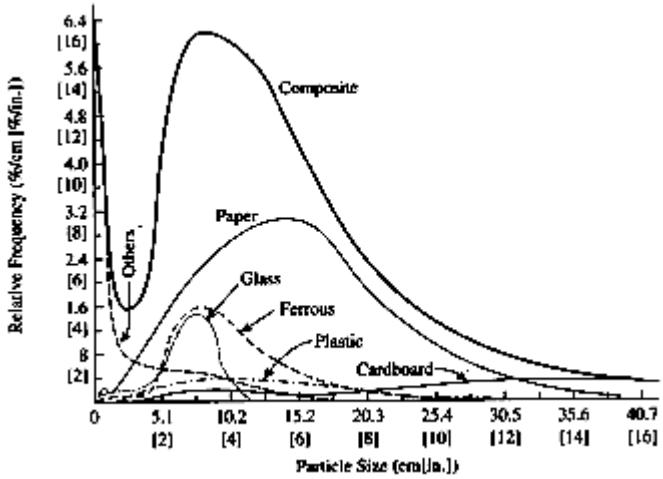


*Figure 1-9: Particle size distribution in FL (J. Ruf 1974)*

Besides these physical properties of particles, there are some important physical/physicomechanical characteristics that include agglomeration, aggregation, bulk density, cohesivity, combustion, compressibility explosion, flowability, packing, permeability, porosity, reactivity, segregation, and shear behavior. These properties influence a particle flow through a WTE combustion chamber. It is a material flow system and can be thought as a black box shown in Figure 1-10. MSW is pushed by feeders, heated, combusted, and, eventually, pushed though the outlet of chamber, changing into ashes. In addition to this solid flow, there is the air and emission gas flows during the MSW combustion.

### 1-4-2. Proximate and ultimate analysis

Proximate Analysis of MSW is used to determine the percent of four components (moisture, volatile matter, fixed carbon, and ash) of MSW and consists of

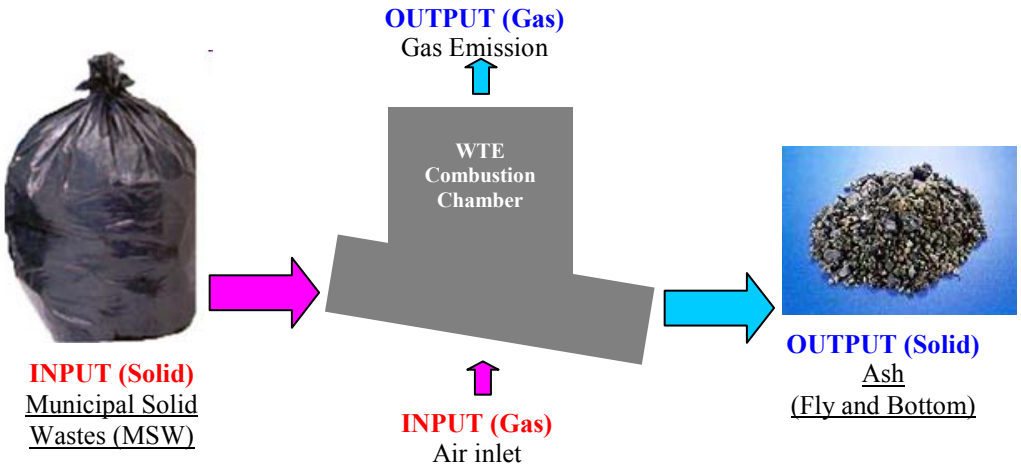


*Figure 1-10: Waste-To-Energy Combustion*

the following tests:

- Moisture (loss of moisture when heated to 105 $^{o}$C for 1 hour)
- Volatile matter (additional loss of weight on ignition at 950 $^{o}$C in covered crucible)
- Fixed carbon (combustible residue left after volatile matter is removed)
- Ash (residue after combustion in an open crucible)

Table 1-3 shows typical proximate analysis data of MSW (Tchobanoglous 1993) and coal (Smoot and Smith 1985).

Ultimate analysis is used to determine the elements C (carbon), H (hydrogen), O (Oxygen), N (Nitrogen), S (Sulfur), and inorganic ash of a sample. To measure weight percent of C, H, and N, a few mg of sample is heated to a temperature of 1000 $^{o}$C and completely combusted in the furnace and N is measured using thermal conductivity detection. O in the sample is measured by the infrared detector in the pyrolysis furnace heated to 1300 $^{o}$C (LECO 1999). S is also measured by the infrared detector but heated from 600 to 1450 $^{o}$C. These detected data are used to characterize the composition of the organic matter in MSW. Data of ultimate analysis of MSW and coal are presented in Table 1-4.

| Types of Waste | Proximate analysis, % by weight | | | |
|---|---|---|---|---|
| | **Moisture** | **Volatile matter** | **Fixed carbon** | **Ash (non-combustible)** |
| Food and food products | | | | |
| Fats | 2.0 | 95.3 | 2.5 | 0.2 |
| Food wastes (mixed) | 70.0 | 21.4 | 3.6 | 5.0 |
| Fruit wastes | 78.7 | 16.6 | 4.0 | 0.7 |
| Meat wastes | 38.8 | 56.4 | 1.8 | 3.1 |
| Paper products | | | | |
| Cardboard | 5.2 | 77.5 | 12.3 | 5.0 |
| Magazines | 4.1 | 66.4 | 7.0 | 22.5 |
| Newsprint | 6.0 | 81.1 | 11.5 | 1.4 |
| Paper (mixed) | 10.2 | 75.9 | 8.4 | 5.4 |
| Waxed cartons | 3.4 | 90.9 | 4.5 | 1.2 |
| Plastics | | | | |
| Plastics | 0.2 | 95.8 | 2.0 | 2.0 |
| Polyethylene | 0.2 | 98.5 | <0.1 | 1.2 |
| Polystyrene | 0.2 | 98.7 | 0.7 | 0.5 |
| Polyurethane | 0.2 | 87.1 | 8.3 | 4.4 |
| Polyvinyl chloride | 0.2 | 86.9 | 10.8 | 2.1 |
| Textiles, rubber, leather | | | | |
| Textiles | 10.0 | 66.0 | 17.5 | 6.5 |
| Rubber | 1.2 | 83.9 | 4.9 | 9.9 |
| Leather | 10.0 | 68.5 | 12.5 | 9.0 |
| Wood, trees, etc. | | | | |
| Yard wastes | 60.0 | 30.0 | 9.5 | 0.5 |
| Wood (green timber) | 50.0 | 42.3 | 7.3 | 0.4 |
| Hardwood | 12.0 | 75.1 | 12.4 | 0.5 |
| Wood (mixed) | 20.0 | 68.1 | 11.3 | 0.6 |
| Glass, Metals, etc. | | | | |
| Glass and mineral | 2.0 | - | - | 96-99 |
| Metal, tin cans | 5.0 | - | - | 94-99 |
| Metal, ferrous | 2.0 | - | - | 96-99 |
| Metal, nonferrous | 2.0 | - | - | 94-99 |
| Residential MSW | 21.0 (15-40) | 52.0 (40-60) | 7.0 (4-15) | 20.0 (10-30) |
| Coal | | | | |
| Pittsburgh bituminous (high volatile) | 2.0 | 36.6 | 55.4 | 6.0 |
| Illinois coal bituminous | 10.1 | 35.9 | 46.7 | 7.3 |
| North Dakota lignite | 29.9 | 29.5 | 33.4 | 7.2 |
| Wyoming subbituminous | 27.8 | 32.9 | 34.3 | 5.0 |
| Kentucky bituminous | 8.6 | 35.2 | 41.5 | 23.3 |

*Table 1-3: Typical proximate analysis data of MSW and Coal* (Tchobanoglous 1993, Smoot and Smith 1985)

| Types of Waste | Ultimate analysis, % by weight | | | | | |
|---|---|---|---|---|---|---|
| | **Carbon** | **Hydrogen** | **Oxygen** | **Nitrogen** | **Sulfur** | **Ash** |
| Food and food products | | | | | | |
| Fats | 73.0 | 11.5 | 14.8 | 0.4 | 0.1 | 0.2 |
| Food wastes (mixed) | 48.0 | 6.4 | 37.6 | 2.6 | 0.4 | 5.0 |
| Fruit wastes | 48.5 | 6.2 | 39.5 | 1.4 | 0.2 | 4.2 |
| Meat wastes | 59.6 | 9.4 | 24.7 | 1.2 | 0.2 | 4.9 |
| Paper products | | | | | | |
| Cardboard | 43.0 | 5.9 | 44.8 | 0.3 | 0.2 | 5.0 |
| Magazines | 32.9 | 5.0 | 38.6 | 0.1 | 0.1 | 23.3 |
| Newsprint | 49.1 | 6.1 | 43.0 | <0.1 | 0.2 | 1.5 |
| Paper (mixed) | 43.4 | 5.8 | 44.3 | 0.3 | 0.2 | 6.0 |
| Waxed cartons | 59.2 | 9.3 | 30.1 | 0.1 | 0.1 | 1.2 |
| Plastics | | | | | | |
| Plastics | 60.0 | 7.2 | 22.8 | - | - | 10.0 |
| Polyethylene | 85.2 | 14.2 | - | <0.1 | <0.1 | 0.4 |
| Polystyrene | 87.1 | 8.4 | 4.0 | 0.2 | - | 0.3 |
| Polyurethane | 63.3 | 6.3 | 17.6 | 6.0 | <0.1 | 4.3 |
| Polyvinyl chloride | 45.2 | 5.6 | 1.6 | 0.1 | 0.1 | 2.0 |
| Textiles, rubber, leather | | | | | | |
| Textiles | 48.0 | 6.4 | 40.0 | 2.2 | 0.2 | 3.2 |
| Rubber | 69.7 | 8.7 | - | - | 1.6 | 20.0 |
| Leather | 60.0 | 8.0 | 11.6 | 10.0 | 0.4 | 10.0 |
| Wood, trees, etc. | | | | | | |
| Yard wastes | 46.0 | 6.0 | 38.0 | 3.4 | 0.3 | 6.3 |
| Wood (green timber) | 50.1 | 6.4 | 42.3 | 0.1 | 0.1 | 1.0 |
| Hardwood | 49.6 | 6.1 | 43.2 | 0.1 | <0.1 | 0.9 |
| Wood (mixed) | 49.5 | 6.0 | 42.7 | 0.2 | <0.1 | 1.5 |
| Wood chips | 48.1 | 5.8 | 45.5 | 0.1 | <0.1 | 0.4 |
| Glass, Metals, etc. | | | | | | |
| Glass and mineral | 0.5 | 0.1 | 0.4 | <0.1 | - | 98.9 |
| Metal, (mixed) | 4.5 | 0.6 | 4.3 | <0.1 | - | 90.5 |
| | | | | | | |
| Coal | | | | | | |
| Pittsburgh bituminous (high volatile) | 77.5 | 5.3 | 8.5 | 1.5 | 1.2 | 6.0 |
| Illinois coal bituminous | 68.5 | 5.0 | 13.8 | 1.3 | 3.5 | 8.1 |
| North Dakota lignite | 69.7 | 3.8 | 13.2 | 1.9 | 1.1 | 10.3 |
| Wyoming subbituminous | 76.3 | 4.4 | 10.8 | 1.1 | 0.5 | 6.9 |
| Kentucky bituminous | 61.0 | 4.4 | 5.6 | 1.4 | 4.3 | 23.3 |

*Table 1-4: Typical ultimate analysis data of MSW and Coal* (Tchobanoglous 1993, Smoot and Smith 1985)

### 1-4-3. Mass reduction

The mass and volume of MSW particles are reduced during the combustion process. The effects of heating rate and sample size in the thermal process are shown Figure 1-11 and 1-12 (Gaur and Reed 1998). Figure 1-12 represents the size effect of mass reduction of 5.8mg and 180mg pelletized baker cellulose. These effects are dependent on heat transfer from the gas film surrounding the particle into the particle.

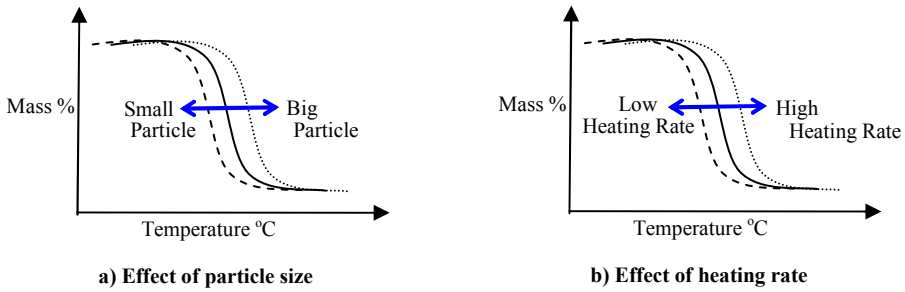


*Figure 1-11: Effects of sample size and heating rate*

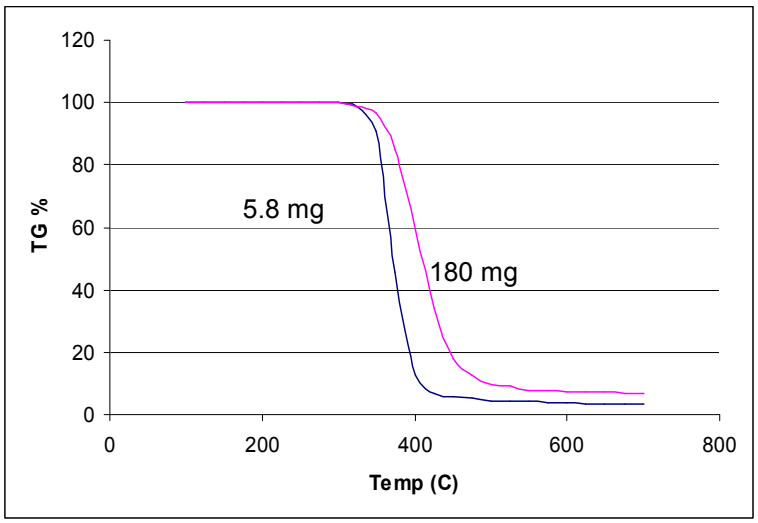


*Figure 1-12: Sample Size effect of pelletized Baker Cellulose, 5.8mg and 180 mg (S. Gaur and T. B. Reed 1998)*

### 1-4-4. Calorific values of different materials

The calorific value (or heating value) of the organic compounds in MSW are the amounts of energy released when the compounds are burned completely. It can be determined using an oxygen bomb calorimeter. The colorific value is dependent on the phase of water or steam in the combustion products. When vapor $H_2O$ is the product of combustion, the calorific value is called Lower Heating Value (LHV). If condensed $H_2O$ is the product of combustion, it is called Higher Heating Value (HHV). *Themelis et. al.* found that composition of organic matter in MSW can be represented by the molecular formula $C_6H_{10}O_4$ (Themelis et. al. 2002) and compared experimental heating values of various waste materials with the percentage of $H_2O$ (moisture) content shown in Figure. 1-13.

The calorific value of the MSW compounds can be determined using elemental composition quantified by ultimate analysis. There are several formulae to calculate calorific values using the elemental composition of MSW.

Dulong's equation had been used by engineers working in coal and wood stoker facilities (Cho et. al 1995):

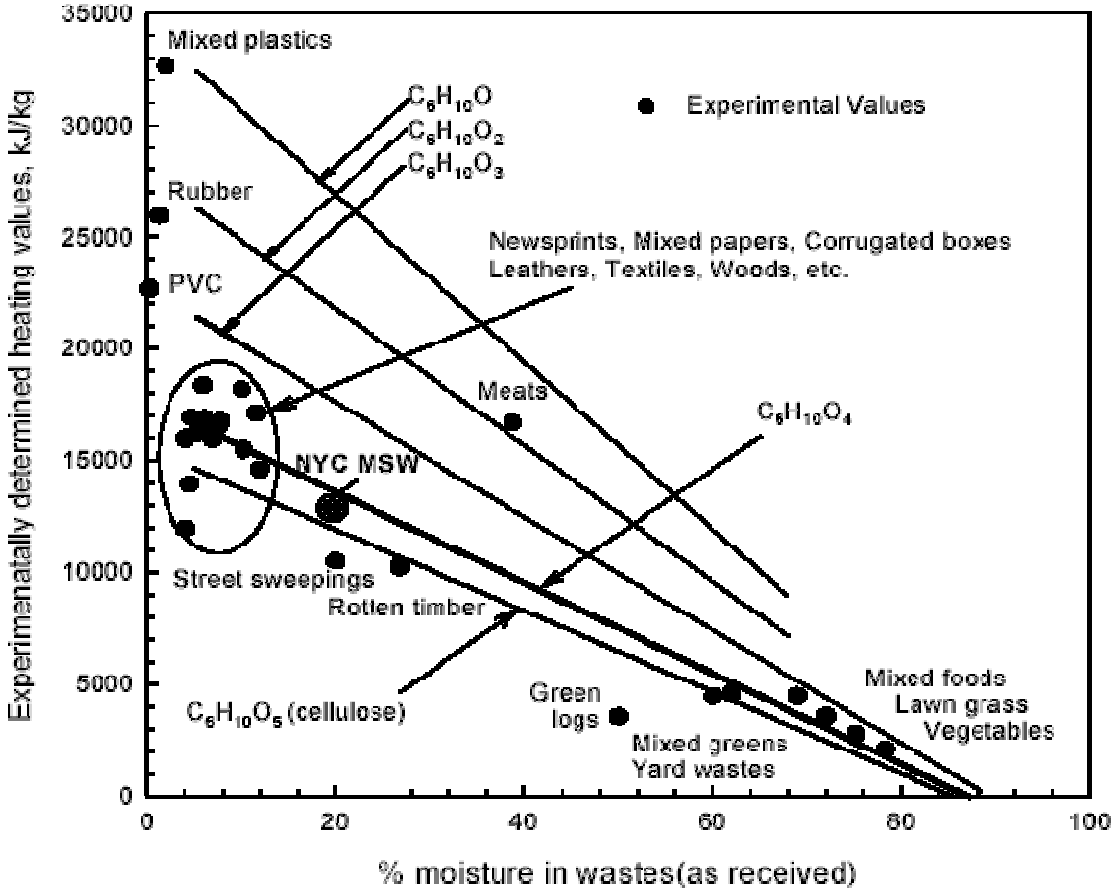


*Figure 1-13: Comparison of experimental heating values of various waste materials* (Themelis *et. al.* 2002)

$$H_h = 81\cdot C + 342.5\cdot(H - 1/8\cdot O) + 22.5S - 6\cdot(9\cdot H + W) \quad \text{(Eq. 1-1)}$$

where $H_h$ is higher heating value, C is carbon fraction (%), H is hydrogen (%), O is Oxygen (%), S is sulfur (%), W is water (%). This equation provides good approximated heating values for fuels that mainly contain carbon, such as coal and wood.

For calorific calculation of MSW, Steuer's equation has been used (Cho et. al 1995):

$$H_h = 81\cdot(C - 3/8\cdot O) + 57\cdot 3/8\cdot O + 342.5\cdot H + 22.5\cdot S + 57\cdot 3/4\cdot O - 6\cdot(9\cdot H + W) \quad \text{(Eq. 1-2)}$$

The heating value of RDF is expressed as follows:

$$H_h = 18400\cdot X_{comb} - 2636\cdot X_{H2O} - 628\cdot X_{glass} - 544\cdot X_{metal}\ \text{kJ/kg} \quad \text{(Eq. 1-3)}$$

where $X_{comb,}$ $X_{H2O,}$ $X_{glass}$, and $X_{metal}$ are the fractions of RDF components.

## 1-5. Physical and chemical transformations of MSW in the bed

The MSW physicochemical transformations in the WTE combustion chamber, as shown 1-14, are composed of three main processes: drying of the surface of solid waste particles, volatilization as the particles may soften and undergo internal transformation, and char combustion processes. In addition to these three processes, the volatiles released from heated solid particles react with oxygen, which is called volatile combustion.

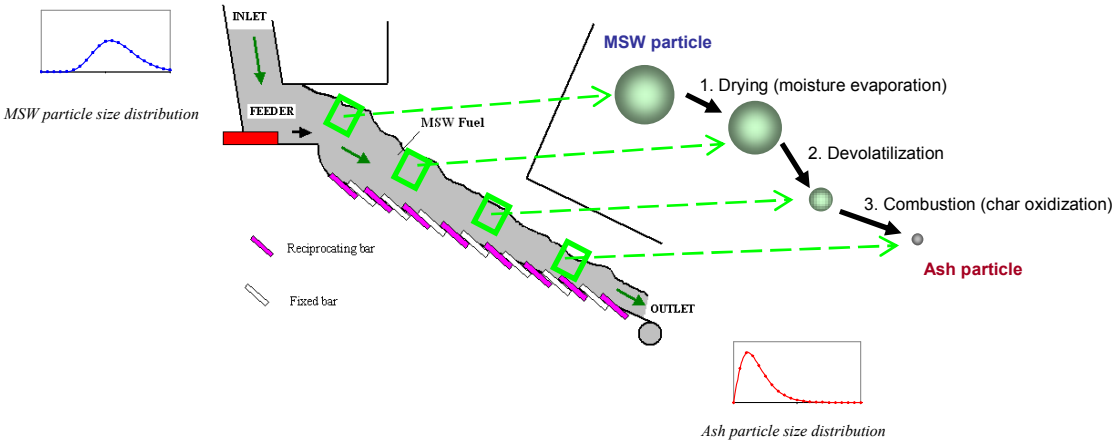


*Figure 1-14: Combustion and transport phenomena of one particle in a MSW bed on the traveling grate*

### 1-5-1. Moisture evaporation in the drying process

The drying process occurs at the surface of solid waste particles just after MSW is fed into the combustion chamber. Heat transferred by convection of the gases surrounding the waste particles and of the primary air injected from the

traveling grate into the MSW bed. The rate of solid waste evaporation can be expressed as:

$$R_{drying} = A_s h_s (C_{H_2O,s} - C_{H_2O,g}) \text{ , when } T_s < 100\text{C}^{\text{o}} \quad \text{(Eq. 1-4)}$$

$$R_{drying} = Q_{ccr} / H_{evp} \text{ , when } T_s > 100\text{C}^{\text{o}} \quad \text{(Eq. 1-5)}$$

$$Q_{ccr} = A_s (h_s (T_g - T_s) + \varepsilon_s \sigma (T_{env}^4 - T_s^4)) \quad \text{(Eq. 1-6)}$$

**1-5-2. Devolatilization in the gasification process**

Volatilization model of first-order reaction process (Badzioch and Hawksley 1970)

$$\frac{dv}{dt} = k(v_\infty - v) \quad \text{(Eq. 1-7)}$$

$$k = A \exp(-\frac{E}{RT}) \quad \text{(Eq. 1-8)}$$

$$v_\infty = Q(1 - v_c)v_p \quad \text{(Eq. 1-9)}$$

where $v$ is the fractional yield of volatiles (mass of volatiles per mass of daf coal), and $v_\infty$ is the hypothetical ultimate yield.

(a) k = 3.12x105 exp[-8961/T] (Badzioch and Hawksley 1970) (Eq. 1-10)

(b) k = 4.3x1014 exp[-27,544/T] (Solomon, et al. 1976) (Eq. 1-11)

A continuous Gaussian distribution of activation energy is another approach to treat pyrolysis (Anthony et al. 1975):

$$\frac{v_\infty - v}{v_\infty} = \frac{1}{\sigma(2\pi)^{\frac{1}{2}}} \left\{ \int_0^\infty \exp\left[ -\left( \int_0^\infty k dt \right) f(E) dE \right] \right\} \quad \text{(Eq. 1-12)}$$

$$f(E) = \frac{1}{\sigma(2\pi)^{\frac{1}{2}}} \exp\left( \frac{-(E - E_0)^2}{2\sigma^2} \right) \quad \text{(Eq. 1-13)}$$

Tchobanoglous et al. reported data about the mounts of volatiles during decomposition processes of the MSW. Table 1-5 and 1-6 shows volatile products and components of MSW with temperature gradient (Tchobanoglous et al. 1985).

| Temperature (K) | Volatiles (kg/kg waste) |
|---|---|
| 755 | 0.123 |
| 921 | 0.186 |
| 1088 | 0.237 |
| 1199 | 0.244 |

*Table 1-5: Volatile products of MSW*

| Component (% vol.) | Temperature (K) | | | |
|---|---|---|---|---|
| | 755 | 921 | 1088 | 1199 |
| $H_2$ | 5.56 | 16.58 | 28.55 | 9.26 |
| $CH_4$ | 12.43 | 15.91 | 13.73 | 10.45 |
| CO | 33.5 | 30.49 | 34.12 | 35.25 |
| $CO_2$ | 44.77 | 31.78 | 20.59 | 18.31 |
| $C_2H_4$ | 0.45 | 2.18 | 2.24 | 2.43 |
| $C_2H_6$ | 3.03 | 3.06 | 0.77 | 1.07 |

*Table 1-6: Composition of volatile matters*

### 1-5-3. Combustion of volatile matter

In the volatilization process, a wide range of different volatile matters are generated. This complex process cannot be treated separately. Therefore, assuming a representative hydrocarbon to be the only combustible product from the volatilization process, the simplified reaction can be presented as follows:

$$C_m H_m + \left(\frac{m}{2} + \frac{n}{4}\right) O_2 \rightarrow mCO + \frac{n}{2} H_2 O \qquad \text{(Eq. 1-14)}$$

$$CO + \frac{1}{2} O_2 \rightarrow CO_2 \qquad \text{(Eq. 1-15)}$$

$$R_{CO} = 1.3 \times 10^{11} C_{CO} C_{H_2O}^{0.5} C_{O_2}^{0.5} \qquad \text{(Eq. 1-16)}$$

$$R_{C_m H_n} = 59.8 T_g P^{0.3} C_{H_2O}^{0.5} C_{O_2} \exp\left(\frac{-12200}{T_g}\right) \qquad \text{(Eq. 1-17)}$$

### 1-5-4. Combustion of fixed carbon within the bed

Fixed carbon in a solid waste particle is combusted and described as following equations:

$$C(solid) + \alpha O2 \rightarrow 2(1-\alpha)CO + (2\alpha - 1)CO_2 \quad \text{(Eq. 1-18)}$$

$$\frac{CO}{CO_2} = 2500 \cdot \exp(\frac{-6420}{T}) \quad \text{(Eq. 1-19)}$$

$$R_{C(solid)} = \frac{C_{O_2}}{\left(\frac{1}{k_r} + \frac{1}{k_d}\right)} \quad \text{(Eq. 1-20)}$$

Eq. 1-20 is char consumption rate expressed by Smoot and Pratt (Smoot and Pratt 1979)

## 1-6. Mathematical modeling for development of WTE technologies

Further development of WTE technologies will depend on a better understanding and application of mass and heat transfer phenomena in the WTE combustion chamber. The transport and combustion phenomena of solid waste particles traveling on the grate systems are controlled by a large number of parameters that depend on the design of the combustion chamber (as explained in Section 1-2 and 1-3) and on the properties of the MSW particles (as described in Section 1-4 and 1-5). Especially, as mentioned in Section 1-4, MSW is a very non-

homogeneous material and the properties of the particles vary widely in terms of size, shape, specific weight, moisture content, energy content (heating value), and chemical composition (Carbon, Hydrogen, Oxygen, Nitrogen, Sulfur, and Ash). In addition, there is large amount of interactions among MSW particles reacting primary air in a high temperature zone of combustion chamber. As the MSW particles travel over the moving grate, they interact with each other and with the flow of primary air though the bed and their temperature, size and composition changes with time and location on the bed (e.g., whether a particle is located near the surface or the bottom of the bed)

One of the most effective ways to understand those transport phenomena and chemical rate reactions is by mathematical modeling of fluid flow though the bed and above the bed, heat transfer between the furnace and particle/gas, mass transfer between particles and air flow, and chemical reactions (i.e. mostly combustion) within the bed and in the chamber above the bed. Simulating these phenomena in a computer is less costly than building physical models and is helpful to develop a better chamber design.

The combustion chamber simulation consists of two major components: 1) a bed model of the drying, volatilization and chemical reactions within the bed, and 2) CFD modeling of the gas flow, heat transfer and gas-phase reactions in the chamber above the grate. These models have been developed separately. Generally, there have

been more studies on CFD chamber modeling because the behavior of emission gases and corrosion of the chamber walls have been the main concerns of both operators of WTE facilities and developers of WTE technologies.

### 1-7. Shortcomings of existing WTE models

There have been several different approaches to model WTE combustion systems in the past (see Chapter 2 in detail). Whereas CFD chamber modeling is widely accepted and used in the WTE industry, the solid waste bed modeling still

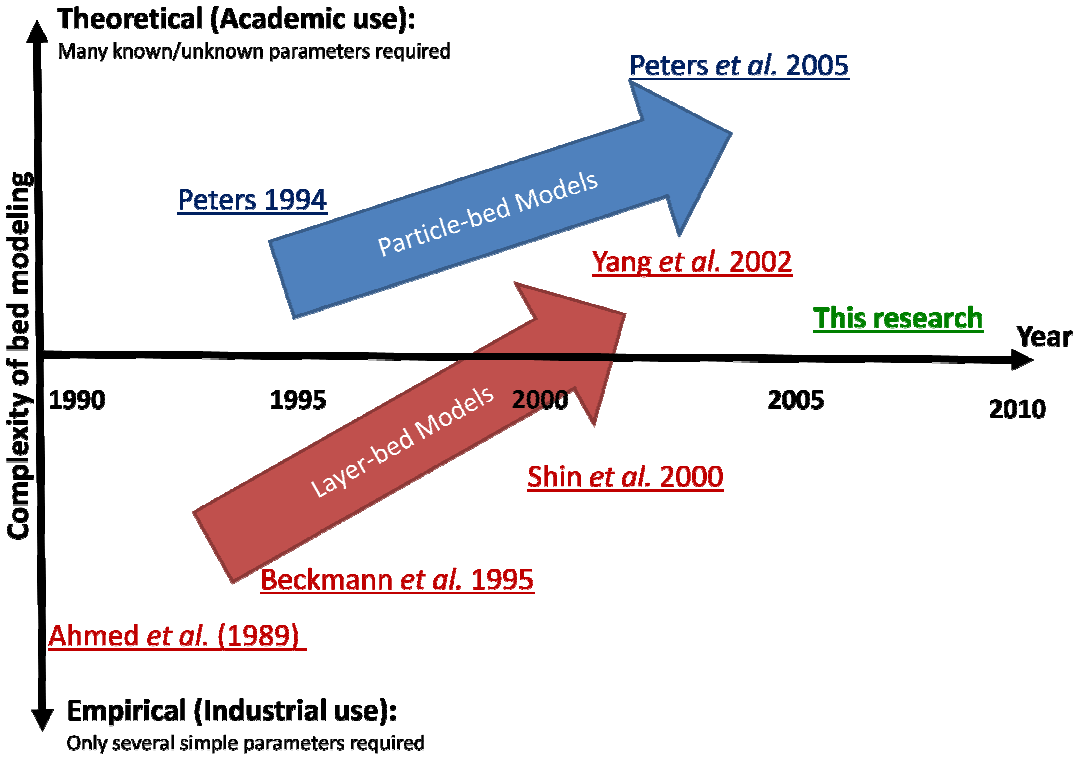


*Figure 1-15: Trend of current bed models*

needs to include an algorithm for overcoming the heterogeneity of MSW gasification and combustion.

Figure 1-15 shows previous studies on bed modeling that can be categorized in two classes: empirical modeling and theoretical modeling.

Empirical models are mainly used for practical basis such as training operators of WTE facilities, predicting approximate results for combustion chamber maintenance, and calculating initial or boundary conditions, like bed surface temperature, as a pre-process of CFD modeling. These models are practical and sometimes called "industry-friendly" because of their simplicity, without long calculation time and need to use extensive computer resources.

Theoretical models are used for academic studies such as establishing new theories, verifying them with experimental results, and sometimes developing new grate systems. These models include complicated MSW flow and combustion. Hence, they need a lot of run-time of computer calculation. Theoretical models, in general, express bed transport and combustion phenomena in more detail than empirical models, but do not represent the heterogeneity of MSW. The problem here is that complicated simulation results do not always agree with the real chamber situation. For example, the Discrete Element Method (DEM) applied in Peters' model is a new approach in order to predict particle movements, but he considers one single spherical particle type such as density (700kg/m3), Young's modulus (10MPa), and shear

modulus (3 MPa) for heterogeneous MSW. This "ideal MSW particle" does not match the diversity of MSW in a real combustion chamber. On the other hand, empirical bed models are too simple to simulate solid waste flow and combustion phenomena. In Shin's model, for example, the interaction between sections of MSW bed, which is agitated by a traveling grate, was not taken into account. Only the height of each section reduced by thermal conversion was discussed in this model. This discrepancy in bed modeling research is due mainly to the heterogeneous characteristics of MSW and the complexity of its physical and thermochemical conversion in a mass-burn combustion chamber.

In addition to those shortcomings of both empirical and theoretical modeling, the current bed models (see the discussion in Chapter 2) are not equipped to predict other effects during the combustion processes on the grates:

1. Continuous variation of solid flow (inlet through outlet, limitation of steady-state bed models)
2. Transient phenomena (channeling through the bed and break-up effects of MSW particles)
3. Mixing of the MSW particles is not taken into account adequately (even though the solid mixing process is one of the principal factors for promoting combustion)

The main reason for these shortcomings is that past studies have considered MSW as one layer, not as particles. Addressing these issues in a novel fashion, i.e. particle-based analysis, can help alleviate some of the problems experienced in current combustor design. Examples of the major problems that need to be addressed are:

1. Worldwide, there are 700 WTE plants with different types of traveling grate systems, such as reverse acting, forward acting, and roller grate. However, there are no methods for evaluating the advantages or disadvantages of various traveling grate systems for mass combustion of non-homogeneous MSW, in terms of throughput, energy, etc.
2. The lack of mixing results in incomplete combustion of solid waste.
3. Unstable combustion caused by the inlet flow of highly non-homogeneous MSW results in unstable burnout point.
4. The channeling of airflow through the grate results in a high excess air requirement and lower temperatures in the chamber. Yang et.al. have been studying this effect though both theoretical and experimental analyses (Yang et. al. 2003).

The relationship among mixing phenomena, chamber designs, and chamber operation on the mass-burn traveling bed is not fully understood and is not fully included in existing bed models. These shortcomings result from lack of quantitative analysis of the movement of MSW particles during the combustion process. In order

to quantify the motion of MSW particles on the various types of grates, some studies using small-scale physical models were carried out. For example, particle tracking tests using 1/15 scale models developed by Lim et al clarified mixing phenomena enhanced by the traveling grates (Lim et al 2001). Residence time of each wooden and ceramic particle was measured using a scale model of forward and reverse acting grate systems (Beckmann et al 2000). Even though these studies were worthwhile, they did not accurately replicate a real combustion chamber and grate using physical scale modeling. One of the difficulties of physical small-scale models has been that the range of particle sizes, densities and shape factors encountered in the MSW fed to WTE combustion chambers is impossible to simulate in small physical models. Also, the physical small-scale models cannot simulate the volatilization and combustion phenomena on the grate that change the density of solids by an order of magnitude.

**1-8. Objectives of study**

The objectives of this doctoral research are mainly to provide a better tool for understanding effects of solid flow and mixing phenomena enhanced by the motion of traveling grate:

1. Developing a mathematical model to characterize and quantify flow and mixing processes of the highly non-homogeneous MSW.
2. Analyzing the relationship between the behavior of solid waste particles and operation parameters (especially, reciprocation speed of moving bars) as well as chamber design parameters (traveling grate)

3. Calibrating and validating mathematical models using full-scale physical model of reverse acting grate with camera observation (analysis of MSW particle movements) and "as-collected" MSW packed bed (collection and analysis of NYC-MSW),

In order to develop an integrated bed model to address the limitations of current bed models described in the previous section (Section 1-7), it is necessary to incorporate two mathematical models based: a bed combustion model, and a bed mixing model under a CFD model, as shown in Figure 1-16.

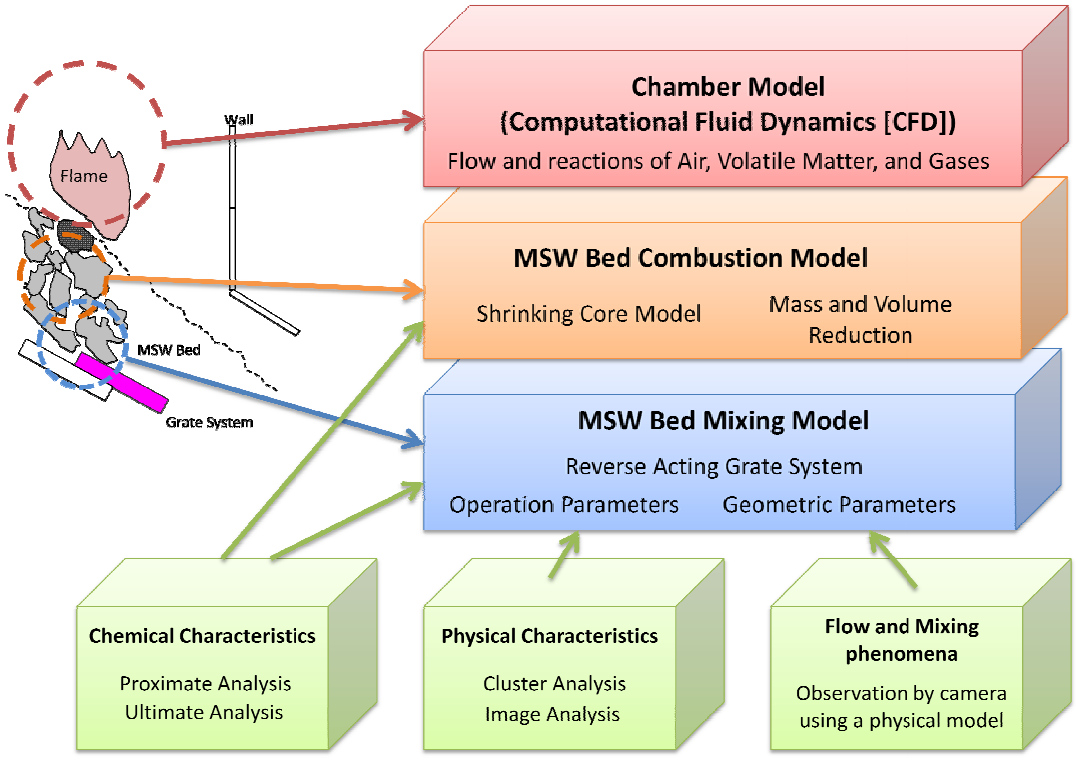


*Figure 1-16: Schematic Diagram of Integrated Modeling*

The bed modeling results have been expressed in terms of two parameters: a) the residence time of particles with different sizes, and b) the mixing diffusion (dispersion) coefficients along the length ($D_l$) of the bed on the grate. These two parameters will be correlated to equipment and operating parameters that can be changed either during design or operation (e.g., diameter, number and speed of rotation of roller grates; number, height, frequency/speed of Martin moving grates).

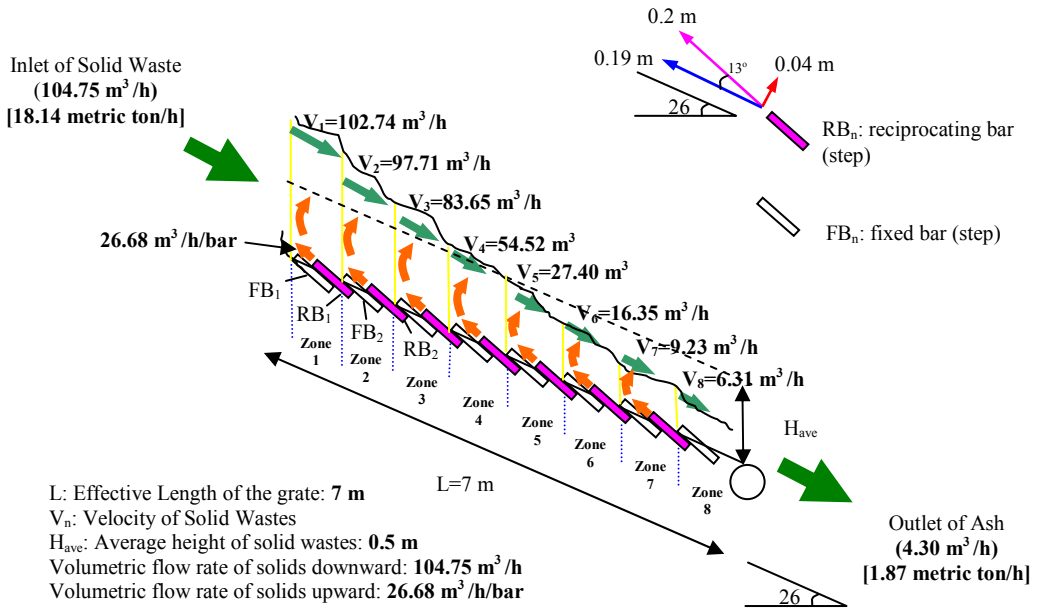


*Figure 1-17: MSW flow and mixing in the reverse acting grate: The MSW particles are subjected to different temperatures and their size and composition change with time and location (e.g., whether a particle is located at the surface or bottom of the bed)*

Figure 1-17 shows the MSW flow and mixing on the reverse acting grate system in a WTE facility. The forces to be considered in the mathematical model are:

a) the gravity force acting on the MSW deposited on the grate; for example, in the absence of any motion of the grate, material deposited on a horizontal plane would form a solids cone of a predictable angle of repose. In the case of an inclined plane (e.g., $26^o$ in the case of the Martin grate), the downward angle of the cone would be proportionally greater.

b) the motion of the grate imposes an additional shear force on the bottom layer of the solids that is in contact with the grate surface. Depending on the "viscosity" of the solids on the grate, this shear force is transmitted to upward layers, similarly to what would happen in a liquid. The combination of gravity and shear forces due to the motion of the grate results in the downward motion of the MSW particles.

The study is based on the dimensions and operating characteristics of an actual industrial WTE plant. The flow rate of MSW fed in the inlet of combustion chamber is 480 short tons per day or 18 metric tons per hour. The specific density of MSW is 500 lb/yd$^3$ or 0.173 tons per cubic meter. Hence, the total volumetric rate of MSW fed by the pusher is 105 m$^3$/hr. If the height of the MSW bed is assumed to be 1.0 meter at any position, the total volume of the MSW bed is 56 cubic meters (8 m in width, 7m in length, and 1 m in height). Therefore, the calculated residence time is

0.53 hour or 32 minutes. However, this residence time calculation of the MSW flow does not include combustion and mixing phenomena: a) volume reduction of MSW during the drying, gasification, combustion processes and b) mixing of MSW due to the motion of the traveling grate.

Regarding MSW volume reduction, as noted earlier, there are mainly three processes: drying, volatilization, and combustion (char oxidization). As shown in Figure 1-18, the mass balance of this WTE chamber system is described as follows,

$$m_{inlet} = m_{drying} + m_{VM} + m_{FC} + m_{outlet} \quad \text{(Eq. 1-21)}$$

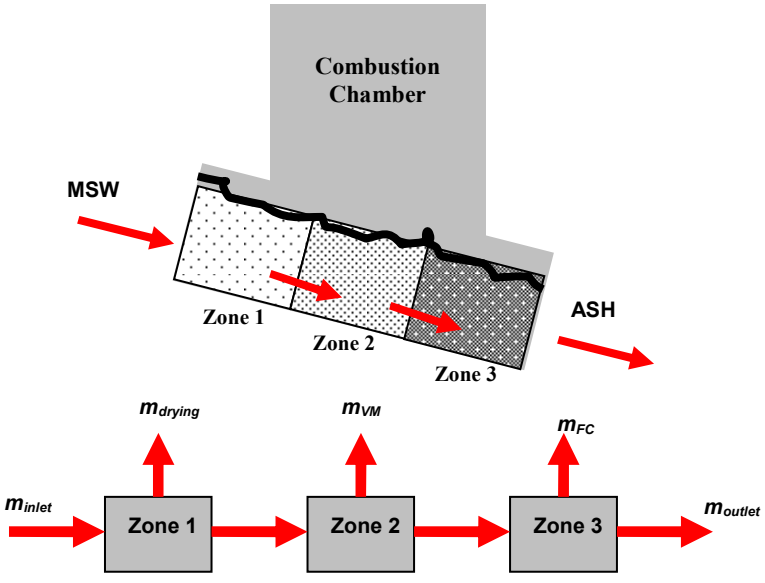


*Figure 1-18: Mass balance of a MSW bed in the combustion chamber*

where, $m_{inlet}$, $m_{drying}$, $m_{VM}$, $m_{FC}$, $m_{outlet}$ are weight % of raw MSW, moisture, volatile matters, fix carbon, and ash, respectively. A typical residential MSW contains about 21% of moisture, 52% of volatile matters, 7% of fixed carbon, 20% of ash (see Section 1-4-2). Since each mass reduction corresponds to a volume reduction, the total volume reduction of MSW in the chamber will be in accordance with this proximate analysis of MSW.

In terms of MSW mixing on a common Martin grate, there are 8 moving bars that reciprocate 12 strokes per hour. Volumetric flow rate of bar motions is 19.7 $m^3$/hr (see Chapter 2 for detail). The MSW flow is described by the dispersion model:

$$\frac{\partial c}{\partial t} = D_e \frac{\partial^2 c}{\partial x^2} - u \frac{\partial c}{\partial x} \qquad \text{for } 0 < x < L \qquad \text{(Eq. 1-22)}$$

where $D_e$ is eddy diffusivity, $u$ is velocity in flow direction, $L$ is length of the combustion chamber, $x$ is distance along reactor, in direction of flow. In dimensionless form where $z = (ut+x) / L$ and $\theta = t / \bar{t} = tu / L$, equation 1-2 becomes

$$\frac{\partial c}{\partial \theta} = \left( \frac{D_e}{uL} \right) \frac{\partial^2 c}{\partial z^2} - \frac{\partial c}{\partial z} \qquad \text{(Eq. 1-23)}$$

where $\left( \frac{D_e}{uL} \right)$ is the inverse of the dimensionless Peclet number, $P_e$. If $P_e$ is smaller than 0.01 (close to zero), dispersion in the MSW flow is negligible and called plug

flow. When $P_e$ is larger than 0.01 the MSW flow has large dispersion and called mixed flow.

The motion of the traveling grate is important in mixing MSW in the bed since the major source of heat transfer to the MSW bed is radiation from flame of volatile matter combustion and chamber walls. If there is no grate motion and the MSW flow has no dispersion (i.e. $P_e < 0.01$), only particles located near the surface of the bed will be heated up and reach the drying and devolatizing temperatures. The inside of the bed will be heated by conduction and then will slowly reach these temperatures (A flame front will move from top to bottom, as it can be seen in a batch reactor). Therefore, for estimating the rate of reactions or heat transfer, the Peclet number $P_e$ of the MSW flow is one of the most important parameters. The projections of the mathematical bed models will be validated by a) numerical analysis of physical characteristics, and b) observation of the MSW particles in the bed using full-scaled physical section model of traveling grate (reverse acting grate) (see Chapter 3 and 5).

In addition to these objectives, this doctoral research hopes to advance the design and operation of WTE combustion chambers for high energy efficiency. This includes assessing of current WTE combustion chamber systems and suggesting the design of a new traveling grate for promoting combustion.

# Chapter 2: Mathematical Modeling

## 2-1. Prior models of grate transport and combustion phenomena

### 2-1-1. Bed modeling (solid waste combustion)

A bed model developed by Ahmed *et al.* (1989) dealt with only pyrolysis reactions of MSW that was simplified to be composed of only cellulosic material. As shown in Figure 2-1, the volume reduction process in the MSW bed is simply proportional to the decomposition rate of cellulose. The MSW bed is ideally well-mixed in the vertical direction. The flame zone above the bed has a constant temperature and it is the heat source for the bed. The calculation method of this bed

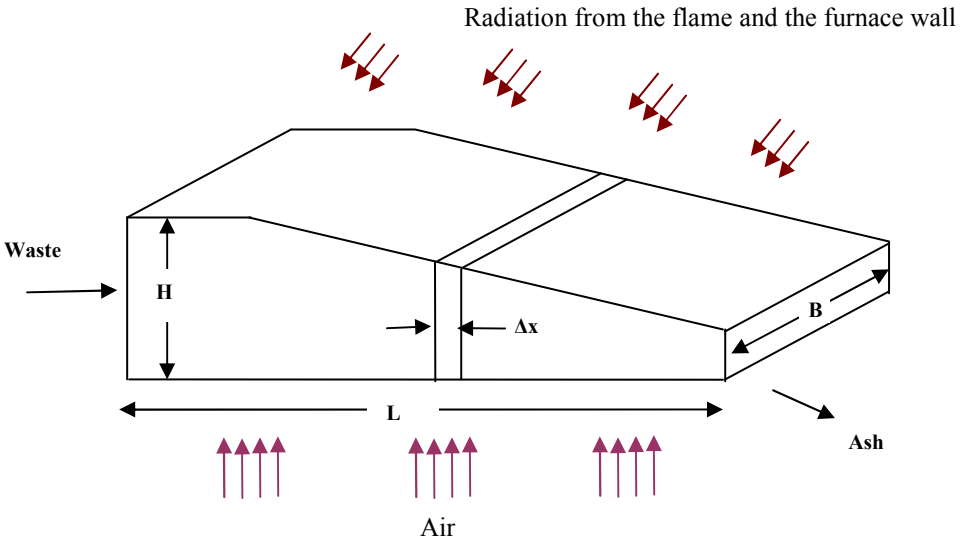


*Figure 2-1: Discretization of the fuel bed (Ahmed et al. 1989)*

modeling incorporated the pyrolysis kinetics, enthalpy of pyrolysis reactions, heat transfer by convection and radiation, kinetics and thermodynamics of volatile matter combustion, and material transport by the traveling grate. In order to examine the effects of the solid feed rates, several parameters are considered such as the air flow rates, the bed and gas temperature profiles, and the height and length of the combustion chamber required for MSW conversion. This study showed simplified trends of these effects, but a detailed quantitative analysis for bed modeling was not undertaken.

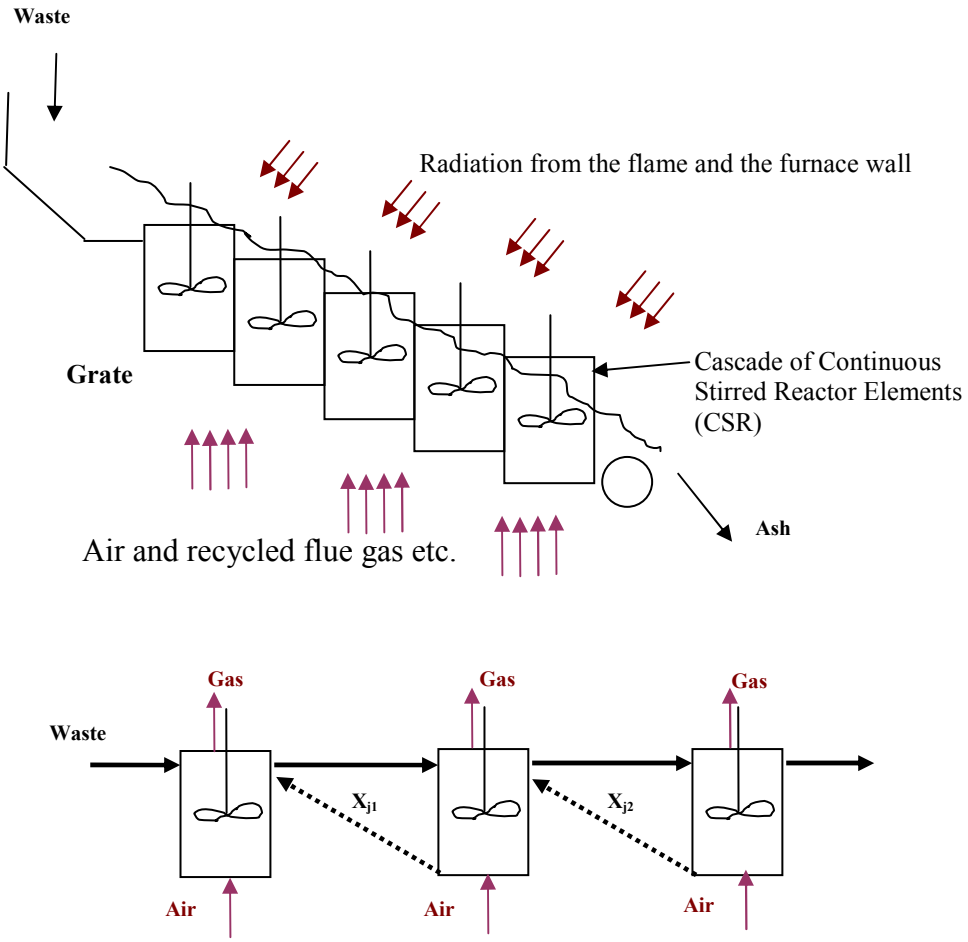


*Figure 2-2: Combustion Steps of a Stoker Firing Process and Model Idea (Beckman 1995)*

Beckmann et al. (Beckmann et al. 1995) considered a combustion chamber as combination of several continuously stirred reactors (CSRs) shown in Figure 2-2. In this bed model they defined an effective reaction coefficient determined by data from a batch-stoker test plant. For both steady state and non steady state conditions modeling results were compared with experimental results. This research concluded

that the model was successful for describing non steady combustion processes of MSW.

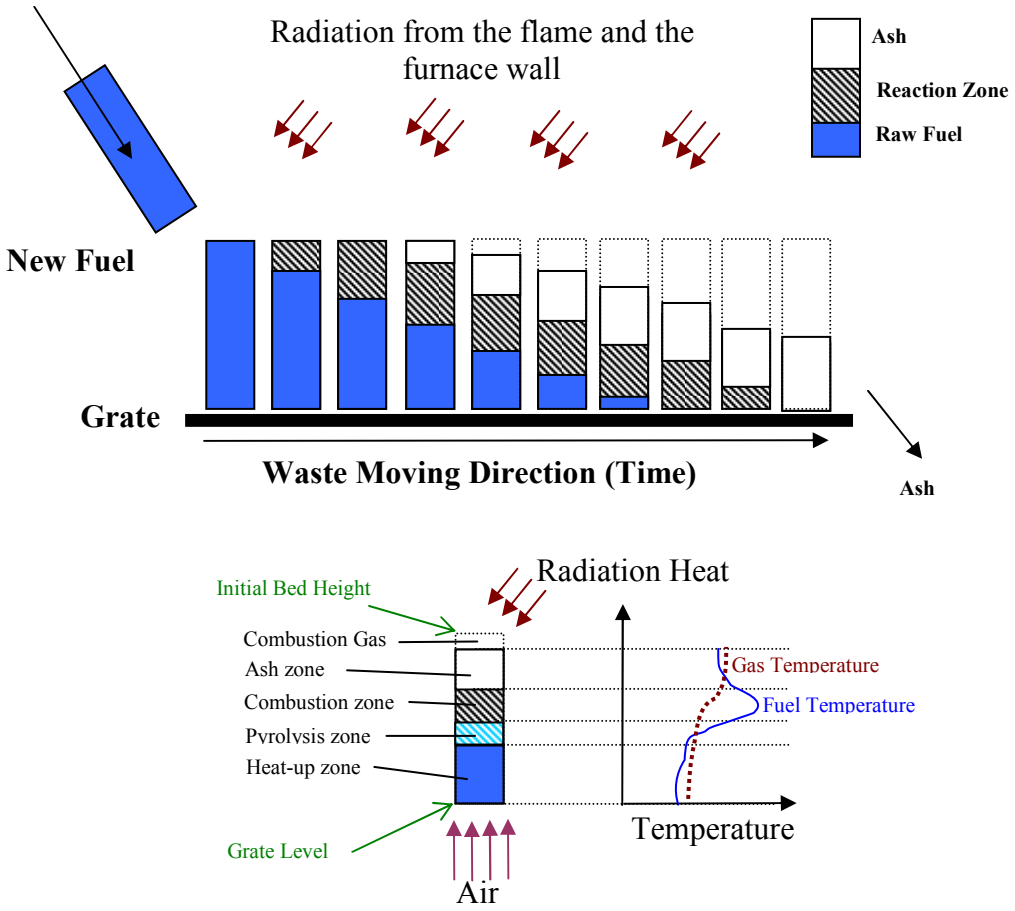


*Figure 2-3: Schematic view of the Combustion in a Solid Fuel Bed (Shin et el., 2000)*

An unsteady one-dimensional bed model was developed by Shin et al. (Shin et al 2000). This bed model consists of a waste shrinkage sub-model and a two-flux radiation sub-model shown in Figure 2-3. Because of heat transfer by radiation from the flame and furnace walls, the temperature on the surface of a MSW bed increases. This transport phenomenon was described in this model and compared with experimental results. The three stages of material conversion such as raw MSW, reacting zone, and ash in the bed were identified. This model results were

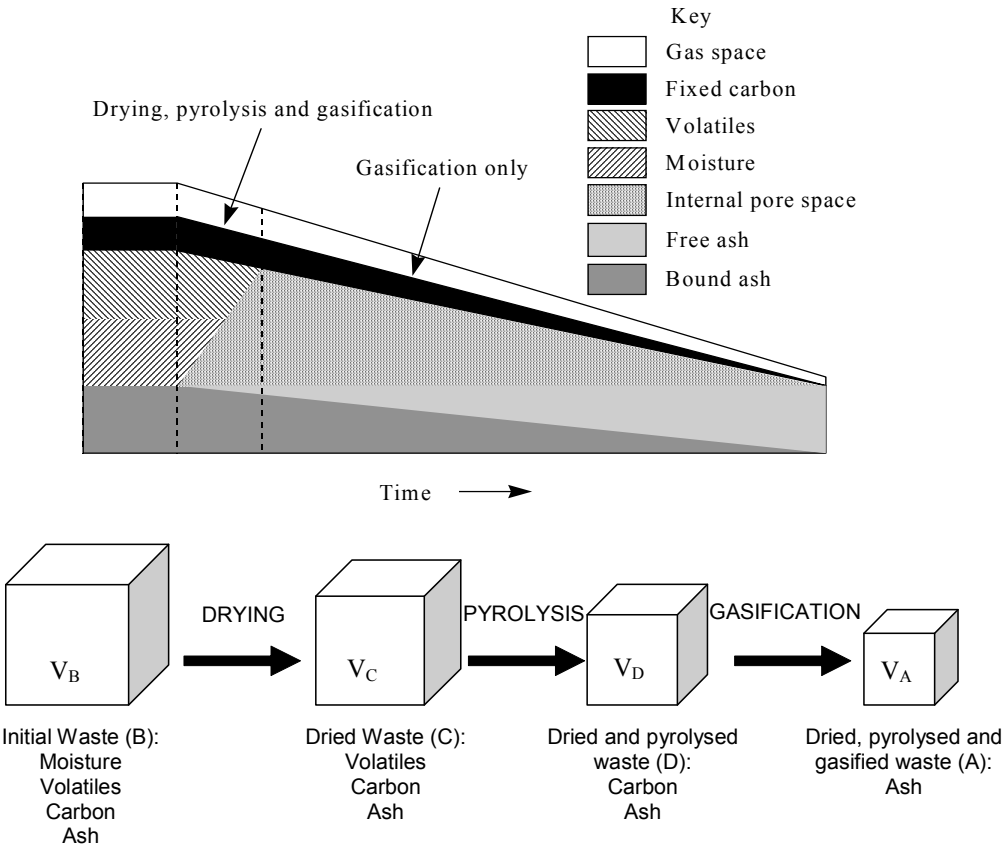


*Figure 2-4: The volume distribution of the various defined components in the bed (Yang et al. 1999, 2002)*

incorporated with a CFD model by Ryu et al. (Ryu et al. 2001).

Yang et al. (Yang et al. 1999, 2002) developed a comprehensive bed model called FLIC shown in Figure 2-4. This two-dimensional bed model was incorporated with various sub-process models and solved the governing equations for mass, momentum, and heat transfer for both gases and solids. FLIC includes several characteristics: Gaussian distribution of activation energies for waste devolatilization, mixing effect between volatile matter and oxidant in the volatile combustion rates, and the momentum equation for the gaseous phase. Validation of this bed model was achieved by means of a bench-top batch furnace used in this study. However, the sub-models are too detailed to determine some coefficients such as the central value and variation of waste activation energy. The FLIC simulation is mainly used by academic researchers when all parameters are known or assumed because MSW is a much more heterogeneous materials than any other material that scientists have ever studied.

Peters et al. (Peters 1994, Peters et al. 2005) present a model for the calculation of an unsteady, three-dimensional flow and combustion phenomena in a packed bed of a solid waste combustion chamber. As shown in Figure 2-5, this bed model simulated a bed comprised of wood particles that mechanically interacted with neighbor particles. On the bases of the results of this study, they developed a new

model for mixing MSW particles on a forward acting grate using the Discrete Element Method (DEM), but it did not include any combustion phenomena.

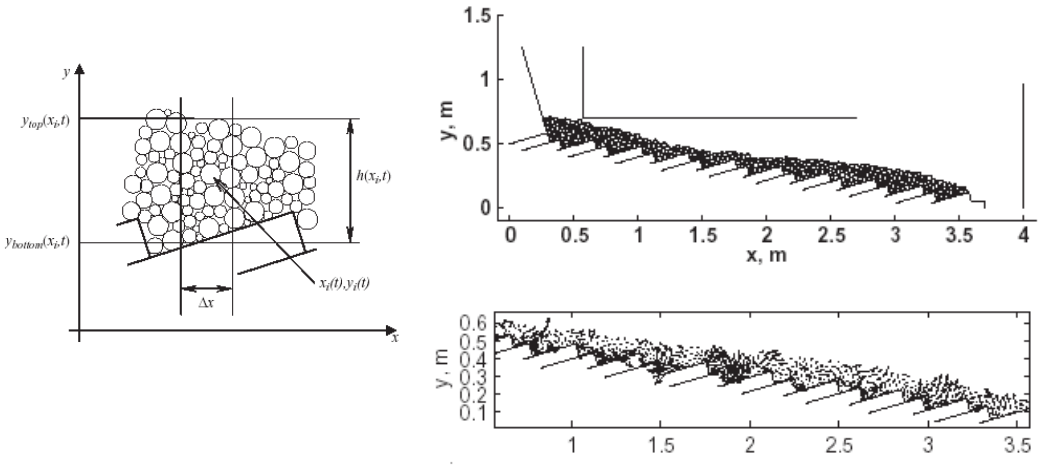


*Figure 2-5: The particle-based model using Discrete Element Method (Peters 1994, Peters et al. 2005)*

Other numerical bed models have been developed for simulating solid waste combustion processes (chemical reactions and mass/heat transfer). CUTEC-Institut has developed a dynamic model for optimizing MSW combustion (Reindorf et al). Wolf has simulated mixing phenomena on a reverse acting grate in waste combustion systems (Wolf, C., 2005). Empirical models have also been developed for training facility operators rather than for research or development. Program codes of them are much simpler than the codes of phenomenal models.

### 2-1-2. Chamber modeling (volatile combustion)

Chamber modeling that uses data computed by a bed model is used to investigate volatile matter combustion above the bed. Volatile matter combustion generated during the thermal conversion process of MSW bed is dependent on the flow and mixing of gases and air. The chemical reactions are carried out between volatile matter and secondary air injected by arrays of nozzles on the chamber walls. The flow of gas and air in the chamber results in turbulence and mixing, depending on temperatures, velocity, and secondary air distribution. In order to calculate these complicated phenomena in the combustion chamber, Computational Fluid Dynamics (CFD) is widely used for chamber modeling.

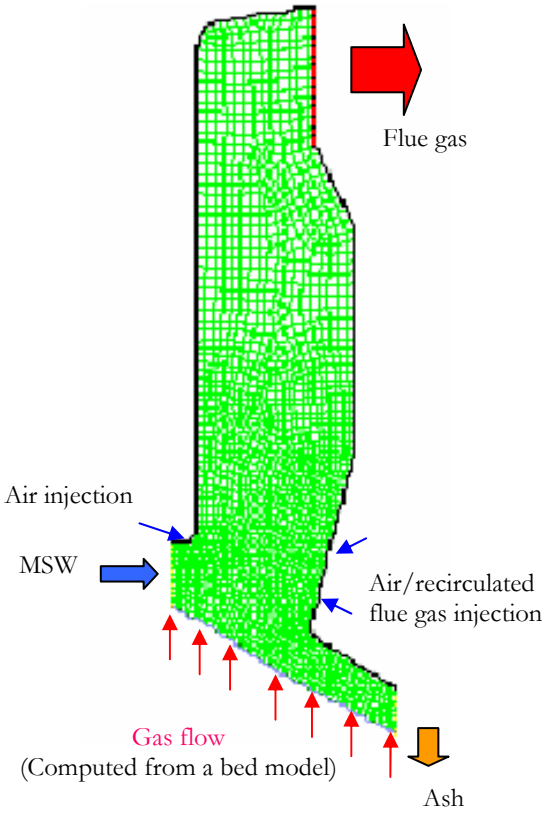


*Figure 2-10: A grid structure of CFD modeling (Nakamura et al.2002)*

Computational Fluid Dynamics (CFD) is concerned with obtaining numerical solutions to fluid flow problems by using the continuity equation (conservation of mass), the Navier-Stokes equation (conservation of momentum), and the energy conservation equations. CFD is one of

the best numerical tools for WTE engineers, and is used for geometric analysis of a new chamber design to calculate air and gas flows as well as for the chemical reactions of volatiles ($C_mH_n$) in the chamber. Figure 1-9 shows the grid structure used for Fluent CDF modeling of the WTE mass-burn combustion chamber in Union County Facility (Nakamura et al. 2002). Commercial CFD software packages such as CFX (ANSYS, Inc.) and Fluent (Fluent Inc.) usually need an additional program sub-code, since CFD does not consider solid waste combustion in a bed.

**2-2. Solids mixing theories**

Solids mixing is widely used in the manufacture of ceramics, glass, plastics, processed food, sand and fertilizers because mixing processes in these industries are necessary for controlling rates of mass and heat transfer and chemical reactions. Mixing processes can be classified in many ways based on the modes of solids flow mixing mechanisms that are involved. There are some types of mixing systems: free-flow systems and fluidized systems. Free-flow systems carry out a process of randomization of particles induced in mechanisms such as diffusion, confection, or both, depending on the type of mixer or traveling grate. Reverse acting grate, forward acting grate, and Roller grate in Mass-burn facilities can be categorized in free-flow mixing. Whereas, fluidized bed systems for MSW can be in fluidized systems that have several effects of bubbles: the fluidized bed is considered to comprise a discontinuous phase of bubbles and a continuous phase of gas and solids. In this

section (2-2), theories of mixing processes in free-flow systems, to which reverse acting grate belongs, have been explained.

Mixing in Free-flow system can be modeled by four types of models: a) diffusion model (Section 2-2-1), b) diffusion-convection model (Section 2-2-2), c) convection model (Section 2-2-3), and d) stochastic model (Section 2-2-4).

**2-2-1. Diffusion model**

Diffusion model for molecules is a possible mixing mechanism of solids. This mechanism is described by Fick's equation:

$$\frac{\partial c}{\partial t} = D_e \frac{\partial^2 c}{\partial x^2} \qquad \text{(Eq. 2-1)}$$

The mixing process can be well characterized by the diffusion model when the mean diameter of binary component particles is same. In order to describe movement of particles in the axial direction, the following equation was applied to the experimental data:

$$\frac{\partial p(x,n)}{\partial n} = D_a \frac{\partial^2 p(x,n)}{\partial x^2} \qquad \text{(Eq. 2-2)}$$

where $n$ is number of revolutions of the mixer, $p(x, n)$ is relative concentration of the particles which is described as follows:

$$p(x,n) = \frac{c(x,n)}{\int_0^L c(x,n)dx} \qquad \text{(Eq. 2-3)}$$

where $L$ is the length of mixer and $c(x, n)$ is particle concentration that is a function of distance and number of revolutions. The solution of Eq. 2-3 is obtained as

$$p(x,n \mid x_0,0) = \frac{1}{\sqrt{4\pi D_a n}} \exp\left[ -\frac{(x-x_0)^2}{4D_a n} \right] \qquad \text{(Eq. 2-4)}$$

where $x_0$ is the initial location of the tracer. This equation can be rewritten in the form of Gaussian distribution as

$$p(x,n \mid x_0,0) = \frac{1}{\sqrt{2\pi\sigma_x^2(n)}} \exp\left[ -\frac{(x-x_0)^2}{2\sigma_x^2(n)} \right] \qquad \text{(Eq. 2-5)}$$

Compared with Eq. 3-3, this equation has variance $\sigma_x^2(n)$ that related to the diffusivity $D_a$, through Einstein's equation, as

$$D_a = \frac{1}{2} \frac{d\sigma_x^2(n)}{dn} \left( \frac{L^2}{n} \right) \qquad \text{(Eq. 2-6)}$$

The diffusivity $D_a^*$ is obtained by

$$D_a^* = D_a N \qquad \text{(Eq. 2-7)}$$

where $N$ is the rotating speed of the mixer. The experimental data shows that the diffusion coefficients of the particles of different densities are larger than those of the particle of the same density.

**2-2-2. Diffusion-convection model**

Diffusion-convection model, as concisely shown in Chapter 1, is described by the diffusion equation (Eq. 1-22) with an additional term including drift velocity. Hwang and Hogg (Hwang and Hogg 1980) examined the mixing of powders flowing over a inclined surface in order to validate the diffusion-confection model. Under steady state conditions, Eq. 1-22 is simplified followings:

$$D_e \frac{\partial^2 c}{\partial x^2} = u \frac{\partial c}{\partial x} \qquad \text{(Eq. 2-8)}$$

Dispersion coefficient of particles, $D_e$, is dependent on shear in the flowing material. From their experiment results, the diffusion coefficient varies linearly with the velocity gradient:

$$D_e = D_e^* \left( 1 + L \frac{\partial u}{\partial y} \right) \qquad \text{(Eq. 2-9)}$$

$D^*$ is the "intrinsic" dispersion coefficient due to random oscillations or fluctuations of the individual particles during flow. The $L$ includes interparticle collisions enhanced by the velocity gradients. These parameters are dependent on the characteristics of the flowing powder and the flow system.

### 2-2-3. Convection model

A convection model is developed to represent convective mixing by a process of forming a striated mixture. This process is a repetitive series of division and recombination. The process of forming a striated RR-mixture (regular packing arrangement mixture with regular pattern), for example, shown in Figure 3-1. There are two striate of a rectangular block. The block is compressed to one-half of its original height, cut into halves, and recombined. Let $x_k^{(N)}$ denote average concentration of a component in cell $k$ ($k$ = 1,2,3,4) after $N$ cycles of the mixing operation. The average concentration distribution after N cycle is expressed by

$$x^{(N)} = P^{(N)} x^{(0)} = [P^{(1)}]^N x^{(0)} \qquad \text{(Eq. 2-10)}$$

where

$$x^{(N)} = \left[ x_1^{(N)} \quad x_2^{(N)} \quad x_3^{(N)} \quad x_4^{(N)} \right]^T \qquad \text{(Eq. 2-11)}$$

$$p^{(N)} = \begin{bmatrix} p_{11}^{(N)} & p_{12}^{(N)} & p_{13}^{(N)} & p_{14}^{(N)} \\ p_{21}^{(N)} & p_{22}^{(N)} & p_{23}^{(N)} & p_{24}^{(N)} \\ p_{31}^{(N)} & p_{32}^{(N)} & p_{33}^{(N)} & p_{34}^{(N)} \\ p_{41}^{(N)} & p_{42}^{(N)} & p_{43}^{(N)} & p_{44}^{(N)} \end{bmatrix} \quad \text{(Eq. 2-12)}$$

For the case shown in Figure 2-11,

$$p^{(1)} = \begin{bmatrix} 1/2 & 1/2 & 0 & 0 \\ 0 & 0 & 1/2 & 1/2 \\ 1/2 & 1/2 & 0 & 0 \\ 0 & 0 & 1/2 & 1/2 \end{bmatrix} \quad \text{(Eq. 2-13)}$$

$$x^{(0)} = \begin{bmatrix} 0 & 0 & 1 & 1 \end{bmatrix}^T \quad \text{(Eq. 2-14)}$$

Hence,

$$x^{(1)} = P^{(1)} x^{(0)} = \begin{bmatrix} 0 \\ 1 \\ 0 \\ 1 \end{bmatrix} \quad \text{(Eq. 2-15)}$$

$$x^{(2)} = [P^{(1)}]^2 x^{(0)} = \begin{bmatrix} 1/2 \\ 1/2 \\ 1/2 \\ 1/2 \end{bmatrix} \quad \text{(Eq. 2-16)}$$

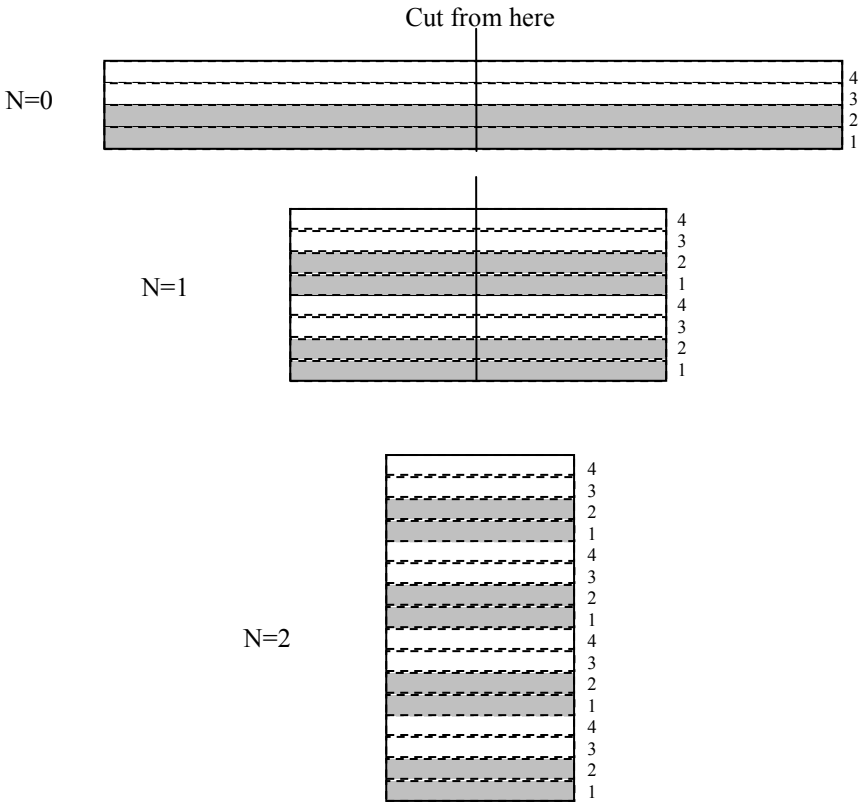


*Figure 2-11: Formation of a striated mixture (Lai et. al. 1978)*

This means that after two cycles, the average concentrations in all the cells becomes uniform.

### 2-2-4. Stochastic model

A non-stationary Markov chain model was applied to the mixing and segregation occurring within vibrated poly-dispersed particulate bed (Chou et. al. 1977). Boss and Dabrowska proposed a stochastic model for the mixing process, during discharge of particles from bins, of multi-component homogeneous solids

(Boss and Dabrowska 1985, 1985). The concentration distribution and the degree of mixing were calculated with the transition matrix in a Markov chain.

The advantages of the stochastic approach are a) that particle distributions and particle motilities can be studied simultaneously; b) the process of mixing can be examined in detail, c) particle movement simulation can be quickly carried out more than Newtonian approach based on the distinct element method (DEM) or particle element method (PEM). In the consideration of these advantages, stochastic approach, based on Markov chains, is chosen in this study (see Chapter 4) for simulating the process of MSW mixing.

## 2-3. Mass and volume reduction model

### 2-3-1. Progressive-Conversion Model (PCM)

Progressive-Conversion Model (PCM), also called Continuous-Reaction Model (CRM), is used when solid reactant is converted progressively throughout the solid particle. In this case the diffusion of gaseous reactant into the particle is rapid more than chemical reaction (Kunii and Levenspiel 1991).

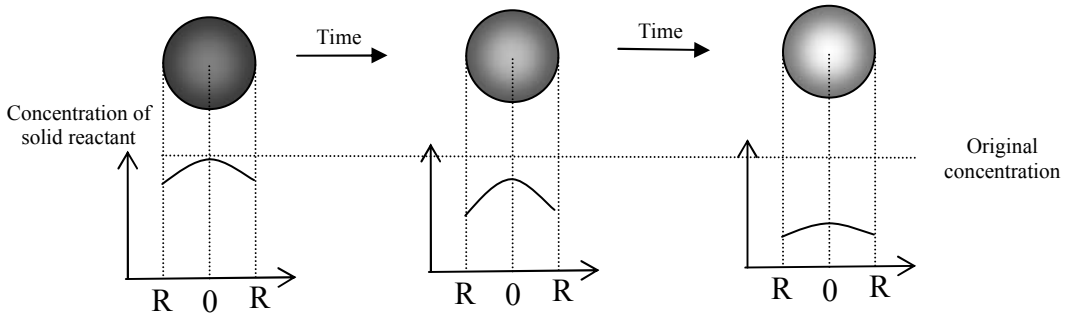


*Figure 2-12: Progressive-Conversion Model (Levenspiel 1999).*

### 3-3-2. Shrinking-Core Model (SCM)

Shrinking-Core Model (SCM), or Unreacted Core model, is used when the diffusion into the reactant particle is slow. The reaction occurs at the outer surface of the particle first. Thus, an unreacted core shrinks in size during reaction, as illustrated in Figure 2-13 (Levenspiel 1999).

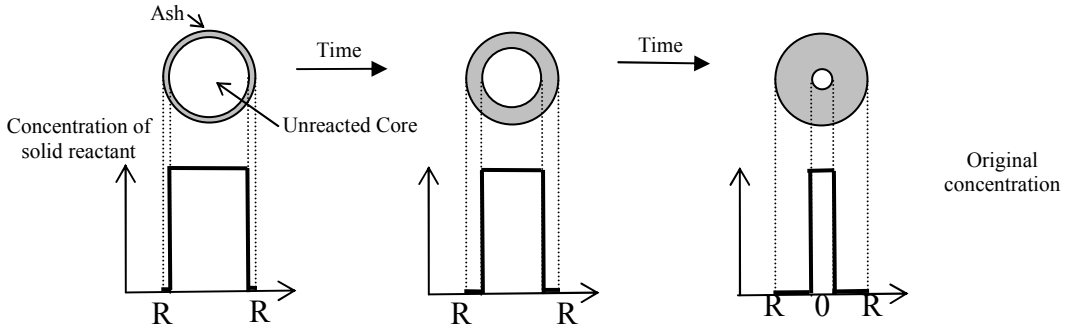


*Figure 2-13: Shrinking-Core Model (Levenspiel 1999).*

A gas contacts a solid particle, reacts with in the particle, and transforms it into product. This kind of heterogeneous reaction may be expressed by the following equation:

A (fluid) +bB (solid) → fluid and solid products. (Eq. 2-17)

In this heterogeneous reaction there are three steps: 1) Diffusion through gas film controls, 2) Diffusion through ash layer controls, 3) Chemical reaction control.

1) Diffusion through gas film controls

The rate of reaction of Eq. 2-17 is

$$dN_B = bdN_A \quad \text{(Eq. 2-18)}$$

Where $N_A$ and $N_B$ are amount of A and B respectively, b is stoichiometric coefficient for B. Thus,

$$-\frac{1}{S_{ex}}\frac{dN_B}{dt} = -\frac{b}{S_{ex}}\frac{dN_A}{dt} = bk_g(C_{Ag} - C_{As}) = bk_g C_{Ag} = const. \quad \text{(Eq. 2-19)}$$

$$S_{ex} = 4\pi R \quad \text{(Eq. 2-20)}$$

where $S_{ex}$ is unchanging exterior surface of a particle, $k_g$ is the mass transfer coefficient, $C_{Ag}$ is the concentration of gaseous reactant A, $C_{As}$ is the concentration of reactant A on the surface of the particle. $C_{As}$ = 0 because no gaseous reactant is present at the particle surface.

The decrease in radius of unreacted core is given by

$$-dN_B = \rho_B dV = \rho_B d\left(\frac{4}{3}\pi r_c^3\right) = -4\pi\rho_B r_c^2 dr_c \qquad \text{(Eq. 2-21)}$$

where $\rho_B$ is molar density of B in the solid and $V$ is the volume of the particle. From Eq. 2-19 and 2-21, the rate of reaction in terms of shrinking radius of unreacted core is given by

$$-\frac{1}{S_{ex}}\frac{dN_B}{dt} = -\frac{\rho_B r_c^2}{R}\frac{dr}{dt} = bk_g C_{Ag} \qquad \text{(Eq. 2-22)}$$

2) Diffusion through ash layer controls

Using the same idea of the gas film control, the rate of reaction is described followings:

$$-\frac{dN_B}{dt} = S_{ex}Q_A = 4\pi r^2 Q_A = 4\pi R^2 Q_{As} = 4\pi r_c^2 Q_{Ac} = const. \qquad \text{(Eq. 2-23)}$$

$$Q_A = D_e \frac{dC_A}{dr} \qquad \text{(Eq. 2-24)}$$

$$-\frac{dN_B}{dt}\int_R^{r_c}\frac{1}{r^2}dr = 4\pi D_e \int_{C_{Ag}=C_{As}}^{C_{Ac}=0} dC_A \qquad \text{(Eq. 2-25)}$$

$$-\frac{dN_A}{dt}\left(\frac{1}{r_c}-\frac{1}{R}\right) = 4\pi D_e C_{Ag} \qquad \text{(Eq. 2-26)}$$

3) Chemical reaction controls

The rate of reaction for the Eq. 2-18 is given by

$$-\frac{1}{S_{ex}}\frac{dN_B}{dt} = bk''C_{Ag} \qquad \text{(Eq. 2-27)}$$

where *k''* is the first-order rate constant for the surface reaction. Replacing Eq. 2-22 in Eq.2-28, the shrinking radius of core is given by

$$-\frac{1}{4\pi r_c^2}4\pi\rho_B r_c^2\frac{dr}{dt}\left(=-\rho_B\frac{dr_c}{dt}\right) = bk''C_{Ag} \qquad \text{(Eq. 2-28)}$$

Shrinking-Core Model (SCM) without ash formation: If a particle burns without ash formation such as pure carbon combustion in air, the shrinking particle will keep getting smaller and finally disappearing. Because there are no ash nor residue layers, the core of the particle is surrounded by gas film illustrated in Figure 2-14. In this case there are two control steps considered: 1) diffusion through gas film controls, and 2) chemical reaction control. The mechanism of chemical reaction controls of SCM without ash formation is the same as that of SCM with ash formation.

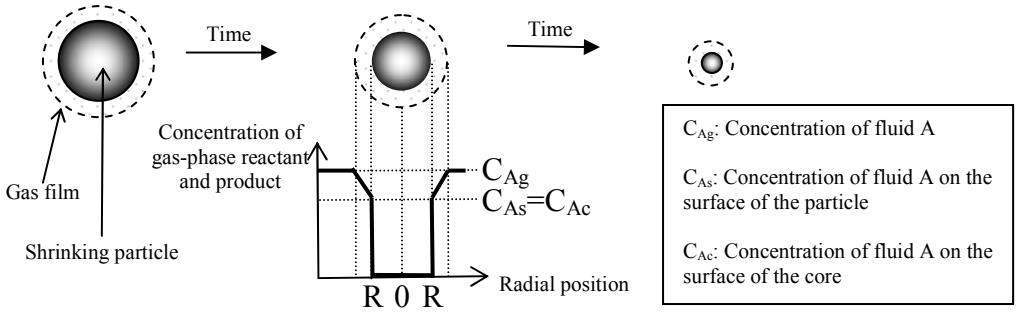


*Figure 2-14: Shrinking-Core Model without ash formation*

1) Diffusion through gas film controls: Mass transfer in a hot air steam to free-falling solids studied by Frossling (1938) gives

$$Sh = 2 + 0.552\,\mathrm{Re}_p^{0.5}\,Sc^{0.333} \qquad \text{(Eq. 2-29)}$$

$$Sh = \frac{k_d L}{D_{AB}} \qquad \text{(Eq. 2-30)}$$

$$\mathrm{Re} = \frac{Lu\rho}{\mu} \qquad \text{(Eq. 2-31)}$$

$$Sc = \frac{\mu}{\rho D_{AB}} \qquad \text{(Eq. 2-32)}$$

Study on mass transfer in order to determine the evaporation of water and benzene drops in air was carried out by Renz and Marshall. Their experimental results were expressed by the following equation:

$$Sh = 2 + 0.6\,\mathrm{Re}_p^{0.5}\,Sc^{0.333} \qquad \text{(Eq. 2-33)}$$

This equation is called the Renz-Marshall equation for mass transfer to spherical particles.

$$k_g \sim \frac{1}{d_p} \qquad \text{(Eq. 3-34)}$$

$$k_g \sim \frac{u^{1/2}}{d_p^{1/2}} \qquad \text{(Eq. 3-35)}$$

Eq. 3-35 expresses particles in the Stokes law regime.

**2-4. Heat transfer through the bed**

All processes in the thermal conversion of backed bed of MSW are governed largely by mass and heat transfer. The MSW bed is an aggregation of particles shown in Figure 2-15. In this section heat transfer, (radiation, convection, and conduction) of a single particle has been described.

As a first step of modeling, heat and mass transfer of the MSW bed is calculated using FLIC (see Figure A-1 in Appendix A). For calculation of volatile combustion CFD modeling is used (see Figure B-2, B-3, and B-4 in Appendix B).

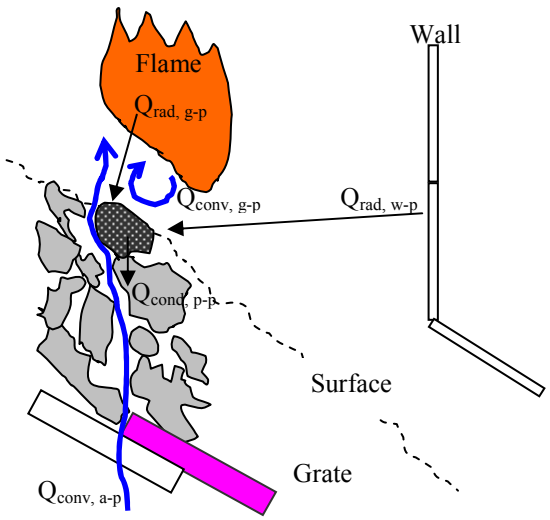


*Figure 2-15: Combustion and transport phenomena of one particle in a MSW*

### 2-4-1. Radiation among walls and particles

As shown in Figure 2-16, at high temperatures, a particle *i* emits a radiative flux and absorb a flux $\dot{q}_{rad,j}$ from all neighboring particles j. The total radiative flux a particle *i* emits is expressed as:

$$\dot{q}_{rad,p-p} = \sum_j F_{i\to j}\alpha\dot{q}_{rad,j} - \varepsilon\sigma\langle T_s\rangle^4 \qquad \text{(Eq. 2-36)}$$

where α and ε are absorption and the emission coefficient, respectively. The <*Ts*> is the surface temperature of a particle *i* that absorbs a flux $\dot{q}_{rad}$ from all neighboring particles *j* and a wall *j* with the view factor $F_{i\to j}$.

### 2-4-2. Radiation between a gas and a particle

The radiative flux a particle *i* emits is expressed as:

$$\dot{q}_{rad,p-g} = \varepsilon'_s \, \sigma(\varepsilon_g T_g{}^4 - \alpha_{g,s} \langle T_s \rangle^4) \qquad \text{(Eq. 2-37)}$$

where $\varepsilon'_s$ is the effective emissivity of MSW and approximated by

$$\varepsilon'_s = \frac{\varepsilon_s + 1}{2} \qquad \text{(Eq. 2-38)}$$

where $\varepsilon_s$ is surface emissivity. $\alpha_{g,s}$ is effective gas absorptivity.

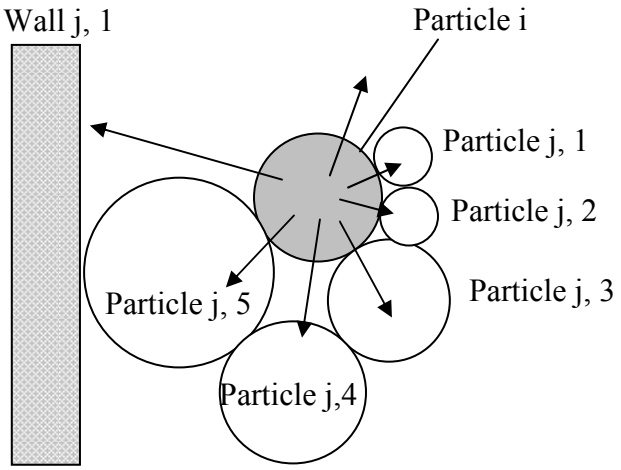


*Figure 2-16: Radiation from particle i to all neighboring particles j*

*Note: For radiation within the fluid phase and from combusting volatile matters will be calculated using CFD software. Fluent has several models for calculating volatile combustion with radiation. The radiative transfer equation (RTE) for an absorbing, emitting, and scattering medium is described as:*

$$\frac{dI}{dl} = -(K_a + K_s)I_b + K_a I_b + \left(\frac{K_s}{4\pi}\right)\int_0^{4\pi} I(\Omega)P(\theta,\phi)d\Omega \qquad \textit{(Eq. 2-39)}$$

*The radiation intensity I is a function of position and direction. The first term on the right-hand side of Eq. 2-36 is absorption and out-scattering loss. The second term shows emission of media. The third one is in-scattering. This integral-differential equation is the third term that is in integral form and should be reduced to differential form to simplify the solving problem.*

**2-4-3. Convection between a particle and the primary air though the bed**

Heat transfer by convection between the primary air and particles is expressed as:

$$\dot{q}_{conv} = h(T_g - T_s) \qquad \text{(Eq. 2-40)}$$

where $h$ is heat transfer coefficient. $T_s$ is the surface temperature of a particle and $T_g$ is the temperature of the primary air.

### 2-4-4. Conduction with two particles

The conductive heat flux between two neighboring particles in contact is estimated by

$$\dot{q}_{cond} = -\frac{1}{1/k_1 + 1/k_2}\frac{\partial T}{\partial r} \approx -\frac{1}{1/k_1 + 1/k_2}\frac{T_{S,1} - T_{S,2}}{\Delta r_{S,1} - \Delta r_{S,2}} \qquad \text{(Eq. 2-41)}$$

where $k_1$ and $k_2$ are conductivities of the two particles. The temperature gradient between two particles is approximated by the surface temperature difference over

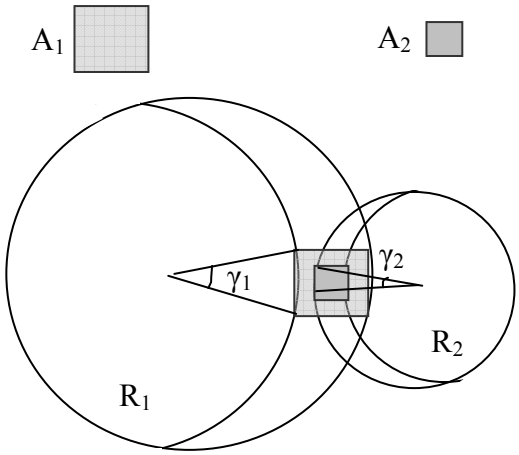


*Figure 2-17: Conduction between two neighboring particles (Peters, B. 2005)*

distance $\Delta r_{S,i}$ from outer particle surface. The contact area is assumed to be quadratic and determined by the contact angles $\gamma_1$ and $\gamma_2$ as shown in Figure 2-17.

**2-4-5. Equation describing mass and heat balance**

Governing Equation of the MSW bed: The governing equations for mass and heat are summarized as follows. For energy (heat) balance of the inside of a single particle,

$$\frac{\partial\left\langle \rho C_p T\right\rangle}{\partial t} = \frac{1}{r^2}\frac{\partial}{\partial r}(r^2 D\frac{\partial\left\langle T\right\rangle}{\partial r} - r^2\left\langle \vec{v}\rho_g C_{p,g} T\right\rangle) + \dot{\omega} \qquad \text{(Eq. 2-42)}$$

Energy balance of the outside of a single particle is describe as:

$$D\frac{\partial\left\langle T\right\rangle}{\partial r}\bigg|_R = \dot{q}_{conv} + \dot{q}_{rad} + \dot{q}_{cond} \qquad \text{(Eq. 2-43)}$$

where $\vec{v}$ is the gas velocity, ρ is the particle density $\rho_g$ is the gas density, $C_p$ and $C_{p,g}$ are the heat capacity of the particle and heat capacity of the gas, respectively. *D* is heat diffusivity and <T> is temperature of the particle surface.

Mass balance of the inside of a single particle:

$$\frac{\partial\left\langle c_i\right\rangle}{\partial t} = \frac{1}{r^2}\frac{\partial}{\partial r}(r^2 D_i\frac{\partial\left\langle c_i\right\rangle^i}{\partial r} - r^2\left\langle \vec{v}c_i\right\rangle) + \dot{\omega}_{ci} \qquad \text{(Eq. 2-44)}$$

Mass balance of the outside of a single particle:

$$-D_{i,eff}\left.\frac{\partial\left\langle c_{G,i}\right\rangle^{i}}{\partial r}\right|_{R}=\beta(\left\langle c_{G,i,R}\right\rangle^{i}-c_{\infty}) \qquad \text{(Eq. 2-45)}$$

where $\vec{v}$ is the gas velocity, $c_i$ is the concentration of component $i$, $\dot{\omega}_{ci}$ is the conversion rate of component $i$. $D_{i,eff}$ is the effective diffusivity of component $i$. $\beta$ is the mass transfer coefficient. $c_{\infty}$ stands for the ambient gas concentration.

Governing Equation of Gas: The governing equations of gas for mass, momentum, energy and species are summarized as follows:

Continuity:

$$\frac{\partial\rho_g}{\partial t}+\nabla\cdot(\rho_g\vec{v}_g)=S_g \qquad \text{(Eq. 2-46)}$$

where $\rho_g$ and $\vec{v}_g$ are the gas density and velocity at a position and time t, respectively. *Sg* includes mass transfer rates between the solid and the gaseous phase due to decomposition processes inside of the particle.

Momentum:

$$\frac{\partial(\rho_g\vec{v}_g)}{\partial t}+\nabla\cdot(\rho_g\vec{v}_g\vec{v}_g)=\nabla\cdot p_g+F(\vec{v}_g) \qquad \text{(Eq. 2-47)}$$

where $p_g$ is gas pressure. The function $F(\vec{v}_g)$ is defined by the following equation:

$$F(\vec{v}_g) = -\frac{\mu}{k}\vec{v}_g \qquad \text{if } Re < 10 \text{ (Darcy)} \qquad \text{(Eq. 2-48)}$$

$$F(\vec{v}_g) = -\frac{\mu}{k}\vec{v}_g - \rho_g C\vec{v}_g\left|\vec{v}_g\right| \qquad \text{if } Re > 10 \text{ (Forchheimer)} \qquad \text{(Eq. 2-49)}$$

where $k$ is the permeability and $K$ and $C$ are constants of the form:

$$K = \frac{d^2 P^3}{150 \cdot (1-P)^2} \qquad \text{(Eq. 2-50)}$$

$$C = \frac{1.75 \cdot (1-P)}{dP^3} \qquad \text{(Eq. 2-51)}$$

Species transport:

$$\frac{\partial(\rho_g Y_{i,g})}{\partial t} + \nabla \cdot (\rho_g \vec{v}_g Y_{i,g}) = S_{Y_{i,g}} + \dot{\omega}_{Y_{i,g}} \qquad \text{(Eq. 2-52)}$$

where $Y_{i,g}$ are mass fraction of $H_2O$, CO, $CO_2$, and $C_mH_n$. $S_{Y_{i,g}}$ is the source term including mass sources due to drying and devolatilization of particles released into the gas phase. $\dot{\omega}_{Y_{i,g}}$ is the gaseous conversion rate of a species $i$:

$$\dot{\omega}_{Y_{i,g}} = \min(\nu_{i,k}\tau_m Y_{i,k}, \sum \nu_{i,k} k_k \exp(\frac{E_{a,k}}{RT_g})) \quad \text{(Eq. 2-53)}$$

$$\tau_m = \frac{1}{t_m} = \frac{1}{C_m \sqrt{\frac{\nu L}{|\vec{v}^3|}}} \quad \text{(Eq. 2-54)}$$

where $t_m$ is mixing time scale, $C_m$ is an empirical constant, $L$ is a characteristic length, $\upsilon$ is the viscosity. $k$ indicates summation of all reactions for a species $i$.

Energy:

$$\frac{\partial(\rho_g e_{i,g})}{\partial t} + \nabla \cdot (\rho_g \vec{v}_g e_g) = \nabla \cdot (\lambda_g \nabla \cdot T_g) - \nabla \cdot \rho_g \vec{v}_g - F(\vec{v}_g)\vec{v}_g + \Gamma + \sum_k \dot{\omega}_{Y_{i,g}} H_{m,i} \quad \text{(Eq. 2-55)}$$

where $\Gamma$ is the heat from walls and the particles. $H_{m,i}$ is the heat generation due to chemical reactions. $\lambda_g$ is the thermal dispersion coefficient. $e_{i,g}$ is the specific internal energy equal to $C_v$

# Chapter 3: Experimental Work

## 3-1. Introduction

### 3-1-1. Study of particle size and shape

Methods of particle size measurement have been much studied particularly in powder technology. These methods are applicable to measurements of MSW particles. This section describes two kinds of particle size analysis: a) sieve analysis and b) image analysis.

#### a) Sieve analysis

The American Society for Testing and Materials (ASTM) provides several standard test methods for sieve analysis, such as C136-05: "Standard Test Method for Sieve Analysis of Fine and Coarse Aggregates" and E-389: "Test for Particle Size or Screen Analysis at No. 4 Sieve and Coarser for Metal Bearing Ores and Related

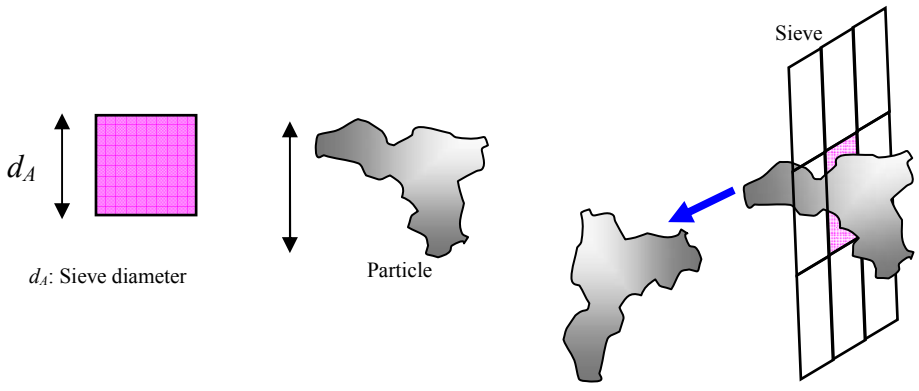


*Figure 3-1: Particle diameter and sieve size*

Materials." These sieve analysis methods have been adopted for MSW (Ruf 1972) in order to measure particle sizes and size distributions defining the sieve diameter ($d_A$) as the diameter of a particle that can pass though sieve size A (Figure 3-1).

**b) Image analysis**

In image analysis, the length, width, perimeter, and area of each particle are measured from digital camera images. An advantage of image analysis is that, it measures both size and shape of particle. It is used mainly for small particles of sands, powders, and grains such as coals, cements, and various chemical compounds. In this study, image analysis has been used because of the above advantage.

**3-1-2. Study of mixing and flow**

There have been two types of modeling of the flow of solids on a combustion grates: small-scale modeling of the full grate or a section of the grate. Lim *et al.* built 1/15-scale models of several grate systems and measured the mixing process due to the movement of the grate using small cubic particles (Lim *et al.* 2001). Figure 3-2 shows the model of the roller grate system and its residence time distribution in the direction of movement of the particles. At time 0 there was a narrow distribution of tracer particles close to the feed end of the grate. The distribution flattened out, that is, there was mixing of tracer particles with the rest, as the material flowed downward.

One of the advantages of small scale models is that they are less costly to build than full scale models, even though substitutional particles made of plastics,

ceramics, or woods must be used instead of real MSW particles. Beckmann and Scholz used clay, wood and ceramic spheres in their scale model of the reverse acting and forward acting grates (Beckmann and Scholz 2000).

On the other hand, section models can be used to reproduce parts of full grate system and examine the mixing process using real MSW particles. However, no one, except Yang et al (Yang et al 2005) has ever such as full scale tests for the study of solid waste mixing on the grate. They measured several mixing diffusion coefficients with different densities (see Table 5-2 in detail)

Because of the size limitation, “as-collected” MSW cannot be used in small-scale models. On the other hand, full-scale grate models have been less applicable for the purpose of solid waste mixing, because of difficulties in construction. However, full-scale models would allow investigating packed beds of real “black bag” MSW collected from local communities. This is an important consideration since “as-collected” MSW samples on a full-scale grate can represent similar geometries and actual combustion chamber conditions of commercial WTE plants. For these reasons, in this study, a full-scale section model of the WTE reverse acting grate was built and actual NYC-MSW particles were used in controlled tests of solids mixing in the section model.

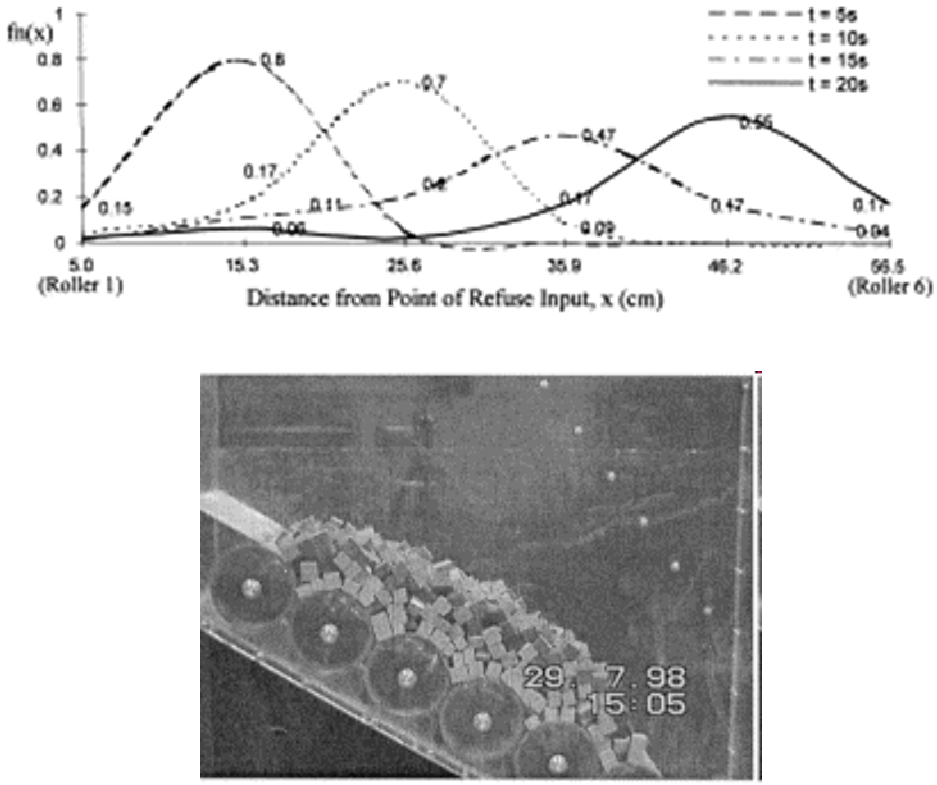


*Figure 3-2: Physical Scale Modeling (Lim et al. 2001).*

## 3-2. Measurement of particle size and Shape Factor (SF) distributions

### 3-2-1. Methodology

**a) Sample collection by field trip in New York City and by WTE facility visit**

Black bags were collected as typical MSW samples in residential areas of the five boroughs (Bronx, Brooklyn, Manhattan, Queens and Staten Island) of New York City. Based on the map shown in Figure 3-3, residential areas of five boroughs were picked as random, where per capita income is the same range. After several black

bags were collected in the five boroughs, 350 particles of MSW were randomly picked up from the black bags.

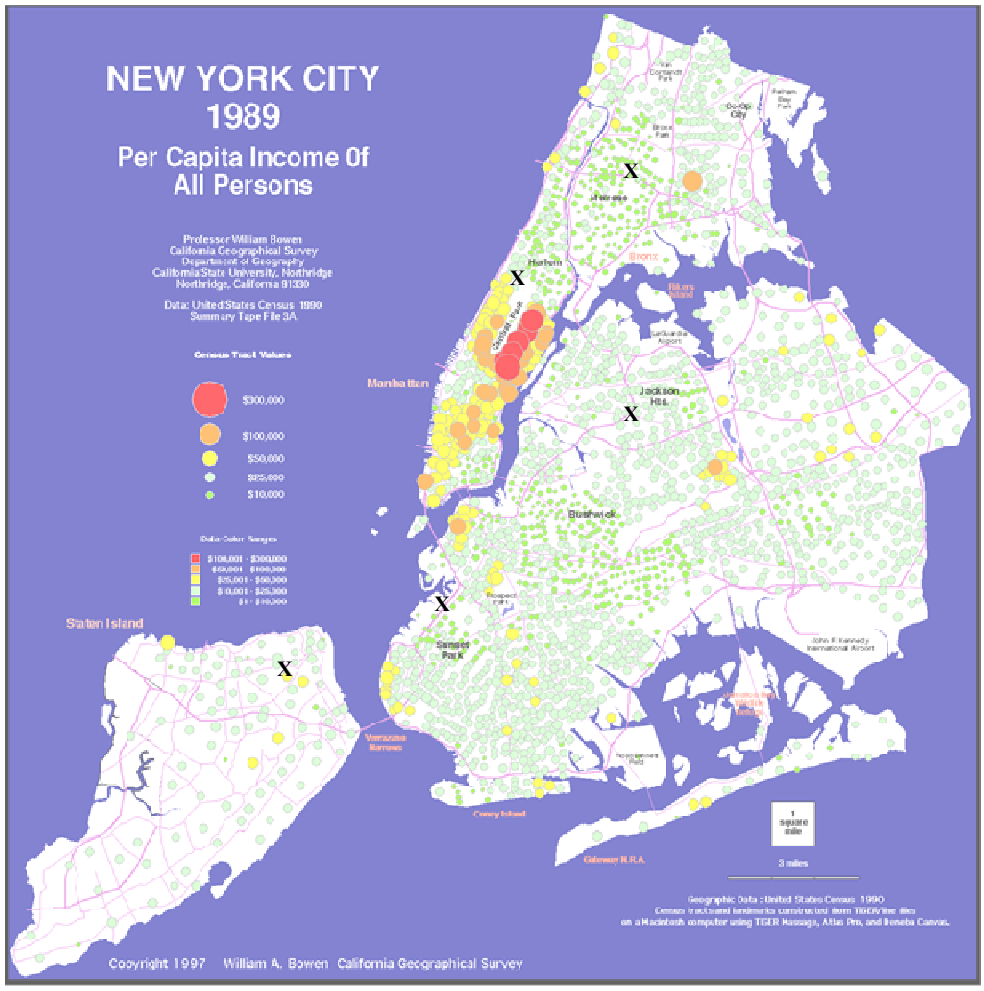


*Figure 3-3: New York City map with per capita income (Bowen 2004). X marks are the locations that black bags were collected*

Samples of combustion residues were randomly collected at the Union County WTE facility of Covanta Energy. Particles of combustion residues, or bottom ash particles, were collected after the bottom ash discharger. Hence, particles are

influenced by this process, such as cracked inside the discharger (water cools down + pressure of the ramp). The residues were sieved using a 1/2 inch (1.27 cm) screen to eliminate fine powder residues and 210 particles were selected.

**b) Sample measurement by image analysis**

Particles of the residue samples were also measured in terms of height, width, area and perimeter in this study. Size and surface area of each particle were measured using the image analyzer (digital camera: Sony PCG-C1VR/BP and software: Able Image Analyzer$^{TM}$ version 2.1) shown in Figure 3-4. There are two steps in image analysis: 1) capturing particle images from the digital camera with color inversion and 2) outlining the shapes of particles regarding length, width, perimeter, and area. Able Image Analyzer$^{TM}$ (Mu Labs 2004) is one of the powerful image analysis software packages and was used in order to measure particle sizes from captured image. It supports image analysis functions that include dimensional, gray scale and

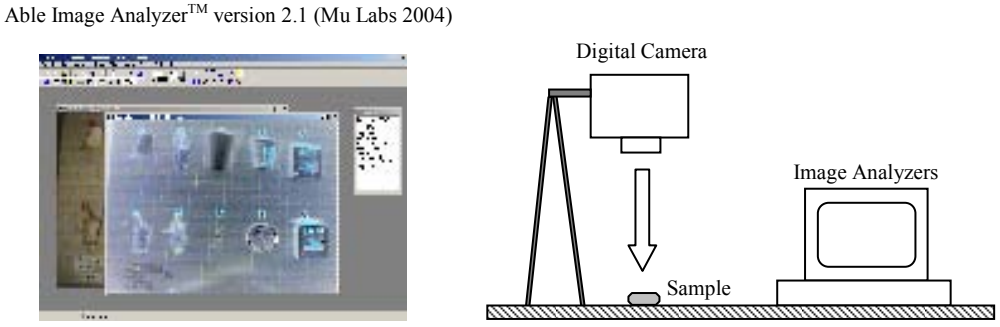


*Figure 3-4: The image analyzer system, outlining the shapes of particles regarding length, width, perimeter, and area*

24-bits color measurements: distance, area, angle, point, line, pixel profile, histogram etc. (from images or selections) with statistics that calculate basic statistics and frequencies. From the image analysis of MSW and ash particles, shape factors for MSW and ash particles were determined.

Cluster analysis was carried out using Clustan Graphics$^{TM}$ version 7.05 developed by Clustan Ltd. (Wishart 2004). This program can be used for a) calculating Tree diagram to investigate similarities of a group compared with other groups and b) drawing scatter plots (multidimensional scaling) to classify MSW and residue particles by shape factors, including aspect ratio, roundness, and spheresity.


*Figure 3-5: Digital camera images of MSW samples (left) and ash samples (right)*

### 3-2-2. Definitions of particle size and shape

Particle Size (diameter): There are many definitions of particle size. Table 3-1 shows various particle diameters. For example, the difference among the Feret, Martin, and Sieve diameters is illustrated in Figure 3-6 (Allen 1997).

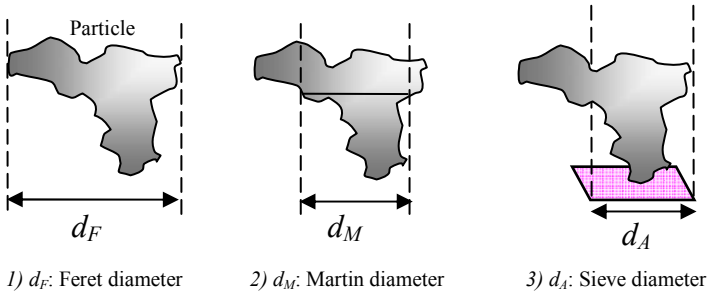


*Figure 3-6: Various types of diameters (Allen 1997)*

| Symbol | Name (diameter) | Definition | Formula |
|---|---|---|---|
| $d_v$ | Volume | Diameter of a sphere having the same volume as the particle | $V = \frac{\pi}{6} d_v^3$ |
| $d_s$ | Surface | Diameter of a sphere having the same surface as the particle | $S = \pi d_s^2$ |
| $d_{sv}$ | Surface-Volume | Diameter of a sphere having the same external surface to volume ratio as the particle | $d_{sv} = (d_v^3 / d_s^2)$ |
| $d_d$ | Drag | Diameter of a sphere having the same resistance to motion as the particle in a fluid of the same viscosity and the same velocity and at the same velocity ($d_d$ approaches $d_s$ when Re is small) | $F_d = 3\pi d_d \eta v$ |
| $d_f$ | Free-falling | Diameter of sphere having the same free – falling speed as a particle of the same density and viscosity | |
| $d_{St}$ | Stokes | Free-falling diameter in the laminar flow region | $d_{St} = \sqrt{(d_v^3 / d_s^2)}$ |
| $d_a$ | Projected area | Diameter of a circle having the same projected area as the particle in stable orientation | |
| $d_p$ | Projected area | Diameter of a circle having the same projected area as the particle in random orientation (mean value of $d_p = d_s$ for convex particles | |
| $d_c$ | Perimeter | Diameter of a circle having the same perimeter as the projected outline of the particle | $P = \pi d_c$ |
| $d_A$ | Sieve | Width of the minimum square aperture through which the particle will pass | |
| $d_F$ | Feret | The distance between pairs of parallel tangents to the projected outline of the particle in some fixed direction | |
| $d_M$ | Martin | Chord length, parallel to some fixed direction, which divides the particle projected outline into two equal areas | |
| $d_R$ | Unrolled | Chord length through the centroid of the particle outline | |

*Table 3-1: Various definitions of particle diameters (Allen 1997)*

Shape factors: The shape of particulate matters is mainly described by shape factors, aspect ratio (AR), roundness (circularity), and sphericity. Aspect Ratio (AR) is described as the following expression (Schneiderhohn 1954):

$$Aspect\ Ratio = \frac{length}{width} \quad \text{(Eq. 3-1)}$$

Roundness (Circularity shape factor) is defined as the following equation (Cox 1927):

$$Roundness = \frac{(perimeter)^2}{4\pi \cdot (surface\ area)} \quad \text{(Eq. 3-2)}$$

Sphericity is defined as the following equation (Wadell 1932):

$$\text{Sphericity } \Phi = \frac{\text{(surface area of a sphere of the same volume as the particle)}}{\text{(actual surface area of the particle)}}$$

(Eq. 3-3)

## 3-3. Physical Modeling

### 3-3-1. Methodology

#### a) Geometry of a physical model

The full-scale physical section model of the reverse acting grate used in this study had the dimensions of 121 cm (4 ft) in length, 91 cm (3 ft) in height, and 61 cm (2 ft) in width and the angle of bed declination to the horizontal was 15 degrees. Figure 3-7 shows the geometry of the full-scale section model. The MSW bed was divided into 16 cells (4 layers × 4 sections), each having a size of 20 × 20 cm. The four bars (2 fixed and 2 reciprocating) have a height of 13 cm and an angle of 15 degrees to the bed (also 45, 30, and 0 degrees can be selected. Martin grate has an angle of 26. Because of weight limitation, 14 degree was chosen in this test). The reciprocating bars traveled 42 cm from the top to the bottom positions, so that the horizontal distance ($42 \cos 14^o = 40.7cm$) was approximately the same as the length of two cells (40cm). Two digital cameras (model: Sony PCG-C1VR/BP and Sabrent SBT-WCCK), positioned above and on the side of the apparatus, were used to monitor the particle movement.

*Note: An ideal full-scale physical model for examining only the effect of grate motions should have an infinite length or, at least, the same length of real combustion chambers. A section model always encounters the limitation of the particle behavior. To minimize the effect of the boundary of the box, the first and last sections located close to the wall of the box were not fed in the stochastic model.*

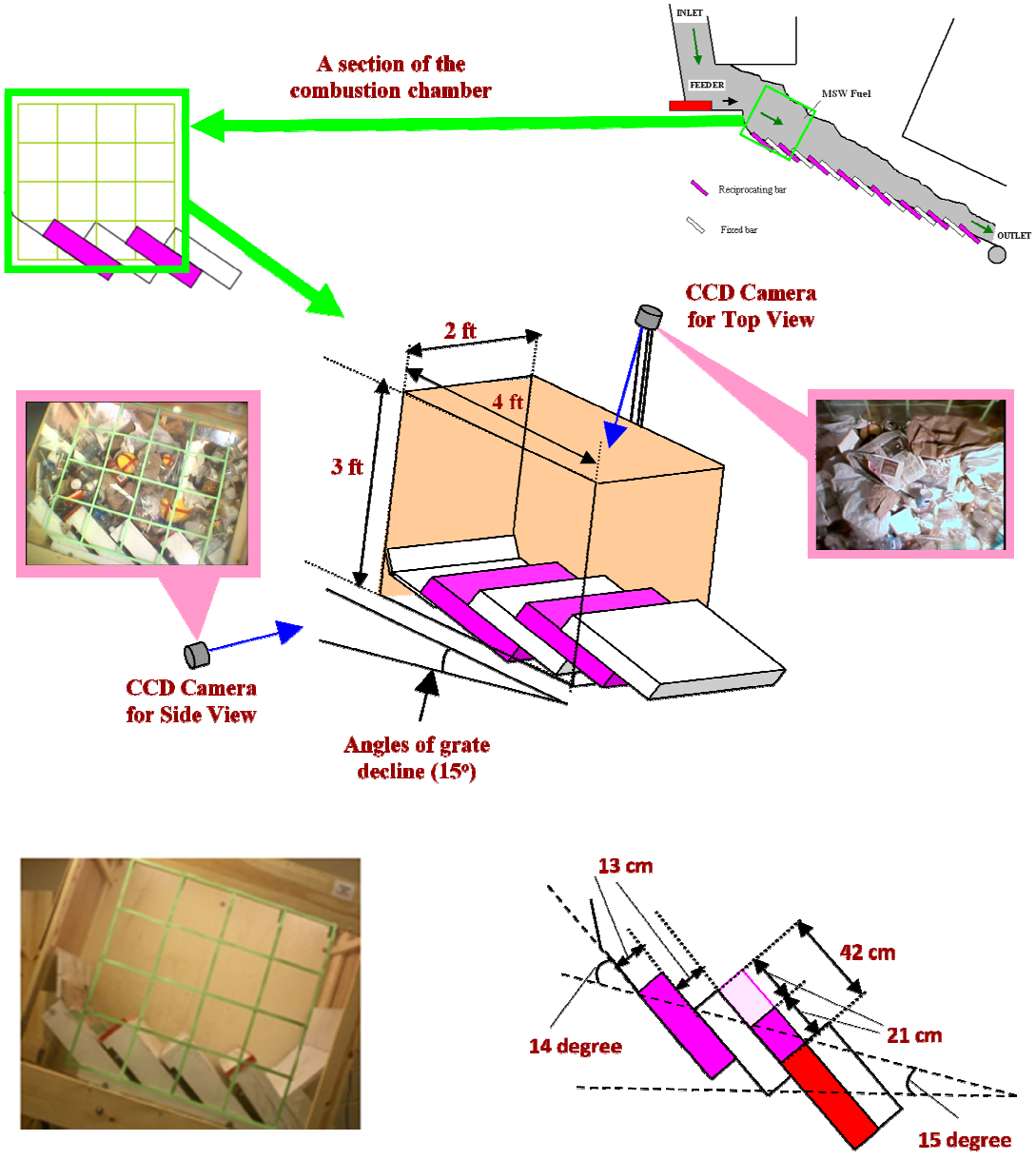


*Figure 3-7: Full-scale physical section model of a combustion chamber: positions of CCD cameras (top) and geometries of reverse acting grate (bottom)*

**b) Making tracers in different size**

Particle tracers were prepared as shown in Figure 3-8. Spherical tracers of small (6 cm), medium (14 cm), and large (22 cm) sizes were made using gap filling insulating foam. These tracers were based on the particle size distribution of NYC-MSW particles: the mean value μ of the size distribution was found to be 14 cm, where $\mu-\sigma \approx 5.8$ cm, and $\mu+\sigma \approx 22.8$ cm. The density of the tracers was 221 kg/m$^3$. This value was more representative of the precompacted MSW and is lower than the typical value of about 297 kg/m$^3$ (500 lb/yd$^3$) (Tchobanoglous 1993), as measured after compression during the collection process.

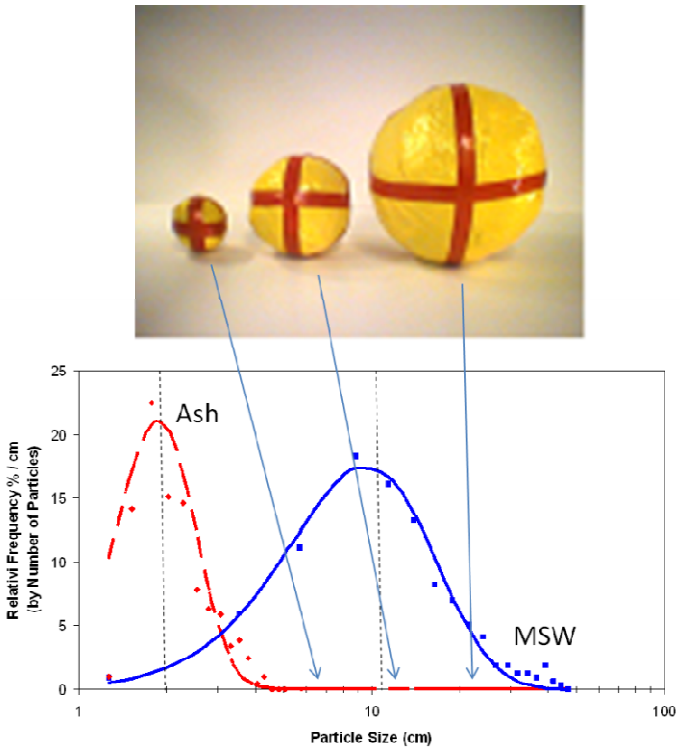

*Figure 3-8: Spherical tracers of different sizes (small 6cm, medium 14cm, large 22cm) (left) and NYC-MSW particle size distributions*


*Figure 3-9: Side views and top views of NYC-MSW beds with 20, 40, 60, and 80 cm heights and angles of chamber bed decline: 15 degree*

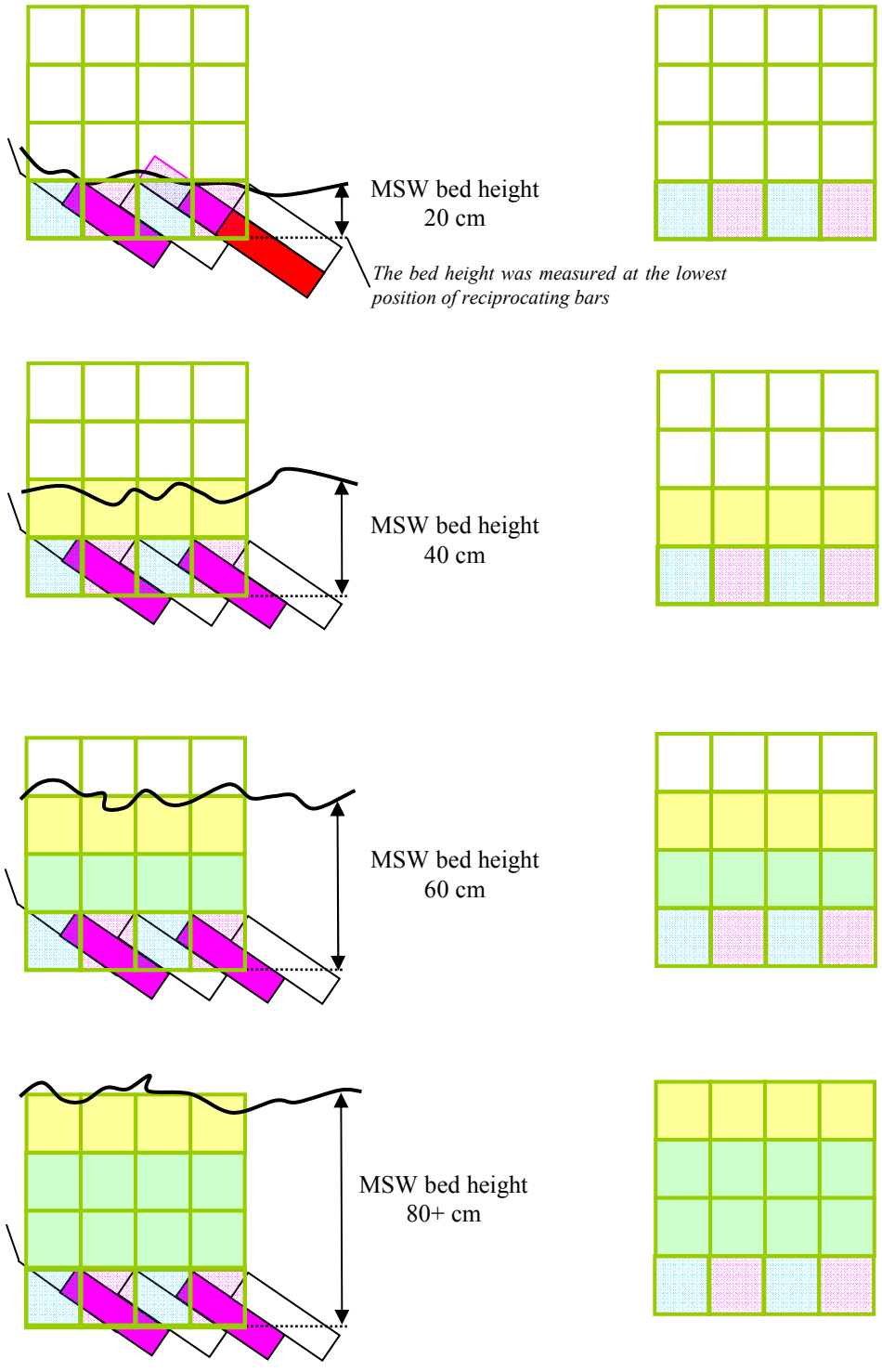


*Figure 3-10: Cell patterns of 20, 40, 60, 80 cm beds*

**c) Loading NYC-MSW particles**

The MSW particles used in the tests were obtained from black bags collected in NYC, as discussed in Section 3-2-1 a) (Figure 3-3). They were loaded into the physical model, along with tracers. Figure 3-9 shows pictures of side and top views that a NYC-MSW bed that was loaded in the full scale section model. The bed heights were 20, 40, 60, and 80 cm and the angle of camber grate declination was 15 degrees to the horizontal, as mentioned earlier. Figure 3-10 shows cell pattern of 20, 40, 60, 80 cm beds.

**d) Operation conditions**

Since this physical model was not motorized, the operation of reciprocating bars was conducted manually. This apparatus enabled the determination of the probabilities of particle movement in each vertical and horizontal position of the packed bed of actual NYC-MSW. After each reciprocation of the moving bars, the tracer positions were recorded by the cameras. Therefore, particles were traced from the original position to the current position after $n$ reciprocations. Because this physical model has neither an inlet nor a feeder, there is no MSW flow pushed into the chamber by means of a feeder. Therefore, a purely mixing phenomena characterization, caused by the reciprocating bars, was experimentally examined. In this “no-feeding” physical model, the motion of the reciprocating bars and gravity were the driving forces that caused the particles to move within the MSW packed bed.

# Chapter 4: Mathematical Work

## 4-1. Mass and volumetric flow of solids and air on the grate

### 4-1-1. MSW flow in the chamber

Unstable combustion of a MSW packed bed flows in a mass-burn chamber is one of the major problems caused by the variability of municipal solid waste (MSW). One reason for the instability of combustion is the extreme variability of the properties of the feedstock. MSW is more complex and non-homogeneous than any other fuel. The physical and chemical properties of MSW directly affect its combustion. Another reason for unstable combustion of MSW is transient phenomena such as the break-up of waste particles and the channeling of combustion air. The resulting unstable combustion of MSW introduces operating difficulties such as fluctuating chamber temperature, low thermal efficiency of the combustion chamber and formation of undesirable compounds (CO, $NO_x$, and dioxin) in the process gas of waste-to-energy facilities.

Some advanced automatic combustion control systems for mass-burn plants have been developed worldwide to stabilize the operating conditions during combustion. For example, Infrared Radiation (IR) sensors are provided in the advanced control systems for image processing and detection of burn out lines. In this system, an auto-regressive model with periodic functions (fuzzy logic) is used in chaos analysis for continuous variation of MSW in the control system. It provides

good control performance for reducing concentration of CO, $NO_x$ and dioxins in the combustion gases (Takatsudo et al. 1999).

Although these new tools have resulted in improved control and operating performance, the continuous variation of the MSW feed into the combustion chamber still makes control of the combustion process difficult. The existing combustion models for mass-burn MSW chambers have used mean values for physical and chemical properties of MSW components, such as proximate analysis and Lower Heating Value (LHV). In this study, a mathematical model for time series analysis of continuous variation of MSW was developed using the Monte Carlo method to simulate stochastic combustion. Additionally, the percolation theory is applied in order to simulate transient phenomena with the bed.

### 4-1-2. Monte Carlo Modeling for MSW feeding and flow

This study presents a time series model for continuous variation of MSW using the Monte Carlo Method. Table 4-1 shows percentages of MSW components and the approximate analysis of various types of combustible dry waste materials in New York City. They are used in this model as an initial distribution. The probability distribution of components of MSW for a uniform distribution $U_k \sim U$ (0, 1) is expressed by

$$X_k \sim \begin{pmatrix} \textit{Paper} & \textit{Cardboard} & \textit{Plastics} & \textit{Textiles} & \textit{Rubber \& Leather} & \textit{Wood} & \textit{Glass} & \textit{Metals} & \textit{Other} \\ 0.266 & 0.047 & 0.089 & 0.047 & 0.002 & 0.022 & 0.05 & 0.048 & 0.046 \end{pmatrix}.$$

(Eq. 4-1)

In order to carry out the computation for the components of MSW, the MATLAB 6 program was used to generate 100 random numbers ($k$ = 100) for each of 100 samples (n = 100).

| Component of waste stream | % in NYC | Weight (metric tons day) | Carbon (% by Weight) | Oxygen (% by Weight) | Nitrogen (% by Weight) | Sulfur (% by Weight) | Ash (% by Weight) |
|---|---|---|---|---|---|---|---|
| Paper | 26.6 | 3144 | 43.5 | 6 | 44 | 0.3 | 0.2 |
| Cardboard | 4.7 | 555 | 44 | 5.9 | 44.6 | 0.3 | 0.2 |
| Plastics | 8.9 | 1052 | 60 | 7.2 | 22.8 | - | - |
| Textiles | 4.7 | 555 | 55 | 6.6 | 31.2 | 4.6 | 0.2 |
| Rubber & Leather | 0.2 | 24 | 69 | 9 | 5.8 | 6 | 0.2 |
| Wood | 2.2 | 260 | 49.5 | 6 | 42.7 | 0.2 | 0.1 |
| Glass | 5 | 591 | 0.5 | 0.1 | 0.4 | <0.1 | - |
| Metals | 4.8 | 567 | 4.5 | 0.6 | 4.3 | <0.1 | - |
| Other | 4.6 | 544 | 26.3 | 3 | 2 | 0.5 | 0.2 |
| Tons per day | | 7292 | 2865 | 372 | 2194 | 42 | 10 |

*Table 4-1 Ultimate analysis of dry stream municipal solid wastes in New York City (Themelis et.al 2002, Tchobanoglous et al. 1993)*

The FLIC two-dimensional bed program (Yang *et al*. 2002) developed by Sheffield University was used, in conjunction with our model for continuous variation of MSW, in order to simulate the combustion process. The FLIC program is used to calculate the fluid flow, heat transfer and combustion reactions in both gaseous and solid phases.

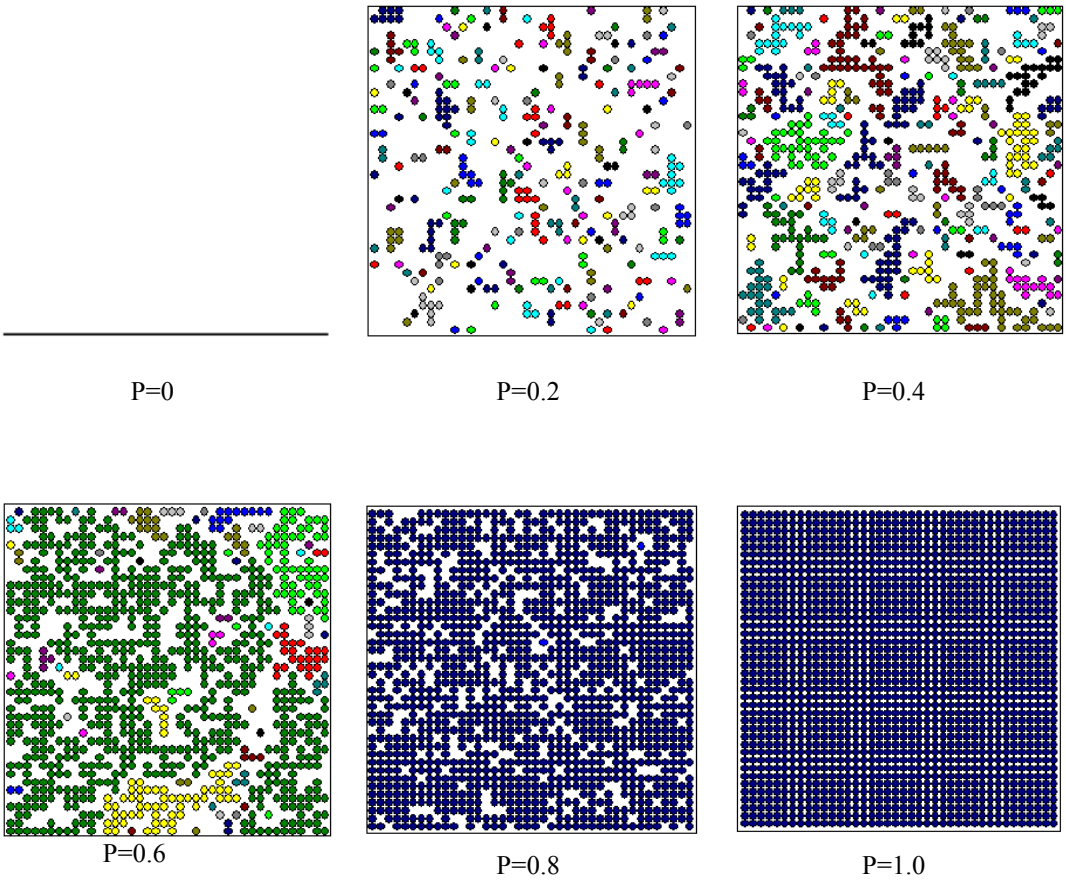


*Figure 4-1. Two-dimensional square lattice site percolation model used in the solid waste on the combustion grate*

Also a model for transient phenomena was developed in this study, based on the percolation theory. The first percolation model, by Broadbent and Hammersley (Broadbent and Hammersley 1957), was primarily concerned with the existence of the 'open path' in a system, in which a large porous stone is immersed in a bucket of water. It has been claimed that percolation theory is a cornerstone of the theory of disordered media, and provides a reasonable model for a disordered medium such as MSW. Although there are two types of percolations (*bond* percolation and *site* percolation), we considered site percolation for transient phenomena in combustion in

this study. There are a number of network models such as Honeycomb, Square, Kagome, Triangular, Diamond, Simple Cubic, BCC and FCC. A network of MSW on the traveling bed of combustion chamber is specified in the model as a two-dimensional square lattice (Figure 4-1) in order to simplify the combustion process. The lattice size L was defined as 40 (40 x 40) for the same reason. We designate each vertex of the lattice $\mathbb{Z}^2$ *open* with probability $p$ and *closed* otherwise. $p_c$ is the critical probability and is defined by

$$p_c = \sup \{p : \quad (p) = 0\} \qquad \text{(Eq.4-2)}$$

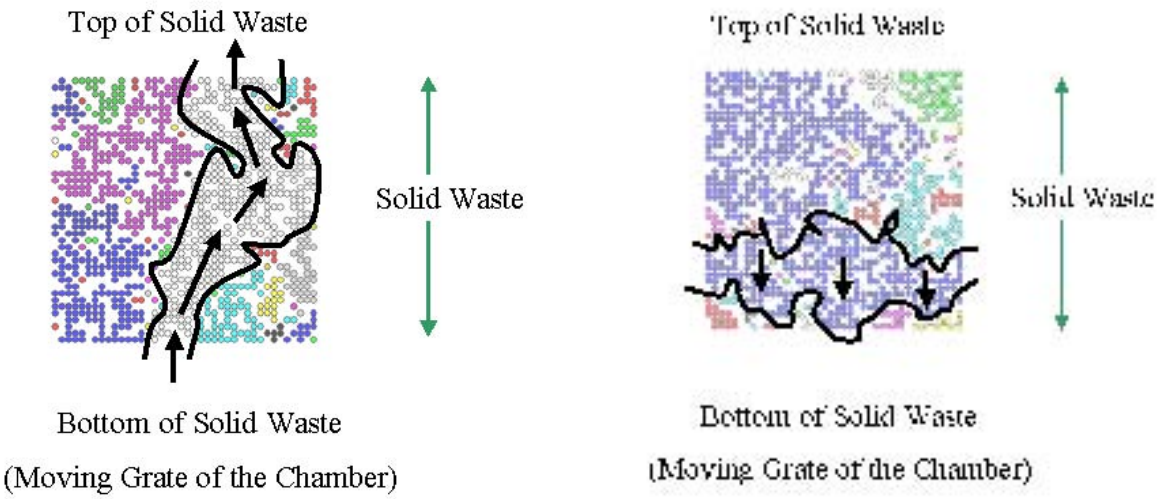


*(a) Channeling* *(b) Break-up (Subsidence)*

*Figure 4-2: Channeling and break-up of MSW bed in the percolation model on the grate*

The current estimate of this critical probability $p_c$ for site percolation in the two-dimensional square lattice is 0.5927 (Grimmett 1991). We assume that

combustion in the lattice proceeds uniformly. The program code for this model was developed using Visual Basic. Figure 4-2 shows the channeling and break-up of MSW on the combustion grate. Channeling usually occurs when particles of solid waste combust and create an empty space vertically through the bed as shown in Figure 4-2 (a). This means at least one cluster reaches both vertical edges of the lattice. Break-up, on the other hand, usually occurs when particles in the middle of the solid waste combust and create a space horizontally as shown in Figure 4-2 (b). This means that at least one cluster reaches both horizontal edges of the lattice in the percolation model.

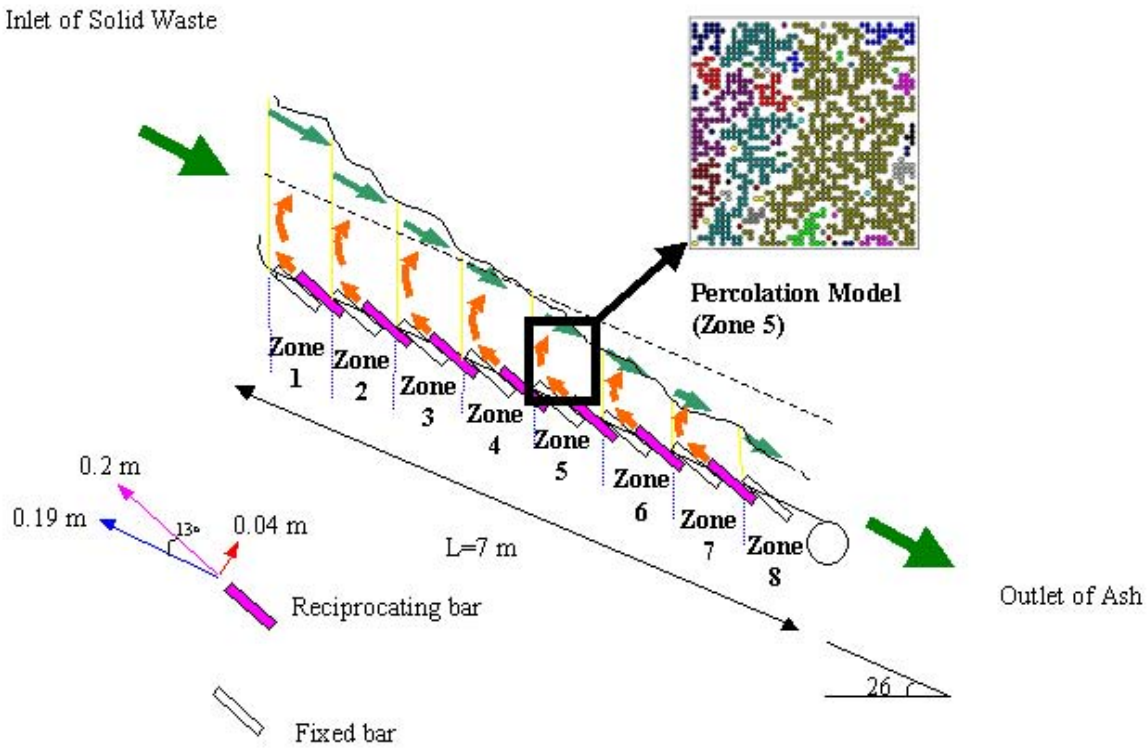


*Figure 4-3: Percolation Model in the combustion chamber*

In our model, we specified the use of the Martin reverse acting grate (Figure 4-3), one of the most popular WTE grates used in the United States. The MSW fed on this grate travels approximately 7.0 m in an hour. We divided the grate into 8 zones, through which MSW runs continuously. Mixing coefficients were assumed to be zero in order to simplify motion of the solid waste. The simulations were performed on a Linux computer (CPU: 1.8MHz, Memory: 256MB) with VMware for Windows 98 environment. It takes approximately two hours to complete one set of the calculations for this model.

**4-2. Stochastic model for MSW particles mixing on the traveling grate**

Simulation of the physical and chemical processes in moving beds is used widely to study combustion and other chemical reaction phenomena in gas-solid systems. Three general types of mathematical models are used for investigating the transport and chemical reaction phenomena in mass burn combustion chambers: Computational Fluid Dynamics (CFD), bed models, and stochastic models. CFD models simulate the fluid flow, heat and mass transfer, and reaction phenomena in the combustion chamber above the traveling grate by solving numerically the continuity and energy conservation equations and the Navier-Stokes equations (conservation of momentum). Numerical bed models of solid waste combustion have been developed since the early 1970s (Essenhigh, R. H. and Kuo, T. J. 1970). Yang, et al. (Yang. et al. 2002) developed a two-dimensional program, called the Fluid Dynamic Incinerator

Code (FLIC). FLIC is graphically interactive and is widely used by WTE engineers to simulate the physical and chemical transformations involved in the drying, volatilization and combustion processes on the grate; however, the combustion process is modeled using typical or average data such as composition, particle size, density and heating value, even though MSW is a very non-homogeneous fuel. Stochastic models, such as the one described in this paper are relatively new, although some researchers have suggested combining mixing models of the traveling bed with experimental work (Lim et al. 2001). Markov chain models have been used in the past to estimate mixing of powders in hoppers (Aoun-Habbache *et al.* 2002) and mixing in fluidized bed reactors. The present study is the first to apply the Markov chain model to the grate of a mass-burn chamber model in order to determine how solid particles move and mix on a moving grate.

**4-2-1. One-dimensional Stochastic model for reverse acting grate**

A model, based on the Markov chain model (Bremaud 1991), was developed to simulate particle flow and degree of mixing as the MSW particles travel over the grate. The first procedural step in the design of the Markov chain model was to divide the solid waste on the bed into several cells ("state" of the system). Then, the transition of particles between these cells with time is examined. In the model, the entire grate was represented by 16 cells and by their respective boundary conditions (Figure 4-4). The computed data were compiled in the form of a transition matrix ***P***

and a state vector ***S(n)*** that describes the particle distribution over the states after *n* transitions.

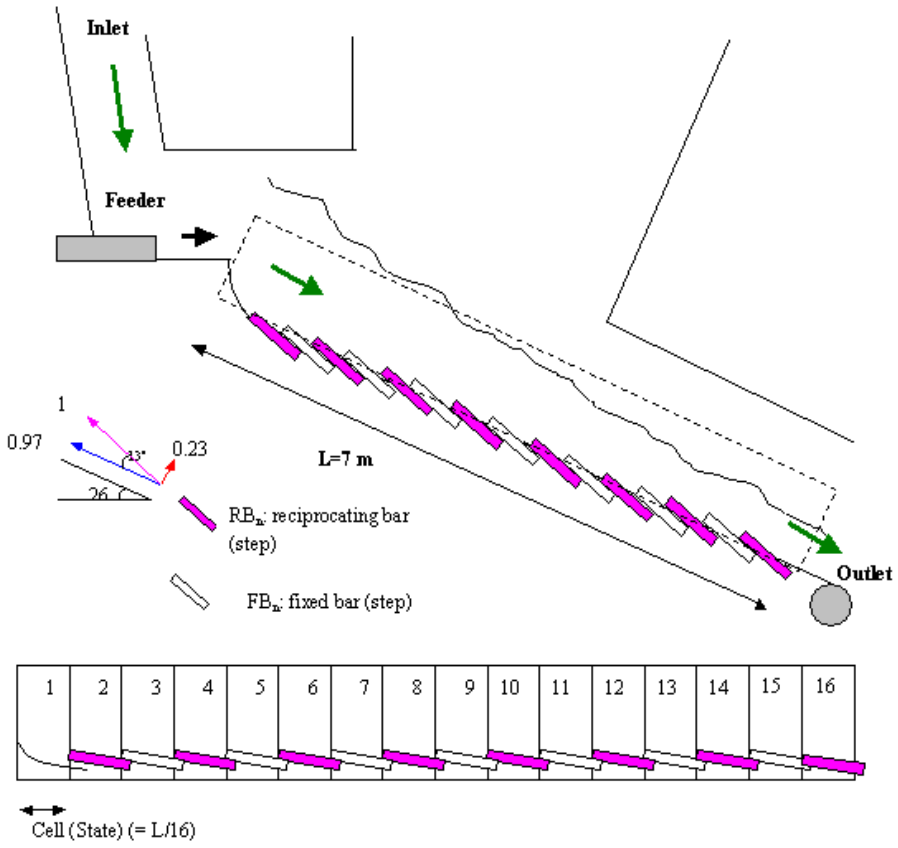


*Figure 4-4: Illustration of the spatial disposition of cells on the reverse acting grate: Each cell represents either the reciprocating bar or the fixed bar.*

The interchange of particles between successive cells ("Transition graph") is illustrated in Figure 4-5.

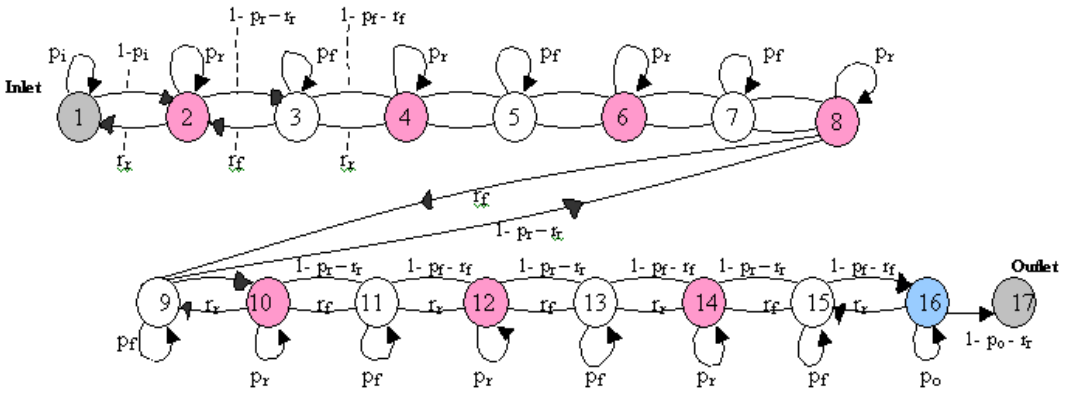


*Figure 4-5: Interchange of particles between successive cells (transition graph): The final cell of this model is cell 17(ash bin); all particles in the MSW feed after combustion eventually arrive at cell 17, although the paths of individual particles differ considerably.*

The Markov chain model assumes that, at each motion of the reciprocating bars (transition), the transition probabilities of the waste particles between adjacent cells do not depend on the previous state in time. The rule governing the particle migration (travel) of the system is expressed by the following equation:

$$\boldsymbol{S}(n) = \boldsymbol{S}(0)\,\boldsymbol{P}^{n} \qquad \text{(Eq. 4-3)}$$

where ***S(n)*** represents the profile of MSW traveling on the chamber bed after n times of double strokes of the reciprocating bars and ***S(0)*** is the initial profile of MSW feed at the inlet (prior to any stroke of the reciprocating bars, i.e., $n=0$); $\boldsymbol{P}^{n}$ is the $n$th power of $\boldsymbol{P}$ (called the n-step transition matrix) of the matrix that contains the probabilities of the solid particle movement. The latter is controlled by feed rate,

particle size and density, geometry of the grate and frequency of reciprocating bars. The transition matrix ***P*** for the movement of the solid waste particles corresponding to the series of cells shown in Figure 4-5 is defined as follows:

$$
\mathrm{P} = \begin{pmatrix}
p_i & 1-p_i & 0 & 0 & 0 & 0 & 0 & 0 & 0 & 0 & 0 & 0 & 0 & 0 & 0 & 0 & 0 \\
r_r & p_r & 1-p_r-r_r & 0 & 0 & 0 & 0 & 0 & 0 & 0 & 0 & 0 & 0 & 0 & 0 & 0 & 0 \\
0 & r_f & p_f & 1-p_f-r_f & 0 & 0 & 0 & 0 & 0 & 0 & 0 & 0 & 0 & 0 & 0 & 0 & 0 \\
0 & 0 & r_r & p_r & 1-p_r-r_r & 0 & 0 & 0 & 0 & 0 & 0 & 0 & 0 & 0 & 0 & 0 & 0 \\
0 & 0 & 0 & .. & .. & .. & 0 & 0 & 0 & 0 & 0 & 0 & 0 & 0 & 0 & 0 & 0 \\
0 & 0 & 0 & 0 & .. & .. & .. & 0 & 0 & 0 & 0 & 0 & 0 & 0 & 0 & 0 & 0 \\
0 & 0 & 0 & 0 & 0 & .. & .. & .. & 0 & 0 & 0 & 0 & 0 & 0 & 0 & 0 & 0 \\
0 & 0 & 0 & 0 & 0 & 0 & .. & .. & .. & 0 & 0 & 0 & 0 & 0 & 0 & 0 & 0 \\
0 & 0 & 0 & 0 & 0 & 0 & 0 & .. & .. & .. & 0 & 0 & 0 & 0 & 0 & 0 & 0 \\
0 & 0 & 0 & 0 & 0 & 0 & 0 & 0 & .. & .. & .. & 0 & 0 & 0 & 0 & 0 & 0 \\
0 & 0 & 0 & 0 & 0 & 0 & 0 & 0 & 0 & .. & .. & .. & 0 & 0 & 0 & 0 & 0 \\
0 & 0 & 0 & 0 & 0 & 0 & 0 & 0 & 0 & 0 & .. & .. & .. & 0 & 0 & 0 & 0 \\
0 & 0 & 0 & 0 & 0 & 0 & 0 & 0 & 0 & 0 & 0 & .. & .. & .. & 0 & 0 & 0 \\
0 & 0 & 0 & 0 & 0 & 0 & 0 & 0 & 0 & 0 & 0 & 0 & .. & .. & .. & 0 & 0 \\
0 & 0 & 0 & 0 & 0 & 0 & 0 & 0 & 0 & 0 & 0 & 0 & 0 & r_f & p_f & 1-p_f-r_f & 0 \\
0 & 0 & 0 & 0 & 0 & 0 & 0 & 0 & 0 & 0 & 0 & 0 & 0 & r_r & p_o & 1-p_o-r_r \\
0 & 0 & 0 & 0 & 0 & 0 & 0 & 0 & 0 & 0 & 0 & 0 & 0 & 0 & 0 & 1
\end{pmatrix}
$$

(Eq. 4-4)

where p is the probability that MSW particles will remain at the same grate position (cell) and r the probability that the particles transit the next grate position (cell). The subscripts f and r in the following expressions represent fixed bars and reciprocating bars, respectively; the subscripts i and o represent inlet and outlet, respectively.

The movement of the reciprocating bars causes an upward motion of the solid waste particles against the downward direction of the feed. Thus, there is a transition from position/cell $k$ ($k$ is the cell number and is a positive integer, $1 < k < 16$) to the two adjacent compartments $k$ - 1 and $k$ + 1 (Figure 4-5). If $k$ is an even number (i.e.. cells #2, 4, 6, 8, 10,…, 14), cell $k$ represents a reciprocating bar. If $k$ is an odd number (i.e., cells #3, 5, 7, 9, …, 15), cell $k$ represents a fixed bar. In order to simulate the mixing phenomena on the actual grate, six probabilities are defined at each cell:

- The probability $p_i$ of particle remaining in state 1 (cell #1).

- The probability $p_r$ of particle remaining on one of the reciprocating bars (cell #2, 4, 6, ….14).

- The probability $r_r$ of transiting to a reciprocating bar (cell #2, 4, 6, ….,14).

- The probability $p_f$ of remaining on a fixed bar (cell #3, 5, ….,15).

- The probability $r_f$ of transiting to a fixed bar (cell #3, 5, ….,15).

- The probability $p_o$ of remaining in outlet state (cell #16)

It should be noted that the probabilities p and r are always positive fractions and the sum of the elements within each row in the matrix $\boldsymbol{P}$ equals one. The values of p and r depend on the feed rate $R_{f,}$, particle size of MSW components S, particle density of MSW components S, state of combustion, frequency of reciprocating bars $R_r$, the length of the reciprocating bars travel L, angle α of chamber bed decline, the

height H and the angle θ of the reciprocating bars. The relationships between probabilities and operating parameters can be expressed as follows:

- For the reciprocating bars (cells #2, 4, 6,….,14),

$$p_r \sim f_r (R_f, S, \rho, R_r, L, \alpha, H, \theta) \quad \text{(Eq. 4-5)}$$

$$r_r \sim g_r (R_f, S, \rho, R_r, L, \alpha, H, \theta) \quad \text{(Eq. 4-6)}$$

$$p_r + r_r < 1 \quad \text{(Eq. 4-7)}$$

and for the fixed bars (cells #3, 5, ….,15),

$$p_f \sim f_f (R_f, S, \rho, R_r, L, \alpha, H, \theta) \quad \text{(Eq. 4-8)}$$

$$r_f \sim g_f (R_f, S, \rho, R_r, L, \alpha, H, \theta) \quad \text{(Eq. 4-9)}$$

$$p_f + r_f < 1 \quad \text{(Eq. 4-10)}$$

The relationships between probabilities are:

- For cell #1, solid waste particles are disposed to move only downward to cell #2, because cell #1 is next to the inlet and new feed enters all the time pushing the older particles downward the grate. Therefore,

$$p_i < 1 - p_i \quad \text{(Eq. 4-11)}$$

- For cell #2 (also, cell #4, 6,…., 14), although the reciprocating bar moves up and down, particles that ride this bar have less chance for transition from cell #3 to

cell #2 and are disposed to remain in cell #3 (same as cells #5, 7, 9,….,15). Therefore,

$$r_r < 1- p_r - r_r < p_r \qquad \text{(Eq. 4-12)}$$

- For cell #3 that represents a fixed bar (same as cells #5, 7, 9,…., 15) particles

| PROBABILITY | ASSUMED VALUE | PROBABILITY | ASSUMED VALUE | PROBABILITY | ASSUMED VALUE |
|---|---|---|---|---|---|
| $p_i$ | 0.4 | $p_r$ | 0.5 | $p_f$ | 0.3 |
| $p_o$ | 0.3 | $r_r$ | 0.2 | $r_f$ | 0.3 |

*Table4- 2: Assumed values of probabilities* satisfying Eqs (4-10), (4-11) and (4-12) for the *transition matrix used in this calculation*

have a high probability to move to the higher cell #2 (same as cells #4, 6, 8,….,14) because the motion of the reciprocating bar below cell #4 pushes particles upward. Therefore,

$$r_f \leq p_f < 1- p_f - r_f \qquad \text{(Eq. 4-13)}$$

The assumed probabilities for satisfying Eqs (4-11), (4-12) and (4-13) are shown in Table 4-2. At this stage of the study it was not possible to define the functions $f_r$ , $f_f$, $g_r$ and $g_f$ in Eqs. (4-5), (4-6), (4-8), and (4-9), because there has not been any experimental study of the mixing phenomena. Further work will be required to estimate values of these parameters, define Eqs (3-21) to (3-26), and then validate the model projections by field tests in an industrial WTE. Since all the solid wastes enter at the inlet of the combustion chamber, the initial state vector $\boldsymbol{S}(0)$ can be formulated as:

$$\boldsymbol{S}(0) = [1 \quad 0 \quad 0 \quad 0 \quad 0 \quad 0 \quad 0 \quad 0 \quad 0 \quad 0 \quad 0 \quad 0 \quad 0 \quad 0 \quad 0 \quad 0 \quad 0]$$

(Eq. 4-14)

This initial state vector represents the state of solid waste in cell #1, the position next to the inlet just after the solid waste is fed on the grate by the pusher at the bottom of the hopper. As stated earlier, the present model examined only one layer of MSW, that in contact with the grate surfaces.

MATLAB 6, an interactive matrix-based program for engineering calculations, was used on a Windows 2000 PC to carry out the matrix calculations required in the Markov chain simulation.

### 4-2-2. Expansion to two-dimensional stochastic model

To develop the two-dimensional Markov chain model of the mass-burn combustion chamber, we defined 5 layers of the MSW fuel above the grate and 32 zones for representing the reciprocating bars and fixed bars of the reverse acting grate. Figure 4-6 shows the total of 160 cells that were defined. The cells express the position where the MSW particles might be located. The average height of the MSW fuel on the grate is assumed as 1 meter. Therefore, the assumed height of each layer is 0.2 meter. The

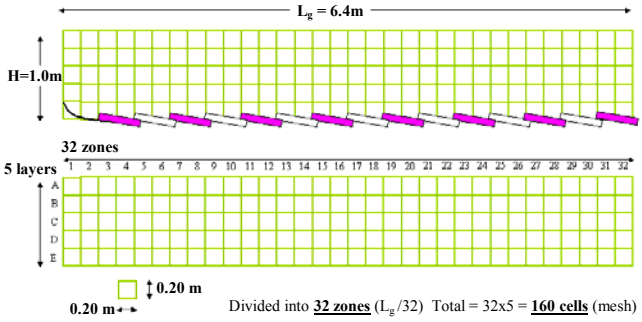


*Figure 4-6: Illustration of the spatial disposition of cells on the reverse acting grate*

rule governing the particle migration on the grate system is expressed by the same equation as Eq. 4-3:

$$\boldsymbol{S}(n) = \boldsymbol{S}(0)\,\boldsymbol{P}^{n} \qquad \text{(Eq. 4-3)}$$

where ***S(n)*** represents the profile of MSW particles traveling on the grate after n times of double strokes of the reciprocating bars; ***S(0)*** is the initial profile of MSW feed at

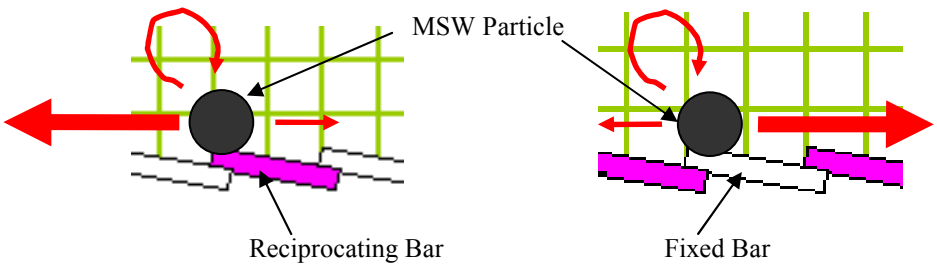


*Figure 4-7: Particle movement by reciprocating and fixed bars*

the inlet (prior to any stroke of the reciprocating bars, i.e., $n = 0$); $\boldsymbol{P}^{n}$ is the $n$th power of the matrix ***P*** (called the n-step transition matrix) that contains the probabilities of the solid particle movement; ***P*** and ***S(0)*** are represented by a 162x162 matrix and a 162x1 matrix, respectively:

$$\boldsymbol{P} = \overset{\longleftarrow\ 162\ \longrightarrow}{\begin{bmatrix} p_{11} & \cdots & \cdots & p_{j,162} \\ \cdots & \cdots & \cdots & \cdots \\ \cdots & \cdots & \cdots & \cdots \\ p_{162,k} & \cdots & \cdots & p_{162,162} \end{bmatrix}} \begin{matrix} \\ \\ \\ \updownarrow\ 162 \end{matrix} \qquad \text{(Eq. 4-15)}$$

$$\overset{\longleftarrow\ 162\ \longrightarrow}{\quad}$$

$$\boldsymbol{S(0)} = \begin{bmatrix} 1 & 0 & \ldots\ldots\ldots\ldots & 0 \end{bmatrix} \qquad \text{(Eq. 4-16)}$$

where $p_{j,k}$ are the probabilities to be measured in future field tests on a Martin grate WTE.. In this section we used assumed values for the probabilities. The rules for determining these probabilities are the same as those for the one-dimension Markov model. This simulation was carried out using the MATLAB 6 program on a Windows 2000 PC. To simplify the complexity of the movement of MSW particles, we simulated the movements without the effect of MSW properties and continuous feeding, i.e., the driving forces in this system are gravity and the movement of the bars.

## 4-3. Size (mass and volume) reduction model

### 4-3-1. Introduction

The size and volume of municipal solid waste (MSW) particles is reduced during the combustion process in the waste-to-energy (WTE) combustion chamber. As they travel over the length of the grate, particles are subjected to drying, volatilization, and char oxidation and finally turn into ash (Figure 4-8). The Martin reverse-acting traveling grate depicted in Figure 1 controls the rate of flow and also enhances mixing. The grate operation is necessary because MSW is much more heterogeneous than coal and other fuels.

Major factors in the size reduction of MSW particles are the physical and chemical transformations occurring on the grate, including drying, volatilization, and combustion. In addition, because of the motion of the moving bars of the Martin grate, some MSW particles break up and their size is reduced. This breakage process can be

numerically expressed as a breakage matrix based on experimental data. For example, Campbell and Webb analyzed roller milling performance and developed a breakage equation (Campbell and Webb, 2001). Before the MSW enters into the inlet of the combustion chamber, the MSW particles are accumulated in the feed hopper from the bottom of which they are pushed into the combustion chamber by the ram feeder. The resulting compaction process can be estimated by means of a ram pressure-density curve, because MSW varies greatly in both densities and compressibility. After the drying, volatilization, and combustion processes in the chamber, MSW particles become ash consisting mostly of non-combustible residues. The particles that are on the surface on the bed, where the temperature rises above 1100 $^{o}$C, are subjected to some fusion and agglomeration, and they form larger particles (clinker). Due to the motion of the traveling grate, clinker particles of ash can break again and their size is finally reduced to the PSD of ash at the outlet of the combustion chamber (Figure 4-8).

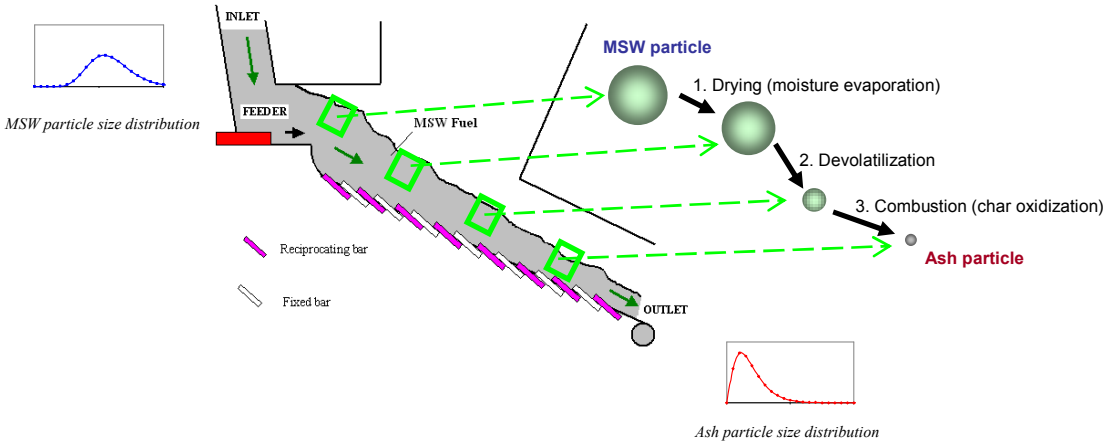


*Figure 4-8: Combustion and transport phenomena of one particle in a MSW bed on the traveling grate*

In order to simulate the size reduction of MSW particles, we modeled the PSD of MSW particles and ash particles and applied the shrinking core model (SCM) to these distributions. Also, Image Analysis was used to determine the PSD of MSW and ash samples. Finally, thermogravimetric analysis (TGA) data was applied on particles of the main constituents of MSW in order to examine the effect of thermal decomposition on particle size.

### 4-3-2. Modeling

Particle Size Distributions (PSDs):

PSDs of MSW and ash were described in this study by using the Gamma function distribution that is expressed as follows:

$$f_p(D) = a \cdot \frac{1}{\beta^{\alpha}\Gamma(\alpha)} D^{\alpha-1} e^{-\frac{D}{\beta}} \qquad \text{(Eq. 4-17)}$$

where a is constant, $D$ is the particle size, and $\alpha$, $\beta$ are positive parameters, respectively. Figure 4-9 shows the gamma distributions for different values of $\alpha$ but constant β.

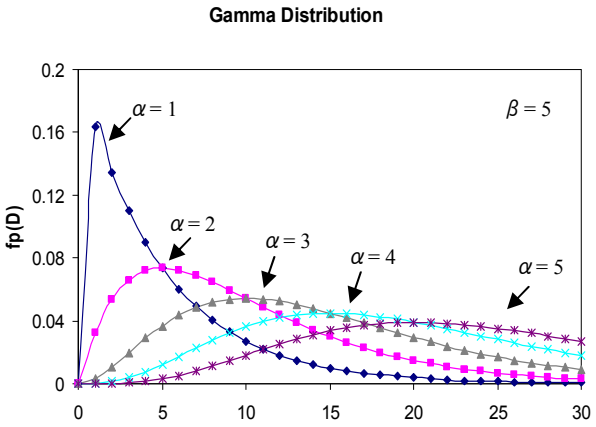


*Figure 4-9: Particle size density function (Gamma distribution) for different values of α (=1, 2, 3, 4, 5) and constant β (= 5)*

Combustion of MSW particles:

The shrinking core model (SCM) is used to simulate the thermal decomposition of MSW particles. The SCM was originally developed by Yagi and Kunii for describing solid and fluid reactions for non-porous particles (Yagi and Kunii 1955). Gbor and Jia developed a SCM combined with PSDs (Gbor and Jia, 2004) The unreacted mass fraction in the core of a particle can be defined as follows:

$$\textit{Unreacted Fraction} = \int_0^{\infty} \left(g(D,t)\right) \cdot \left(f_p(D)\right) dD \qquad \text{(Eq. 4-18)}$$

where $g(D, t) = 1 - X_D$ is the unreacted fraction and $X_D$ depends on the type of the controlling regime, such as diffusion through gas film, diffusion through ash layer, or chemical reaction control.

$g(D, t) = 0$ for $0 < D < D_t$

and $g(D, t) = 1 - X_D$ for $D_t < D < D_{max}$

Therefore, the overall conversion for all particle sizes (X) is

$$X = 1 - \int_{D_t}^{D_{\max}} g(D,t) \cdot a \cdot \frac{1}{\beta^{\alpha}\Gamma(\alpha)} D^{\alpha-1} e^{-\frac{D}{\beta}} dD \qquad \text{(Eq. 4-19)}$$

A large part of the size reduction of MSW is due to thermal decomposition that occurs at temperatures below 400 $^{o}$C and can be expressed as follows:

$$MSW \rightarrow moisture + volatile\ matters + char \qquad \text{(Eq. 4-20)}$$

For this reaction, $g(D,t) = 1 - X_D = \left(1 - \frac{k_{rn} t}{D}\right)^3$ (Eq. 4-21)

where $k_{rm} = k_r D$, $D_t = k_{rn} t$, and $k_r = k_1 C_{Ag} / \rho R$. R is radius of particles ($R = D/2$).

Other possible size reduction phenomena that are not included in this model:

*(1) Compaction of MSW particles:* The size of MSW particles can be reduced due to compaction. When MSW particles are fed into the chamber, the feeder compresses them and they become smaller than the particles in black bags as collected.

*(2) Breakage of MSW particles:* As the particles travel on the reverse acting grate, some of them break due to movement of the traveling grate and mechanical interaction with neighboring particles. For example, a glass bottle fed into the chamber may break into hundreds of small pieces.

## 4-4. Stochastic model for MSW mixing combined with a flow

The first procedural step in the design of the stochastic model was to divide the MSW bed into several cells (mesh grid shown in Figure 4-10, same as in 4-6). In a commercial WTE plant, a reverse acting grate, whose total length is 6.4m, has 8 moving bars and 8 fixed bars and the initial MSW bed height is 1m. We divided the bed into 32 sections along the axial direction and 5 layers along the horizontal direction, resulting in a total of 162 cells including the inlet and ashbin cells. The particle movement probabilities were determined from experimental data and used to formulate a transition matrix ***P***.

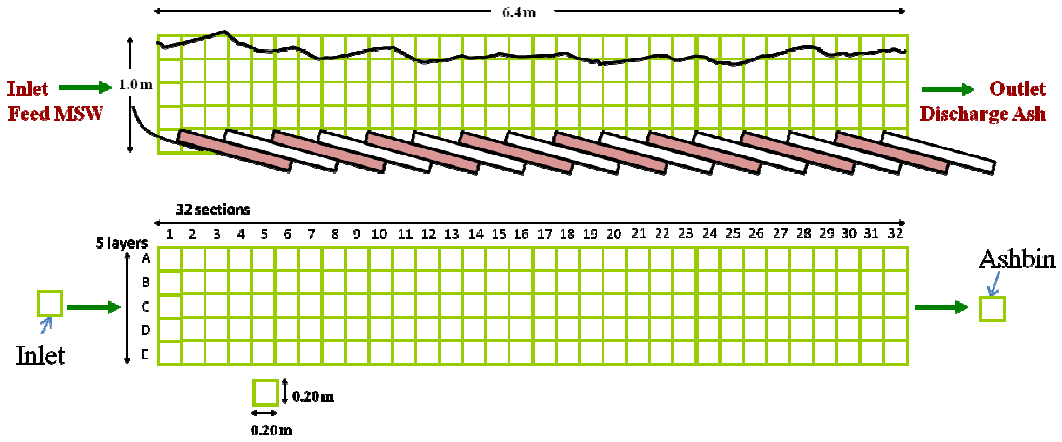


*Figure 4-10: MSW bed on the reverse acting grate of a WTE plant showing divided cells (mesh) for the stochastic simulation*

The stochastic process employed in the mathematical model is called a Markov Chain and assumes that, at each reciprocation of the moving bars, the transition probabilities of the waste particles between adjacent cells are independent of the previous state in time. The rule governing the particle migration of the system is expressed by the following equation:

$$\boldsymbol{S}(n) = ( \boldsymbol{F}^{k} \cdot \boldsymbol{P} )^{n} \cdot \boldsymbol{S}(0) \qquad \text{(Eq. 4-22)}$$

where $\boldsymbol{S}(n)$ represents the profile of MSW traveling on the chamber bed after $n$ times of reciprocations of the moving bars and $\boldsymbol{S}(0)$ is the initial profile of MSW feed at the inlet (prior to any reciprocation of the moving bars, i.e., $n = 0$). $\boldsymbol{F}^{k}$ is the $k$ th power of matrix $\boldsymbol{F}$ that controls the MSW flow in the packed bed pushed by the feeder at the combustion chamber inlet. $k$ is the ratio between MSW feed flow rate and the frequency of the reciprocating bars. If there is no inlet feeder flow, then $k = 0$ and $\boldsymbol{F}$ becomes the identity matrix that neither affects $\boldsymbol{P}$ or $\boldsymbol{S}(0)$. The dimension of the flow matrix $\boldsymbol{F}$ is 162-by-162. The elements of $\boldsymbol{F}$ that we used are shown in Figure 4-11 and their corresponding cells and directions are shown in Figure 4-12. There are several different types of feeding systems, such as feeding bars and screws that are currently employed in mass-burn combustion chambers. In order to simplify a MSW flow caused by a feeder, we considered it as a plug flow. In this type of flow system, since particles travel only from section $i$ to the next section $i+1$ in a given layer, all transition probabilities $p_{i,i+1} = 1$, except for the exit location probabilities $p_{33,34}$, $p_{65,66}$, $p_{97,98}$, and $p_{129,130}$ (= 0). This is because particles at the exit position in each layer (the

32nd section) cannot transition back to the inlet position for these 4 cells. All other $p_{i,j}$ are equal to zero. Since the MSW flow greatly depends on the type of feeding system and chamber geometry, further study is needed to determine the elements of flow matrix $\boldsymbol{F}$, specific to the particular operational conditions.

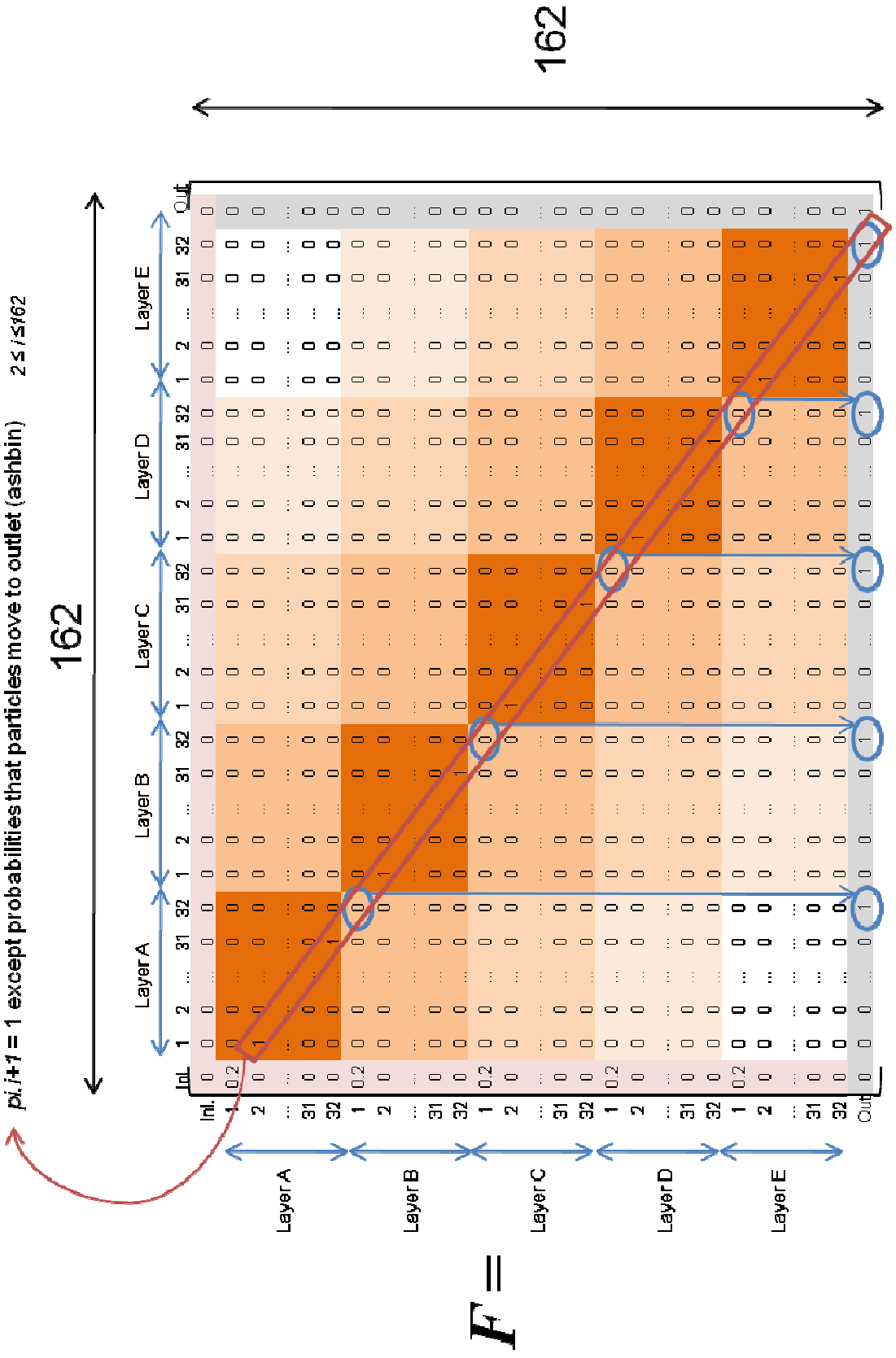


*Figure 4-11: The elements of the flow matrix* ***F***

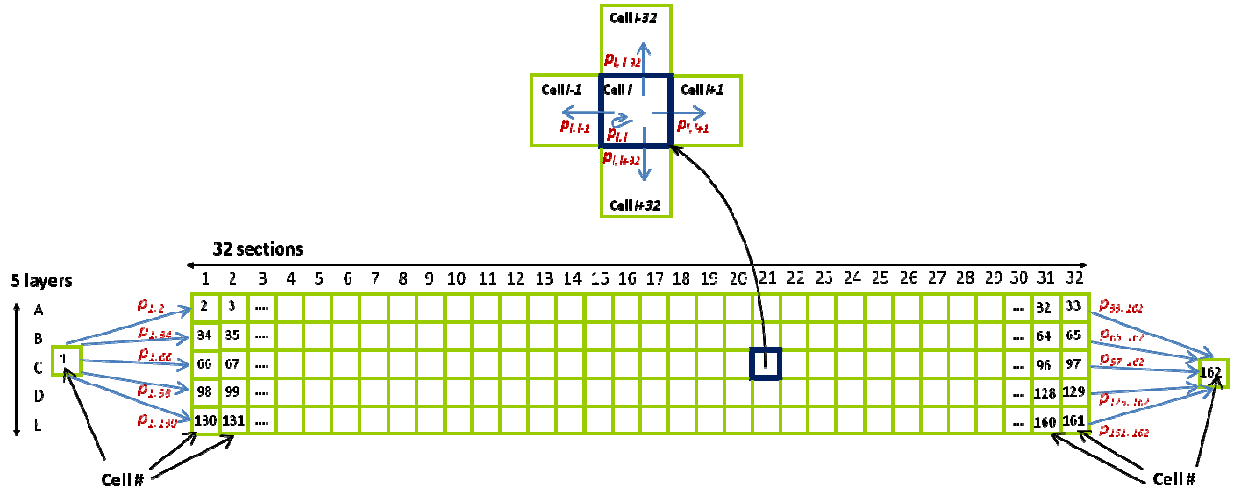


*Figure 4-12: Diagram of probabilities and directions of the flow for each cell of the MSW bed on the grate*

***P*** is the transition matrix that contains the probabilities predicting the solid particle movement due to the motion of the reciprocation bars. As shown in Figure 4-13, the size of the transition matrix is 162-by-162 including a total of 26,244 probabilities, as the same size of flow matrix ***F***. The main diagonal ( $p_{1,1}$, $p_{2,2}$ ,....., $p_{i,i}$, ..., $p_{162,162}$ ) elements represent the probabilities that the MSW particles remain in the same cell. As also shown in Figure 4-12, $p_{i,i+1}$ is the probability that the particle transits from cell *i* to the neighbor cell *i+1* (along the flow direction) and $p_{i,i-1}$ is the probability from cell *i* to cell *i-1* (opposite to the flow direction). $p_{i,i+32}$ is the probability that the particle moves to the cell in the layer directly below the current cell location(from cell *i* to cell *i+32*) and $p_{i,i-32}$ is the probability that it moves to the cell in the neighboring layer above (from cell *i* to cell *i-32*). It should be noted that the probabilities in the transition matrix ***P*** are always positive fractions and the sum of the elements within each row of the matrix ***P*** equals one.

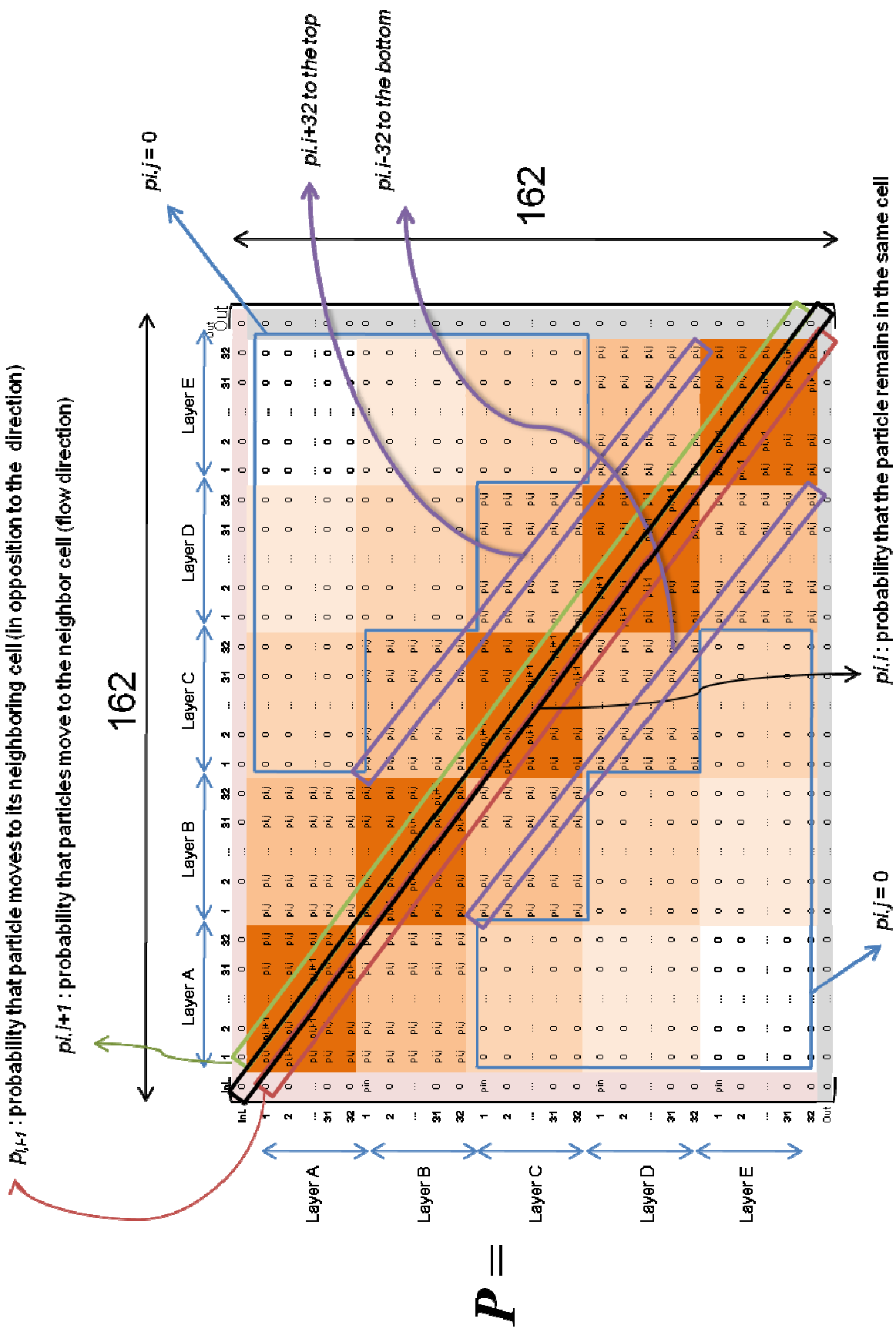


*Figure 4-13: The elements of the transition matrix* ***P***

The transition probabilities were determined using measured data from the full-scale experimental cross-section model. The grate system of an actual combustion chamber has 8 moving bars as shown in Figure 4-10, whereas the physical section model employs 2 moving bars as shown in Figure 3-7. The predictive capability of the stochastic model was expanded by employing 8 moving bars to match a full-length grate system. Based on the fact that the residence time of a real combustion chamber roughly ranges from 30 to 120 min (sometimes a particle stays shorter or longer than this range), a typical value for the MSW feed in this model was set at a time of 64 min for traveling the total chamber length of 6.4m (32cells): i.e. 2min/cell.

Since all of the solid waste enters at the inlet of the combustion chamber, the initial state vector ***S(0)*** can be expressed as:

$$\boldsymbol{S}(0) = [1 \quad 0 \quad \cdots \quad 0 \quad 0] \qquad \text{(Eq. 4-16)}$$

This initial state vector, whose size is 1×162, represents the state of the solid waste in the inlet cell, whose position is at the bottom of the hopper adjacent to the feeder bar.

In order to carry out the matrix calculations required in this stochastic simulation, MATLAB 7.1 was used on a Windows XP PC.

# Chapter 5: Results and Discussion

## 5-1. Results from experimental work

### 5-1-1. Particle size and shape distributions

Figure 5-1 shows the particle size distributions (PSDs), sphericity distributions, aspect ratio distributions (ARDs) and roundness distributions of MSW and ash particles. As shown in Figure 5-1-a, the peak of MSW PSD, about 10 cm, shifts to the peak of the ash PSD, about 2 cm, during the combustion process. Also, the tail of the MSW PSD is larger than that of the ash PSD. In Sphericity Distributions (Fig 5-1-b), two peaks of MSW and ash particles are located between 1.5 and 2. The two peaks are ranging from 1.2 to 1.4 in Aspect Ratio Distributions (Figure 5-1-c) and from 1.3 to 1.4 in Roundness Distributions (Figure 5-1-d), respectively. Either ash distribution has a higher peak than MSW distribution. This means ash particles are more homogeneous in size, sphericity, aspect ratio, and roundness than the MSW particles.

In the combustion chamber, the MSW particles are mixed by the movement of the acting grate and heated up. The most important phenomenon during size and shape change processes is volatilization, since around 300 $^{o}$C MSW particles usually

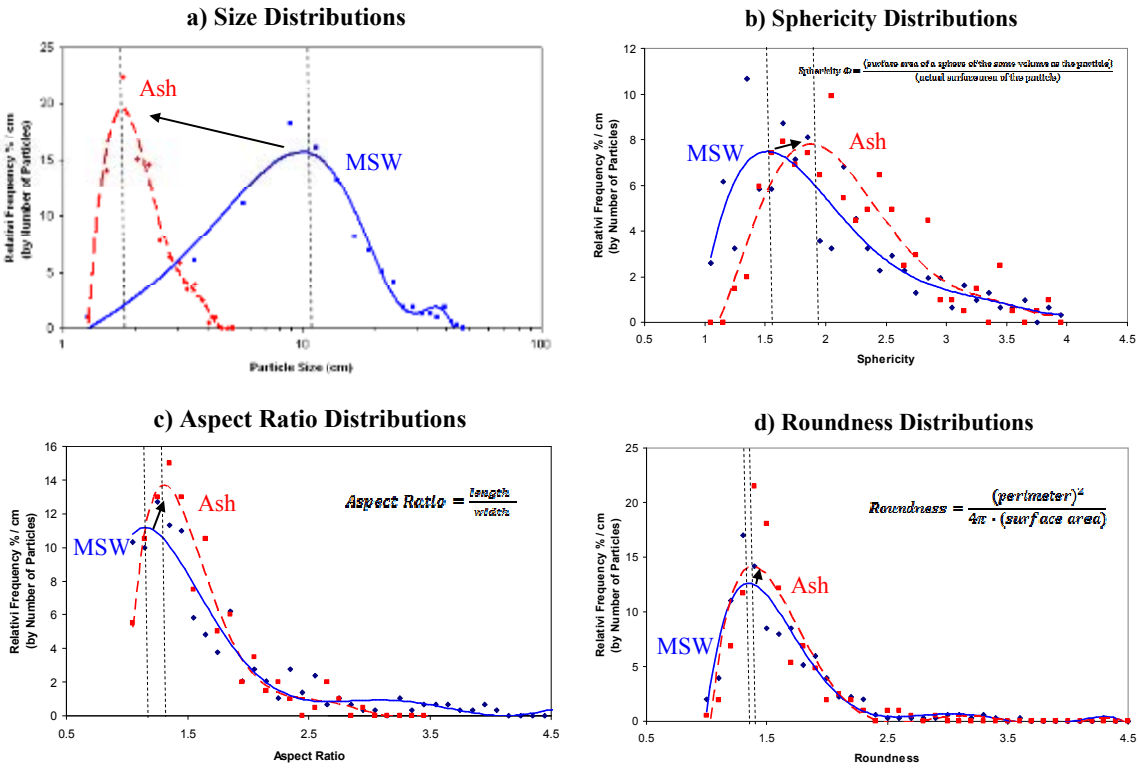


*Figure 5-1: Distributions by particle numbers of residential MSW and combined ashes in NYC a) Particle size distributions (PSDs), b) Sphericity distributions, c) Aspect Raito distributions (ARDs), d) Roundness distributions*

start generating volatile matter and their mass and volume decrease rapidly. This particle shrinkage results in size reduction and shape change of MSW particles. Then the MSW particles distributions get closer to ash distributions. Finally, the

combustible MSW particles become ash during the char gasification stage (fixed carbon oxidization).

The particle size distributions (PSDs), sphericity distributions, aspect ratio distributions (ARDs) and roundness distributions of MSW and ash particles were analyzed. The peak of MSW PSD is around 10 cm and shifts to the peak of ash PSD, around 2 cm, during the combustion process. Also, the "tail" of the MSW PSD is larger than that of ash PSD. In sphericity distributions, the peak of the MSW particles was found to be at 1.5 and of the ash particles at 2. The Aspect Ratio Distributions are 1.2 and 1.4 and the Roundness Distributions 1.3 and 1.4, respectively.

**5-1-2. Probabilities from full-scale physical model**

Figures 5-2 to 13 show particle movement and the state diagrams (transition graph) of small, medium, and large tracer particles at different heights (20, 40, 60, and 80 cm) of the MSW bed. A tracer particle in each cell has a different behavior. For example, a tracer located in the cells at layer E moves very quickly because it is pushed by a reciprocating bar.

Figure 5-14 shows the measured probabilities of small, medium, and large particles that remain in the same cell location of a NYC-MSW packed bed after one reciprocation of its moving bars. These probabilities in layer E, at the bottom of the bed, are lowest for small and medium particles. For large particles, no experimental data could be obtained because the small and medium particles occupied layer E and tended to remain at the bottom so that large particles could not transit there. These probabilities showed that 22% of small particles and 8% of medium particles stay in layer E while the rest of them (78% of small and 92% of medium particles) move to a neighboring cell because of the motion of a reciprocating bar.

Layer B is where small and medium particles have the second lowest probabilities and large tracers have the lowest. Approximately 50% for any one of the three sizes remain in layer B while the rest of them move to other cells. Retention probabilities for the middle of the MSW bed (layers C and D) are much higher with values up to 81%. Since the MSW was loaded up at the height of 80 cm, layer B is at

the top of the bed and a tracer on the free surface moves more because there are fewer particles acting on it to constrain its motion. Particles in this top layer were sometimes observed to be easily rolling along the free surface, a type of motion that is unavailable to particles in the lower layers.

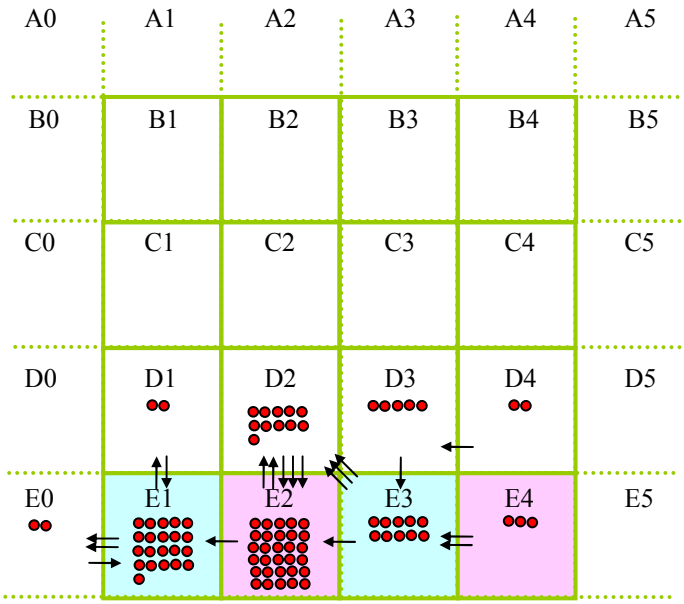


*Observed particle movements: Number of the circles in a cell means how many a tracer particle stayed in the cell per reciprocating motion of moving bars. One arrow indicates a movement and direction of a particle tracer into a neighbor cell during a reciprocating motion of moving bars.*

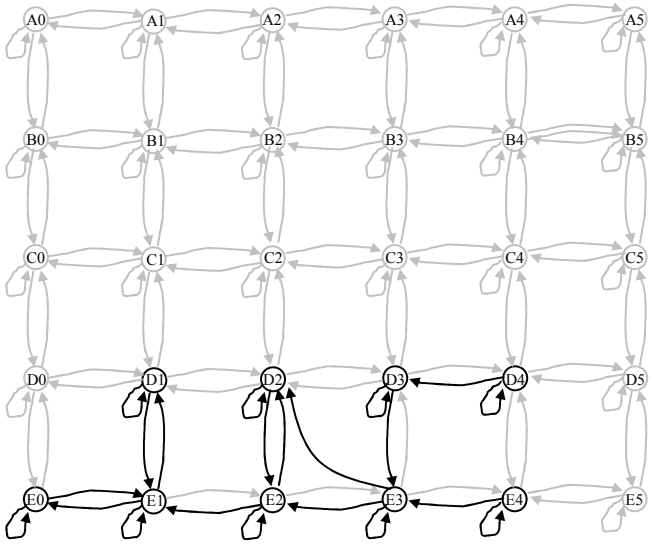


*Corresponding state diagram*

*CCD image from Side view of the bed*

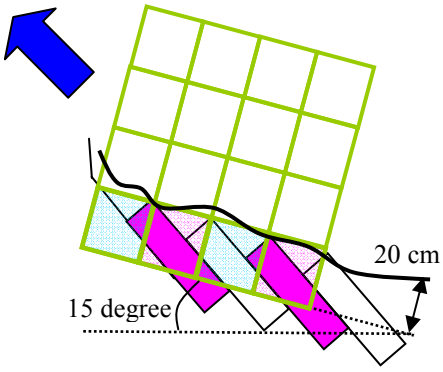


*Solid bed divided by20cm×20cm cells*

*Grate inclination: 15°*
*Bed solid: Mixed MSW*
*Tracer: 6 cm sphere tracer*
*Original bed height: 20 cm*

*Figure 5-2: Observed particle movements and corresponding state diagram*

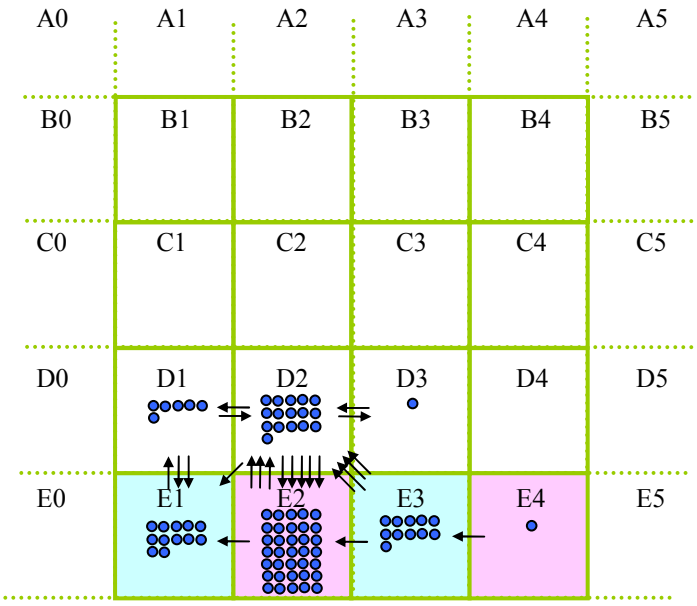


*Observed particle movements: Number of the circles in a cell means how many a tracer particle stayed in the cell per reciprocating motion of moving bars. One arrow indicates a movement and direction of a particle tracer into a neighbor cell during a reciprocating motion of moving bars.*

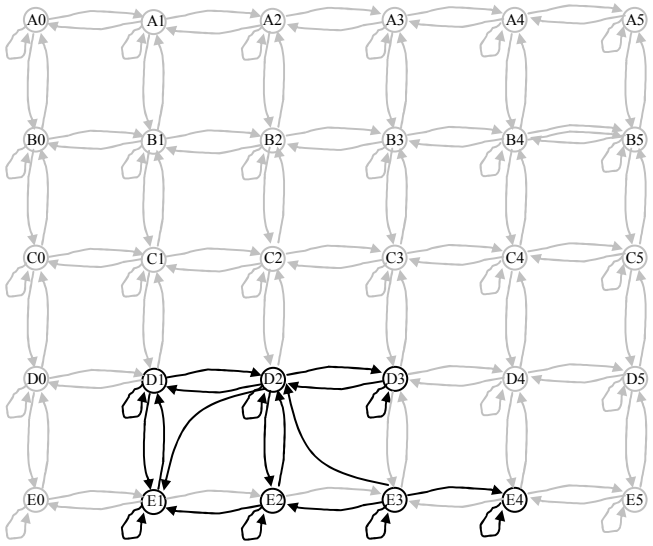


*Corresponding state diagram*

*CCD image from Side view of the bed*

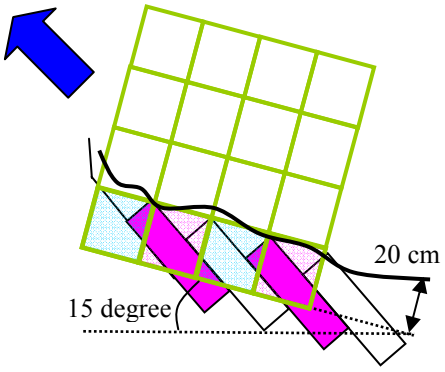


*Solid bed divided by20cm×20cm cells*

*Grate inclination: 15°*
*Bed solid: Mixed MSW*
*Tracer: 14 cm sphere tracer*
*Original bed height: 20 cm*

*Figure 5-3: Observed particle movements and corresponding state diagram*

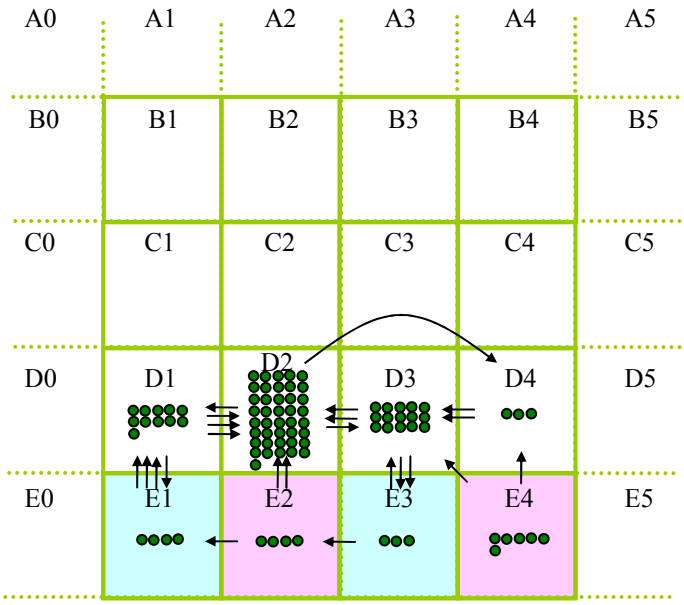


*Observed particle movements: Number of the circles in a cell means how many a tracer particle stayed in the cell per reciprocating motion of moving bars. One arrow indicates a movement and direction of a particle tracer into a neighbor cell during a reciprocating motion of moving bars.*

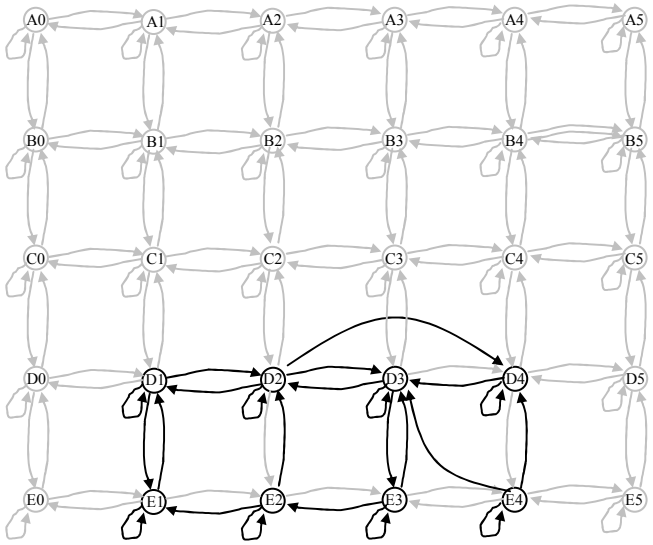


*Corresponding state diagram*

*CCD image from Side view of the bed*

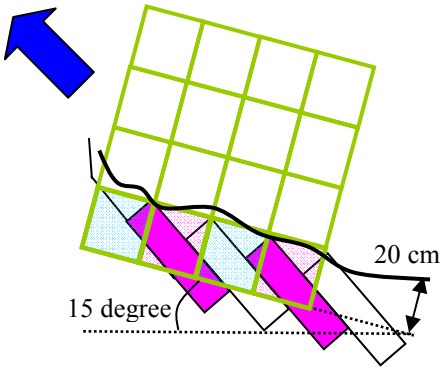


*Solid bed divided by20cm×20cm cells*

*Grate inclination: 15°*
*Bed solid: Mixed MSW*
*Tracer: 22 cm sphere tracer*
*Original bed height: 20 cm*

*Figure 5-4: Observed particle movements and corresponding state diagram*

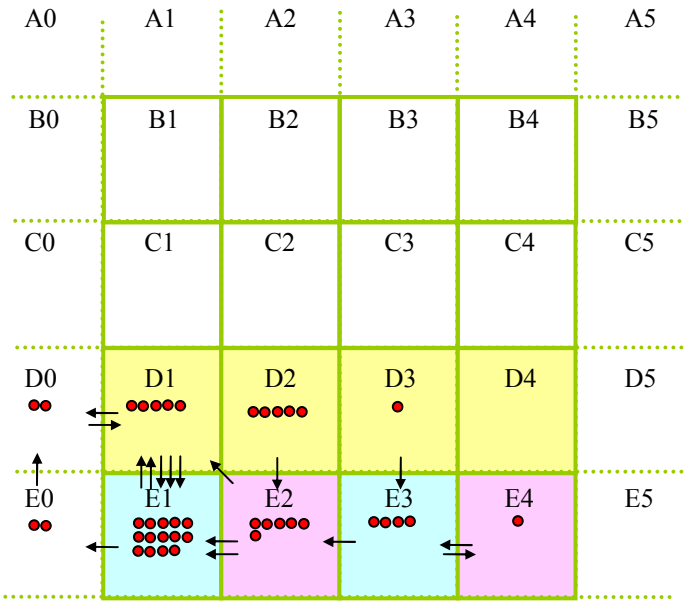


*Observed particle movements: Number of the circles in a cell means how many a tracer particle stayed in the cell per reciprocating motion of moving bars. One arrow indicates a movement and direction of a particle tracer into a neighbor cell during a reciprocating motion of moving bars.*

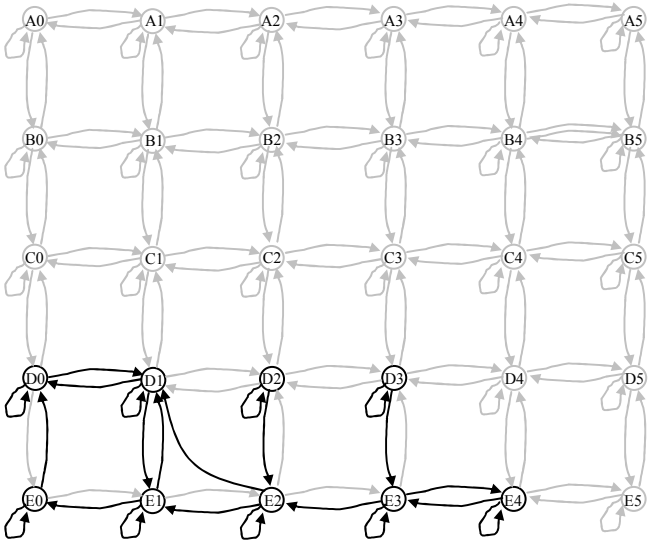


*Corresponding state diagram*

*CCD image from Side view of the bed*

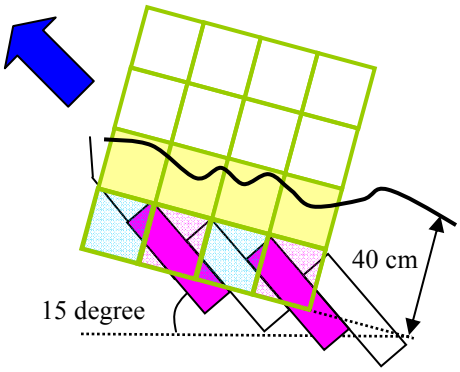


*Solid bed divided by20cm×20cm cells*

*Grate inclination: 15°*
*Bed solid: Mixed MSW*
*Tracer: 6 cm sphere tracer*
*Original bed height: 40 cm*

*Figure 5-5: Observed particle movements and corresponding state diagram*

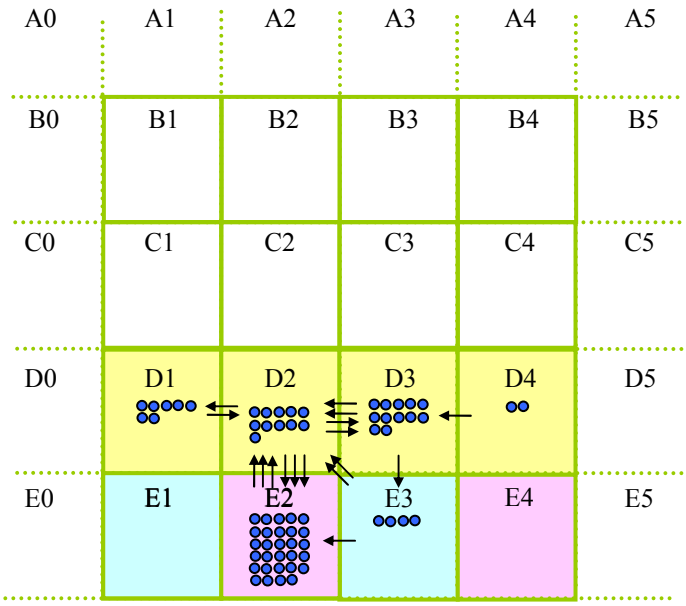


*Observed particle movements: Number of the circles in a cell means how many a tracer particle stayed in the cell per reciprocating motion of moving bars. One arrow indicates a movement and direction of a particle tracer into a neighbor cell during a reciprocating motion of moving bars.*

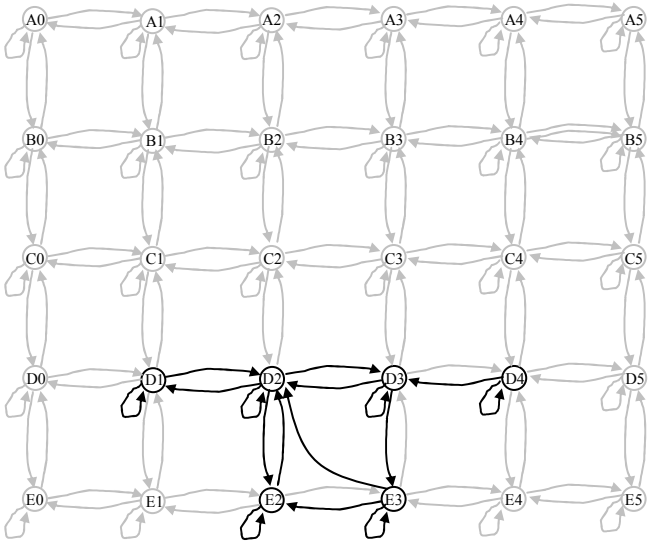


*Corresponding state diagram*

*CCD image from Side view of the bed*

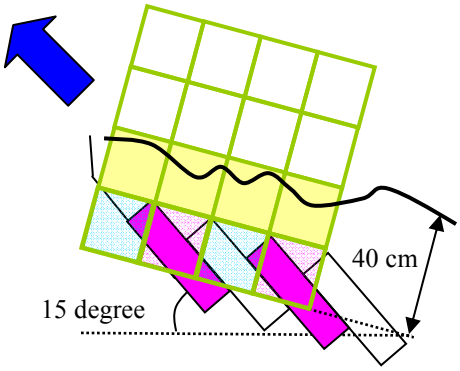


*Solid bed divided by20cm×20cm cells*

*Grate inclination: 15°*
*Bed solid: Mixed MSW*
*Tracer: 14 cm sphere tracer*
*Original bed height: 40 cm*

*Figure 5-6: Observed particle movements and corresponding state diagram*

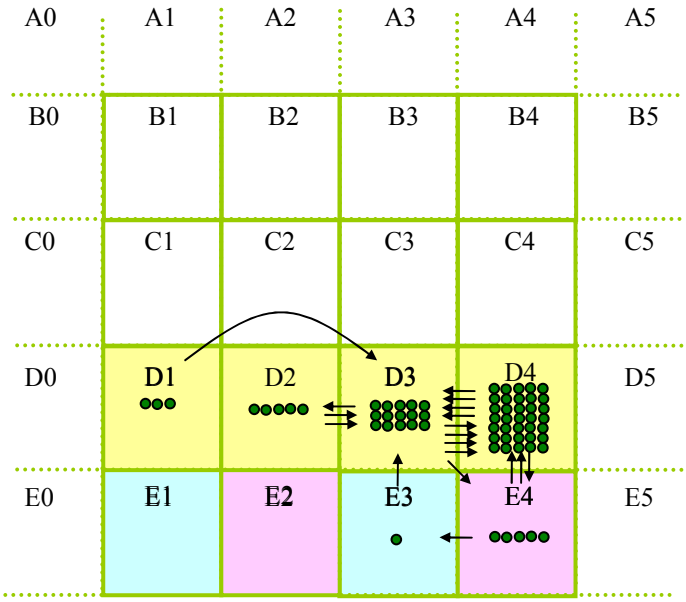


*Observed particle movements: Number of the circles in a cell means how many a tracer particle stayed in the cell per reciprocating motion of moving bars. One arrow indicates a movement and direction of a particle tracer into a neighbor cell during a reciprocating motion of moving bars.*

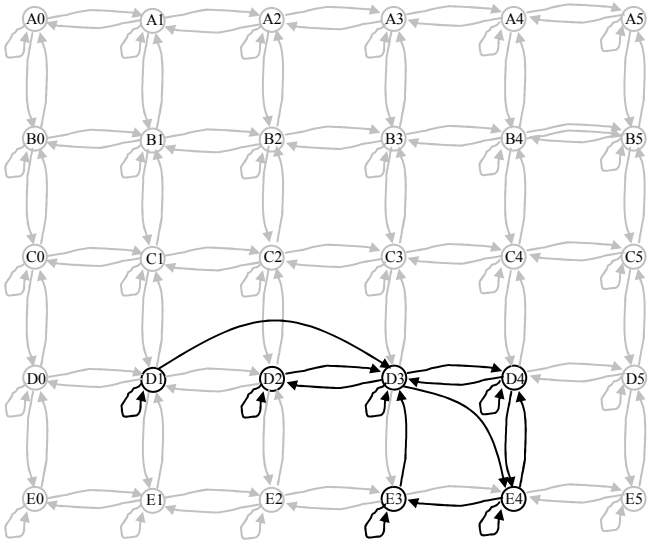


*Corresponding state diagram*

*CCD image from Side view of the bed*

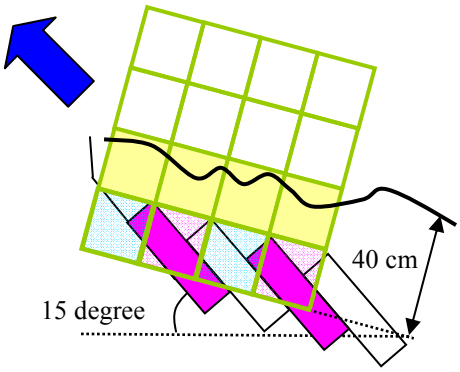


*Solid bed divided by20cm×20cm cells*

*Grate inclination: 15°*
*Bed solid: Mixed MSW*
*Tracer: 22 cm sphere tracer*
*Original bed height: 40 cm*

*Figure 5-7: Observed particle movements and corresponding state diagram*

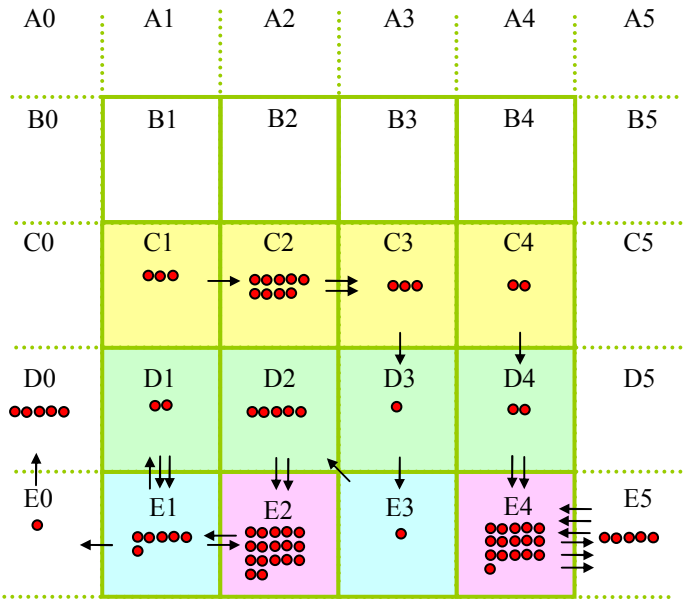


*Observed particle movements: Number of the circles in a cell means how many a tracer particle stayed in the cell per reciprocating motion of moving bars. One arrow indicates a movement and direction of a particle tracer into a neighbor cell during a reciprocating motion of moving bars.*

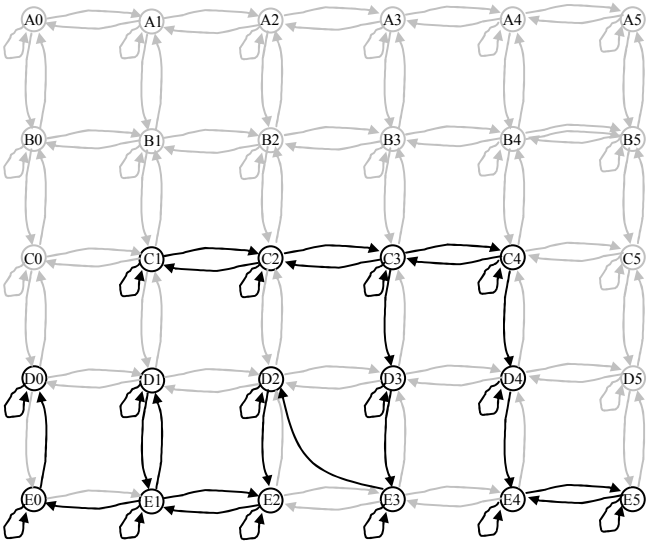


*Corresponding state diagram*

*CCD image from Side view of the bed*

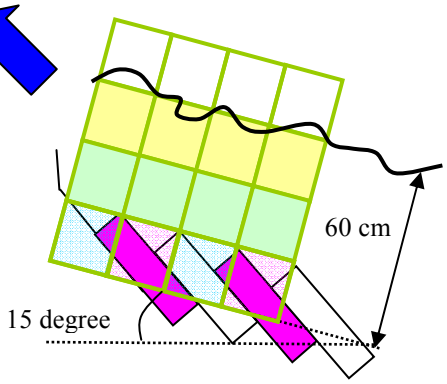


*Solid bed divided by20cm×20cm cells*

*Grate inclination: 15°*
*Bed solid: Mixed MSW*
*Tracer: 6 cm sphere tracer*
*Original bed height: 60 cm*

*Figure 5-8: Observed particle movements and corresponding state diagram*

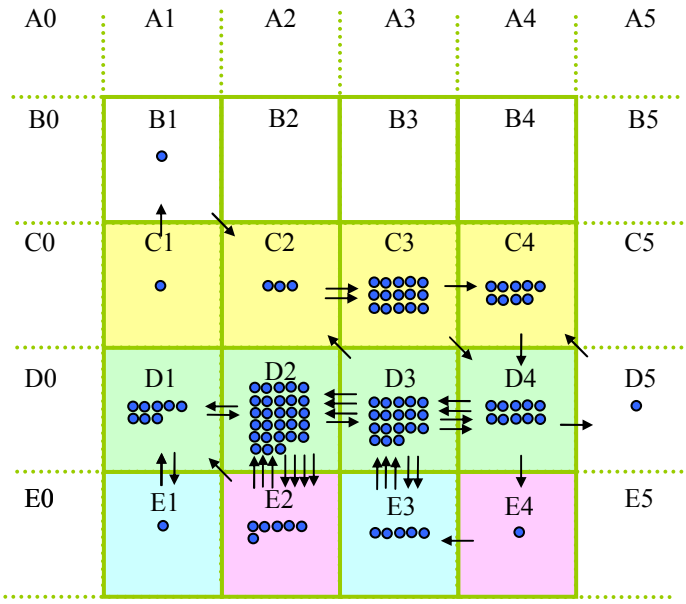


*Observed particle movements: Number of the circles in a cell means how many a tracer particle stayed in the cell per reciprocating motion of moving bars. One arrow indicates a movement and direction of a particle tracer into a neighbor cell during a reciprocating motion of moving bars.*

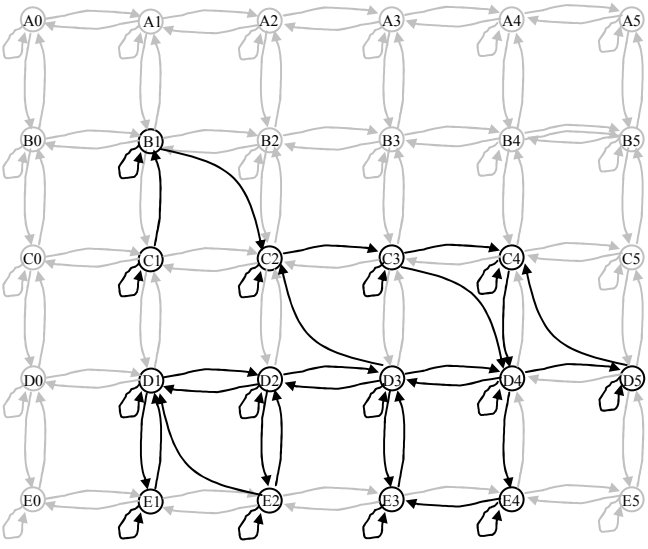


*Corresponding state diagram*

*CCD image from Side view of the bed*

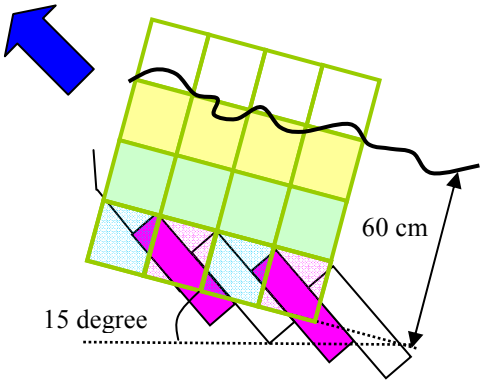


*Solid bed divided by20cm×20cm cells*

*Grate inclination: 15°*
*Bed solid: Mixed MSW*
*Tracer: 14 cm sphere tracer*
*Original bed height: 60 cm*

*Figure 5-9: Observed particle movements and corresponding state diagram*

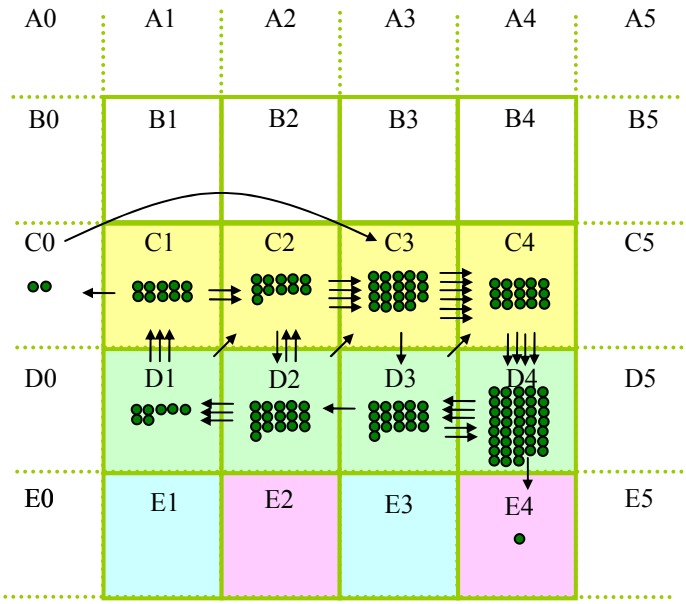


*Observed particle movements: Number of the circles in a cell means how many a tracer particle stayed in the cell per reciprocating motion of moving bars. One arrow indicates a movement and direction of a particle tracer into a neighbor cell during a reciprocating motion of moving bars.*

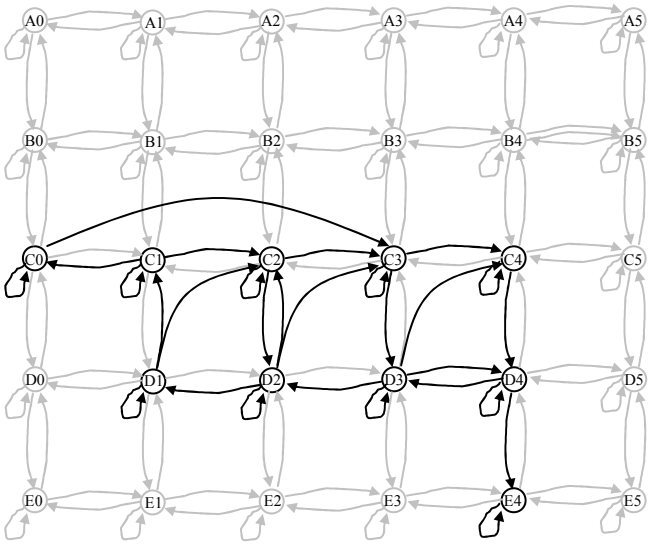


*Corresponding state diagram*

*CCD image from Side view of the bed*

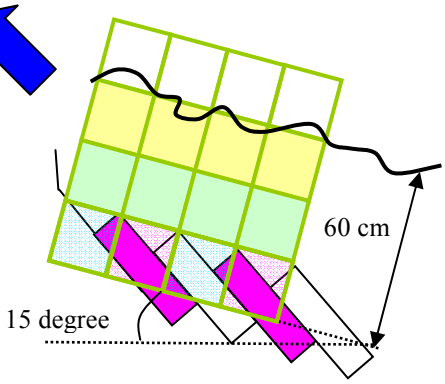


*Solid bed divided by20cm×20cm cells*

*Grate inclination: 15°*
*Bed solid: Mixed MSW*
*Tracer: 22 cm sphere tracer*
*Original bed height: 60 cm*

*Figure 5-10: Observed particle movements and corresponding state diagram*

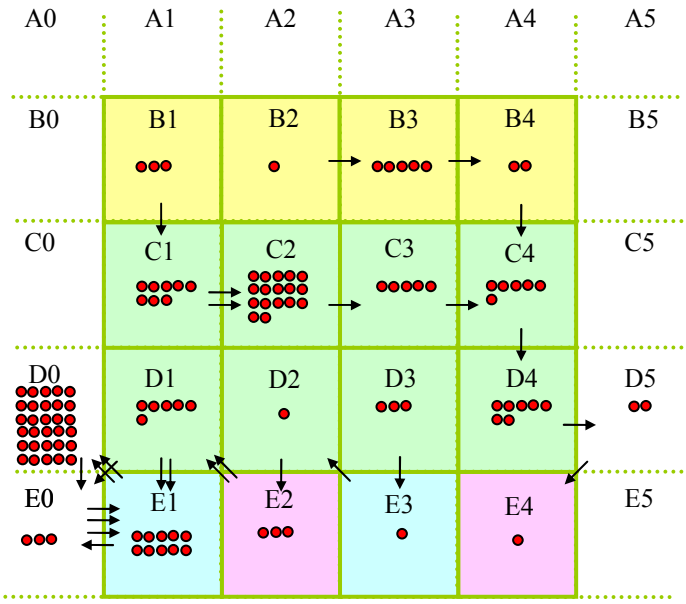


*Observed particle movements: Number of the circles in a cell means how many a tracer particle stayed in the cell per reciprocating motion of moving bars. One arrow indicates a movement and direction of a particle tracer into a neighbor cell during a reciprocating motion of moving bars.*

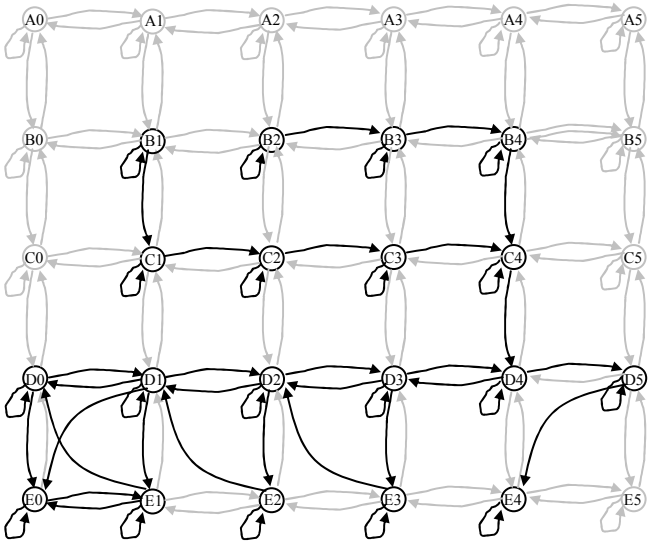


*Corresponding state diagram*

*CCD image from Side view of the bed*

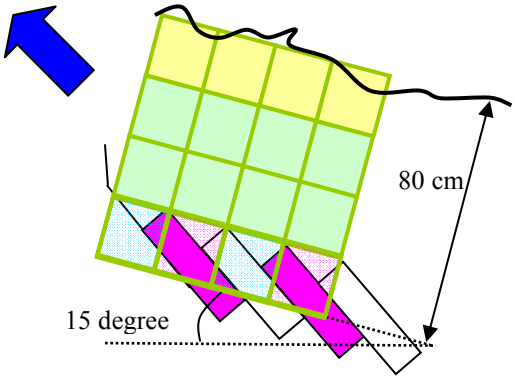


*Solid bed divided by20cm×20cm cells*

*Grate inclination: 15°*
*Bed solid: Mixed MSW*
*Tracer: 6 cm sphere tracer*
*Original bed height: 80 cm*

*Figure 5-11: Observed particle movements and corresponding state diagram*

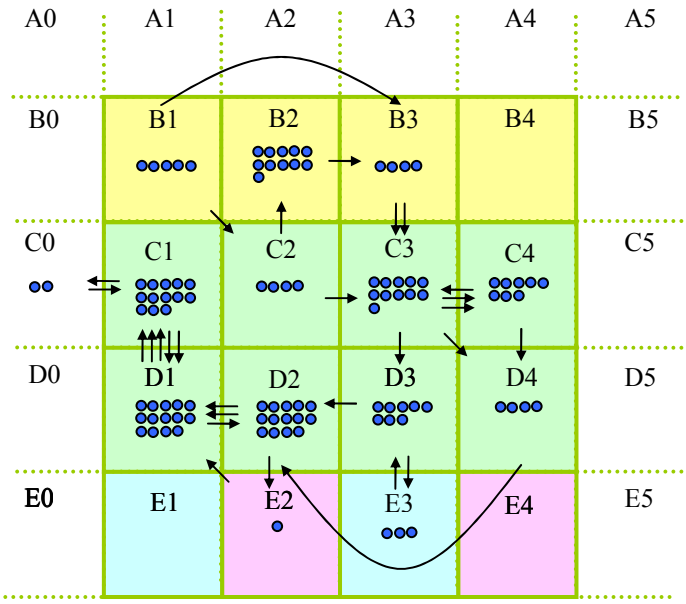


*Observed particle movements: Number of the circles in a cell means how many a tracer particle stayed in the cell per reciprocating motion of moving bars. One arrow indicates a movement and direction of a particle tracer into a neighbor cell during a reciprocating motion of moving bars.*

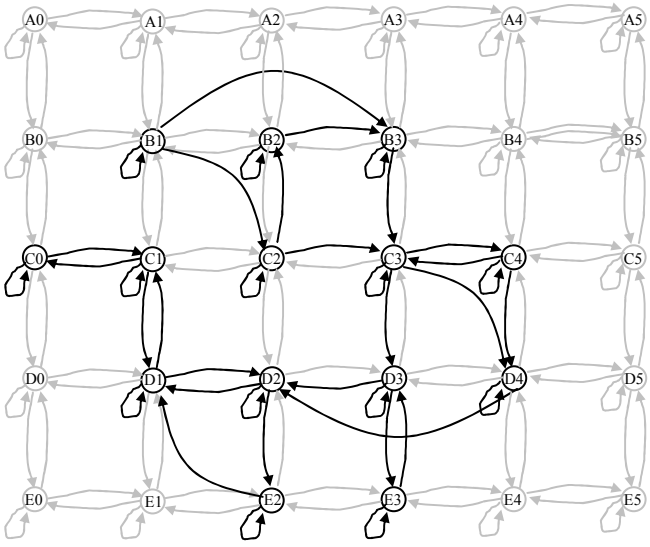


*Corresponding state diagram*

*CCD image from Side view of the bed*

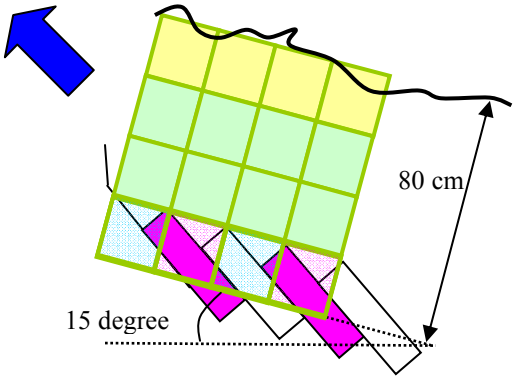


*Solid bed divided by20cm×20cm cells*

*Grate inclination: 15°*
*Bed solid: Mixed MSW*
*Tracer: 14 cm sphere tracer*
*Original bed height: 80 cm*

*Figure 5-12: Observed particle movements and corresponding state diagram*

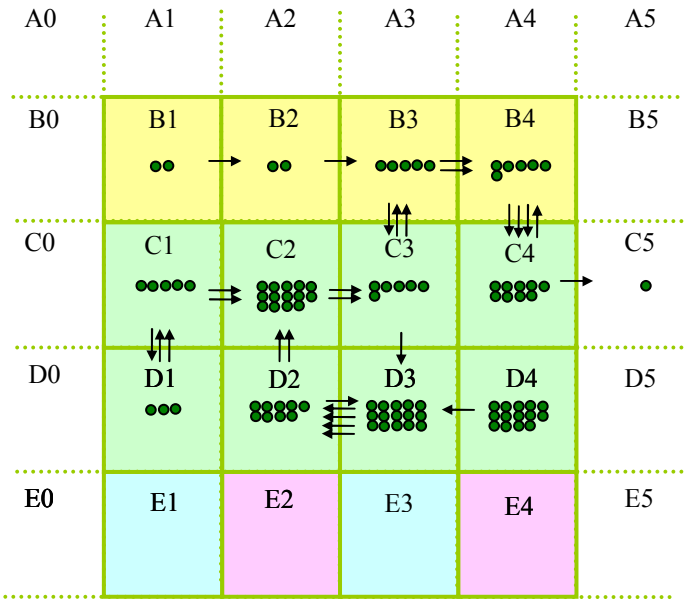


*Observed particle movements: Number of the circles in a cell means how many a tracer particle stayed in the cell per reciprocating motion of moving bars. One arrow indicates a movement and direction of a particle tracer into a neighbor cell during a reciprocating motion of moving bars.*

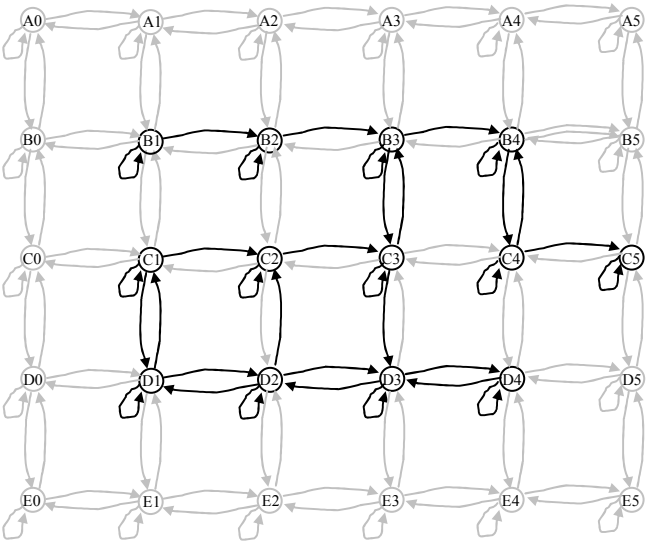


*Corresponding state diagram*

*CCD image from Side view of the bed*

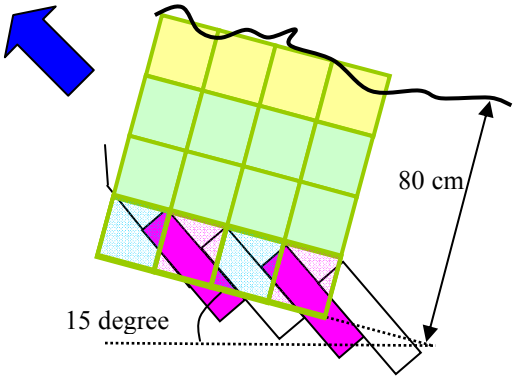


*Solid bed divided by20cm×20cm cells*

*Grate inclination: 15°*
*Bed solid: Mixed MSW*
*Tracer: 22 cm sphere tracer*
*Original bed height: 80 cm*

*Figure 5-13: Observed particle movements and corresponding state diagram*

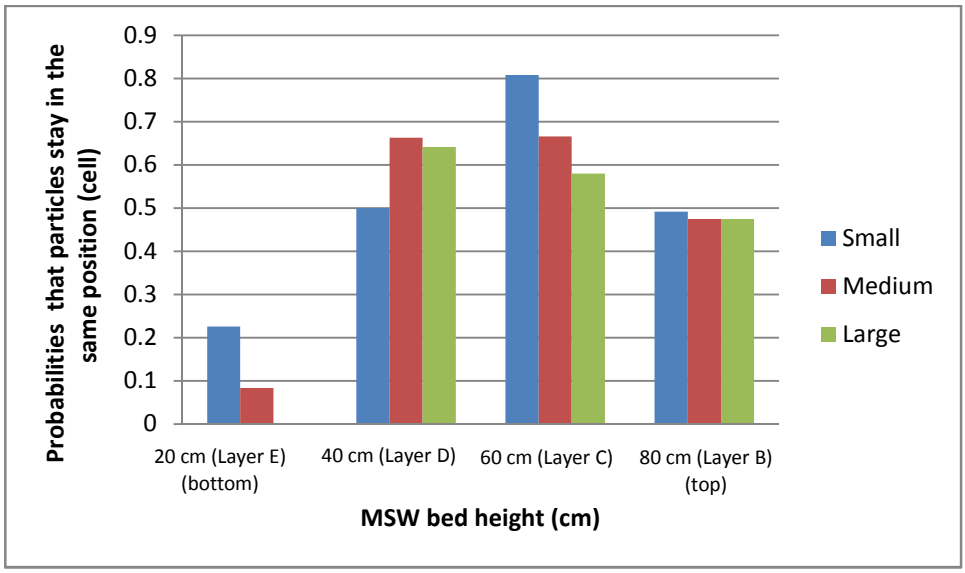


*Figure 5-14: Measured probabilities that particles stay in the same position (cell) after one reciprocation of the moving bars*

## 5-2. Results from mathematical work

### 5-2-1. Mass and volumetric flow of solids (Monte Carlo simulation results)

Figure 5-15 shows the simulation results for continuous variation of the components of MSW generated in New York City. The abscissa shows the MSW sample number. Each sample has several components and, together, they define a

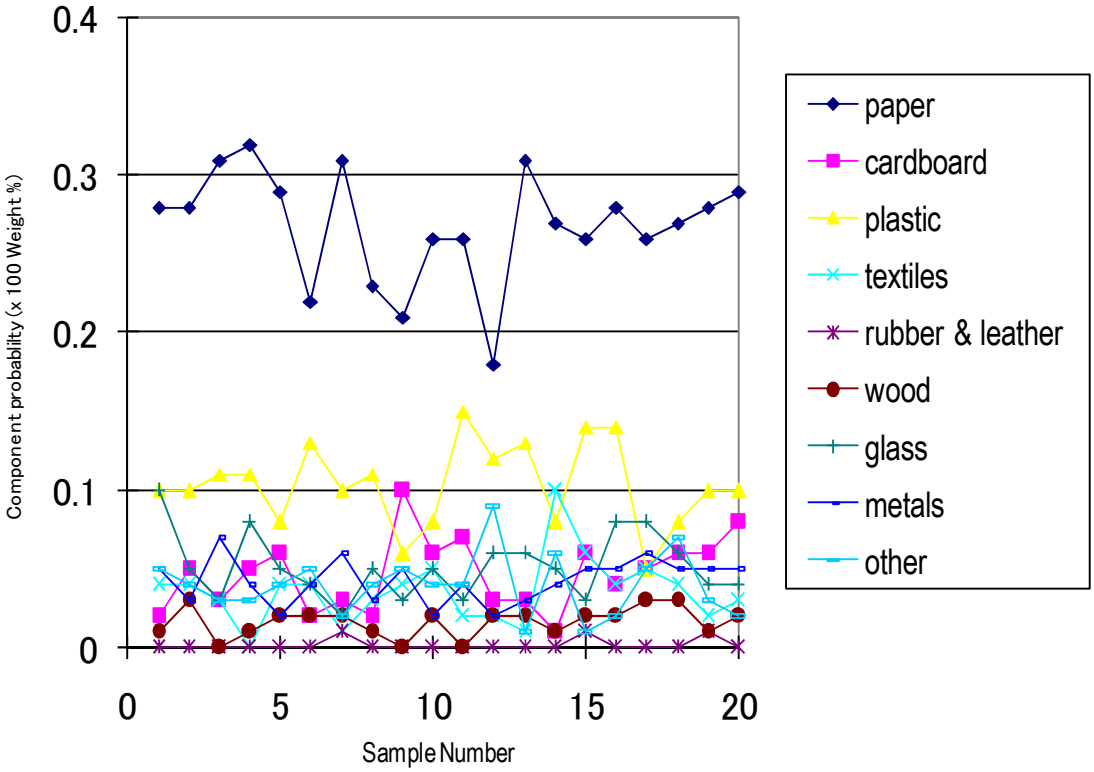


*Figure 5-15: Time series of continuous variation of MSW components by Monte Carlo simulation*

time series for continuous variation of MSW. The first 20 of the 100 samples used are shown in Figure 5-15. The time series made by these samples specifies one of the initial conditions to simulate the combustion process.

The simulation results using the above samples are shown in Figure 5-16. The solid temperature is highest in the middle of the grate which is located around Zone 4, as shown in Figure 5-16 (a) (see Appendices in detail). Near the inlet of the combustion chamber, temperatures of solid waste remain under 371 K because moisture evaporation occurs in this stage and combustion of most components of MSW is limited. Figure 5-16 (b) shows the residual ash in solid (mass %) (see Appendices in detail). From the middle of the grate to the ash discharge end of the grate, the MSW burns well and generates ash until it reaches the burn-out line, which is in Zone 8. Figure 5-16 (c) shows the simulation results of percolation model for transient phenomena (break-up and channeling). It is based on the calculation result of residual ash shown in Figure 5-16 (b). From Zone 5 to Zone 8, each combustion probability is nearly equal to or exceeds the critical probability $P_c$. This indicates that the possibility of break-up and channeling of solid waste after Zone 5 is high and channeling is observed in the lattice of Zone 5.

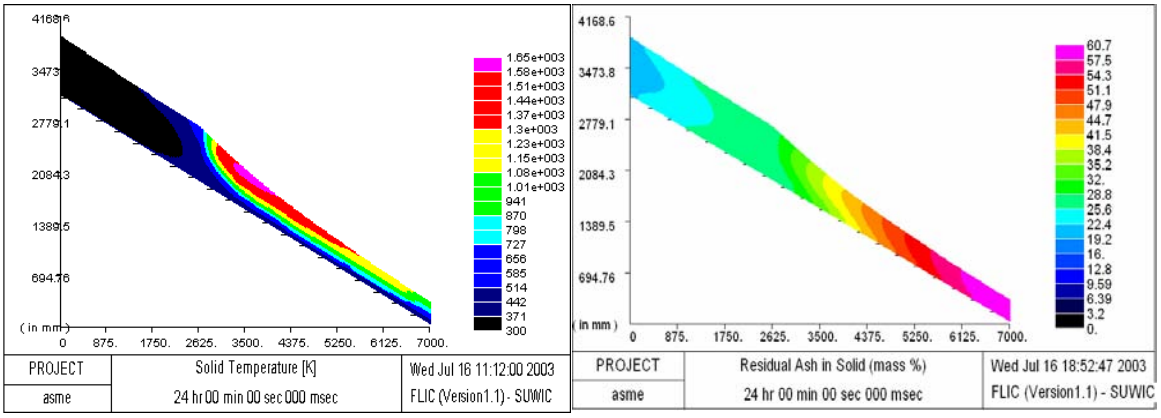


*(a) Solid temperature (K)* *(b) Residual ash in solid (mass %)*

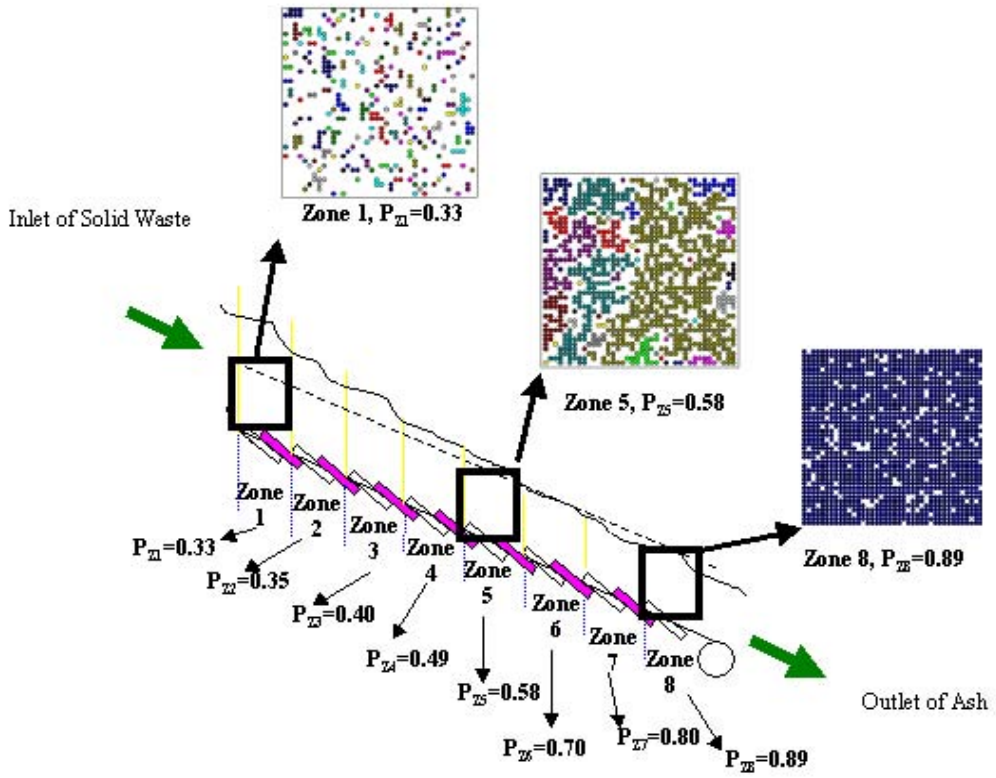


*(c) Result of percolation model for transient phenomena (break-up and channeling)*

*Figure 5-16: Calculation results of the MSW combustion on the Martin grate*

Figure 5-17 shows how much combustion is completed by volume % in the each zone. We assumed that MSW from inlet of the chamber consists of 20 % volumetric voids, i.e., $P_v$ = 0.2. Therefore, for example, solid waste in Zone 1 burns only 13 volume % of total solid waste. The most important combustion phenomena and their most probable occurrences are shown in Figure 5-18. In this study, we assumed $P_v$ = 0.2. $P_c$ is 0.5927 because we specified a square lattice for this percolation model. $P_{ch}$ is the channeling probability and, between $P_c$ and $P_{ch}$, channeling is generated frequently. $P_a$ is the ash probability. This means the burn-out line which means the remaining solid waste does not contain combustible matter. Break-up occurs between $P_{ch}$ and $P_a$.

The simulation results of this combustion model with continuous variation of MSW have provided the temperatures and percentage of residual ash by weight. From that, the volume change (%) from waste to ash has been calculated and the combustion probabilities for each zone have been estimated. The percolation model has shown the mechanism of transient phenomena such as channeling and break-up of solid waste. The governing parameters such as void probability $P_v$, channeling probability $P_{ch}$, critical probability $P_c$, and ash probability $P_a$ were found by this model.

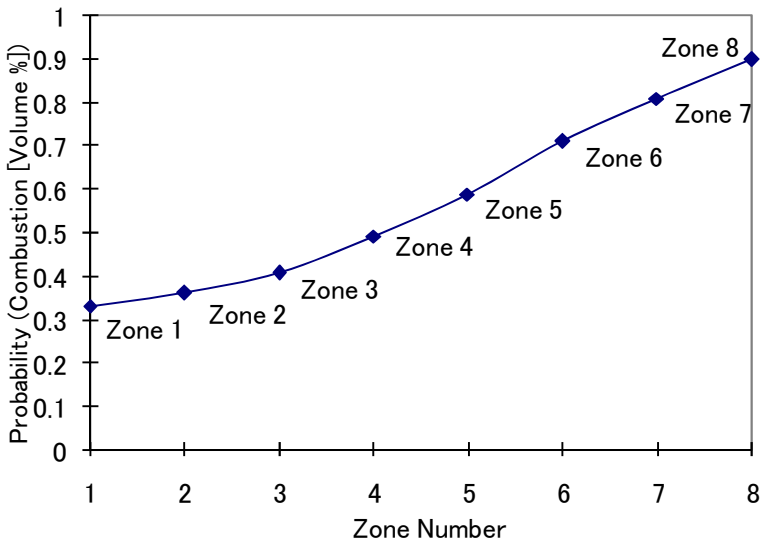


*Figure 5-17: Combustion probability in each zone*

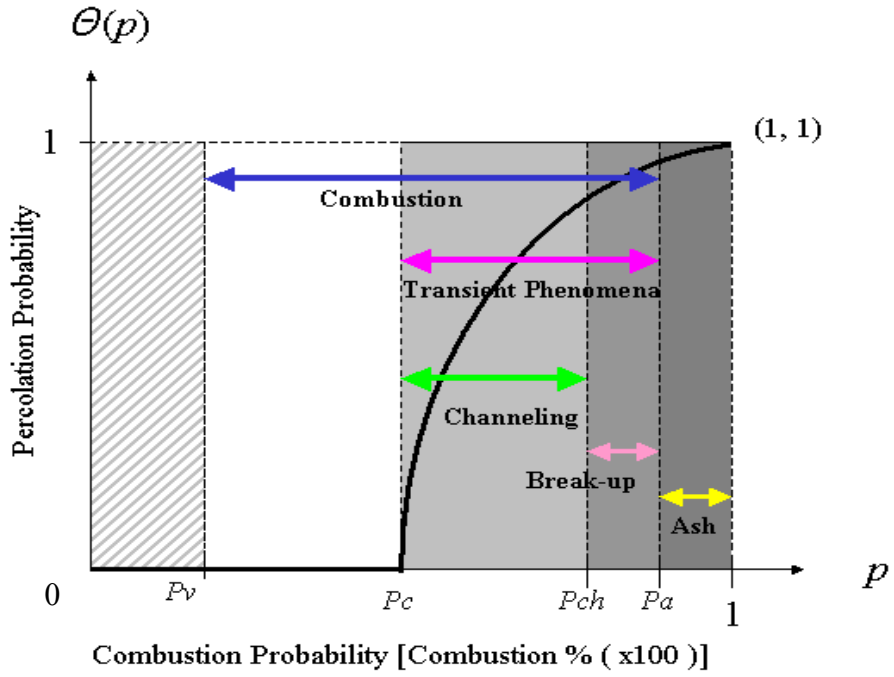


*Figure 5-18: Transient phenomena during the combustion process*

### 5-2-2. Simulation results from the stochastic model for MSW mixing

#### a) One-dimensional simulation

Figure 5-19 shows a simulated "random walk" that represents the particle movement based on a calculation over 46 steps (the required number of calculations varies between different time series because of the stochastic nature of the simulation results). Cell #1 represents the feed end of the grate and cell #16 the end of the grate where the ash falls to the ash pit below. Cell #17 denotes the state of bottom ash. This graph shows how a hypothetical solid particle travels over the reverse acting grate. At each motion of the reciprocating bar, the particle may remain in the same cell or move to the adjacent cell, downward or upward, due to the upward motion of the bars. At the #2 and #5 cells, the particle seems not to move for a while, which, in a multi-layer model of the bed on the grate, would result in mixing with the next layer up (see next section 5-2-2-b, Two-dimensional simulation). The lower graph in Figure 5-19 provides a visual illustration of the behavior of a particle on the moving grate, based on the results of the matrix calculation. The particle actually moves back and forth between cells as indicated by the solid line. For example, between cells #11 and #12, the particle travels back and forth because of the action of the reciprocating bar.

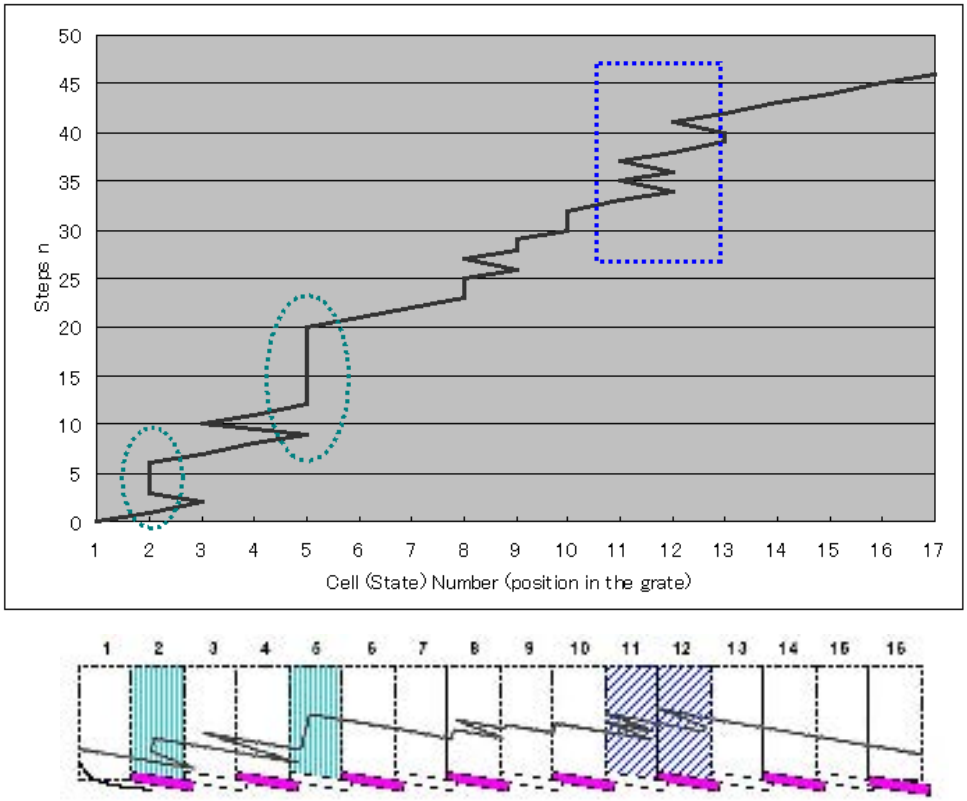


*Figure 5-19: Simulation results of the movement of a solid waste particle on the Reverse Acting Grate: Top graph: tracing a behavior of one particle on the bed. In cells #2 and 5 the particle seems to stay put for a while. In cells #11 and 12, the particle goes back and forth because of the movement of the reciprocating bar. Bottom graph: Visualization of the particle travel based on the results of the calculations shown on top graph.*

Figure 5-20 shows the residence time distributions of solid waste particles with successive motions of the reciprocating bars. Under the combination of downward gravity and upward motion of the reciprocating bars, all particles travel gradually to the outlet. The peak of each particle distribution profile is displaced toward the outlet and the profile becomes much flatter. The solid particles that move slower (particles in the left part of each profile in Figure 5-20 have been pushed

upward by the reciprocating bars. This action contributes to mixing partly combusted material with newly fed solid wastes.

It is evident that solid wastes that are more mixed have a better chance of

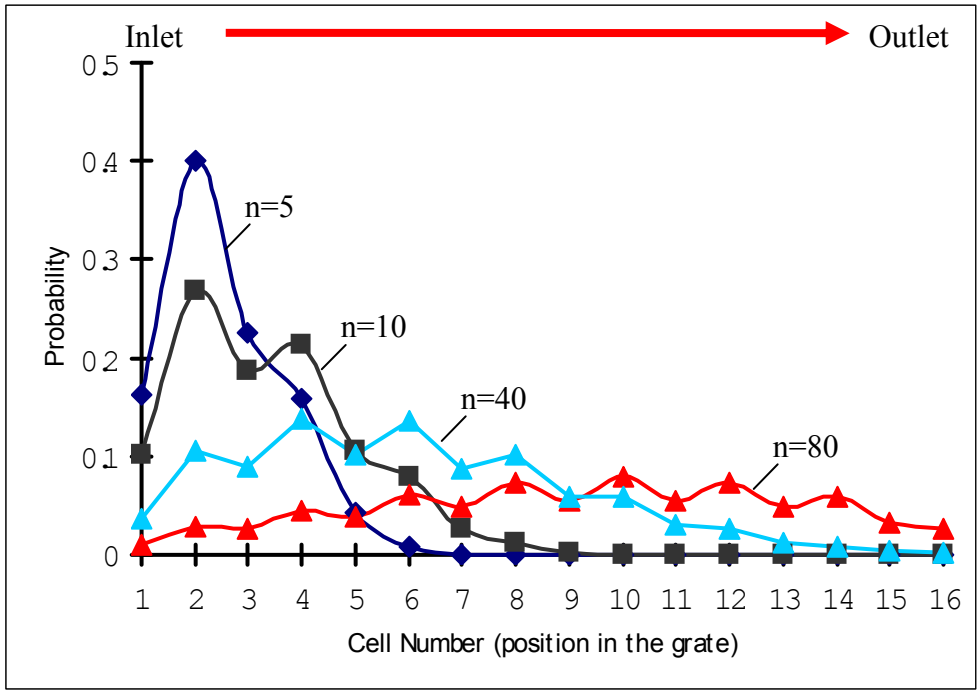


*Figure 5-20. Change in tracer particles distribution profiles over grate with number of movements of reciprocating bars (n=5, 10, 40, 80). The regular perturbations in the n=40 and n=80 profiles are due to the effect of alternatively passing over stationary and reciprocating bars.*

being combusted completely. On the other hand, solid particles that travel faster than the bulk of the solid wastes (particles in the right part of the each profile in Figure 5-20 will not burn completely. Without additional feed coming in, the probability of particles staying in a specific cell, after an infinite number of movements (step $n = \infty$, approaches zero, because all solid particles travel toward the outlet and eventually reach it.

In summery of this section, a new method for investigating mixing on the grate of a WTE combustion chamber, using the one dimensional stochastic model, was presented. This method may provide a useful for predicting the actual path of particles, for a certain grate configuration (frequency of reciprocation bar motion, length of travel, etc.). This information would contribute to the characterization and quantification of the mixing process. In the first test of the one-dimensional stochastic model presented in this section, the bottom layer of the bed, which is in contact with the bars of a reverse acting Martin grate, was simulated. Based on these calculation results, a two-dimensional stochastic model (multi-layer model) for MSW mixing was developed in order to expand the single layer of MSW bed to the multi-layer. The following section (5-2-2-b) shows the results of a two-dimensional stochastic simulation of MSW particle mixing.

**b) Two-dimensional simulation**

Figure 5-21 shows the MSW particle distributions with successive motions of the reciprocating bars. Since the reciprocating bars move at a constant frequency (a typical value is around 11-13 strokes/hour), Figure 5-21 represents residence time distributions (RTD) over the grate. The peak of each distribution is moved toward the outlet of the chamber because all solid waste particles travel from the inlet to the outlet, affected by the motion of the reciprocating bars in combination with the downward force of gravity. The effect of particles passing alternatively over fixed and

reciprocating bars results in the regular perturbations eminently shown in the $n$ = 40 and 80 profiles.

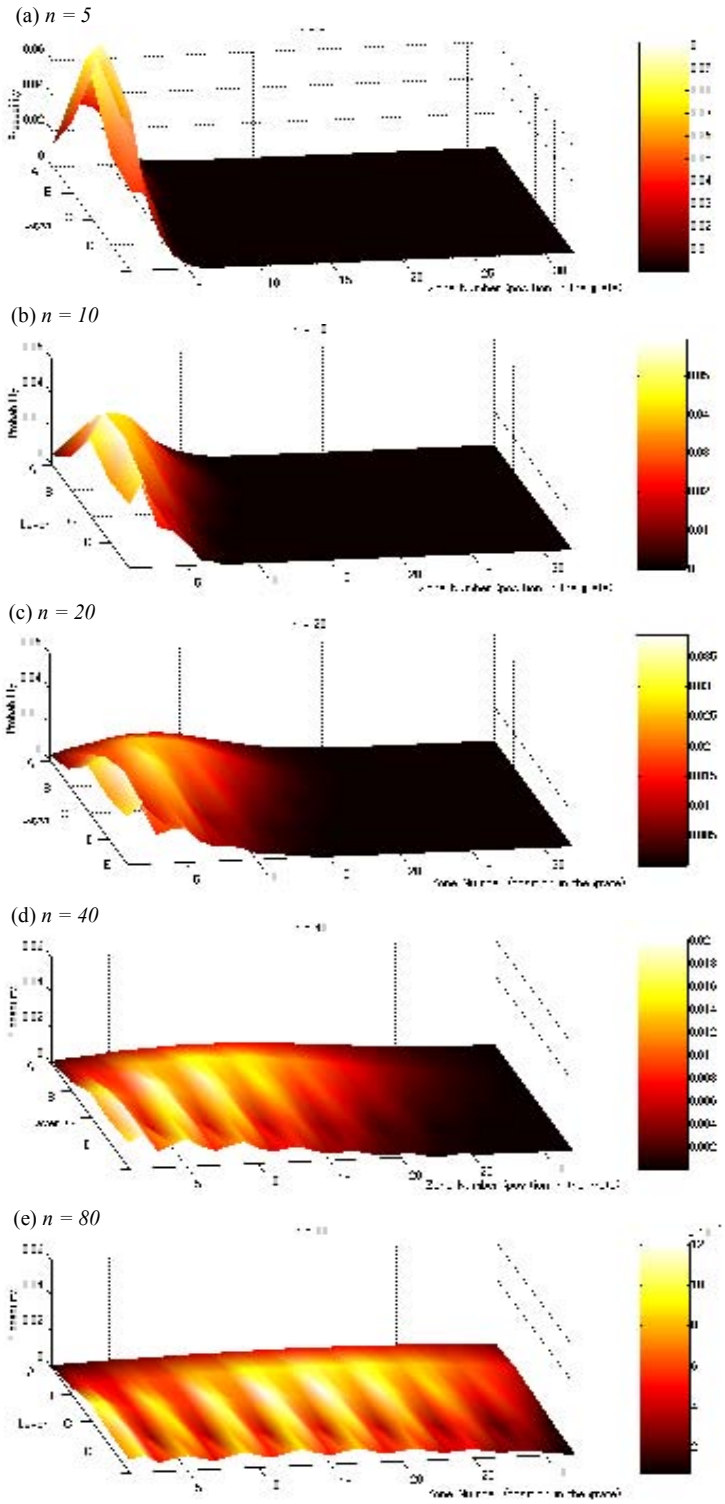


*Figure 5-21: Change in particle distribution profiles over grate with number of movements of reciprocating bars (a) n=5, (b) n = 10, (c) = 20,(d) n = 40,(e )n= 80*

Figure 5-22 shows the motion (paths) of traveling MSW particles in layers of the MSW fuel above the reverse acting grate for various numbers of reciprocating motions. According to the assumptions made in defining probabilities within the matrix ***P***, particles in layer A exhibit the highest movement toward the outlet because layer A is near the surface of the MSW fuel and some particles can slip on the surface or roll down along the surface. The particle path in Figure 5-22 (a) shows that this particle travels mainly in the layer A and B where the probabilities of the movement forward to the outlet direction are higher. In the case of Figure 5-22 (a), the step number n is smallest ($n$ = 67) than in the other cases (i.e., 5-22 (b), (c) and (d)) and the particle has the shortest residence time on the grate. The particle can be located in the surface layer where chemical reaction rates are high, although it has the shortest residence time and path. The path of a particle shown in Figure 5-22 (b) indicates that this particle remained for a long period of time in zones 25-30.

These zones include the burnout point and the particle must be almost ash in an actual combustion chamber. The case shown in Figure 5-22 (c) expresses mixing of the particle in the first half of the chamber (zones 1 to 16). On the other hand, the rest of the path along the second half of the grate (zones 17 to 32) seems smoother. The bottom layer E is the nearest layer to the reciprocating bars and particles in this layer are exposed to the driving force of the reciprocating bars against the feed direction. Figure 5-22 (d) shows a path of a MSW particle that reached ash bin when

$n$ = 401. This indicates mixing of this particle near zone 10 and between zone 20 and 25, due to the movement of the reciprocating bars.

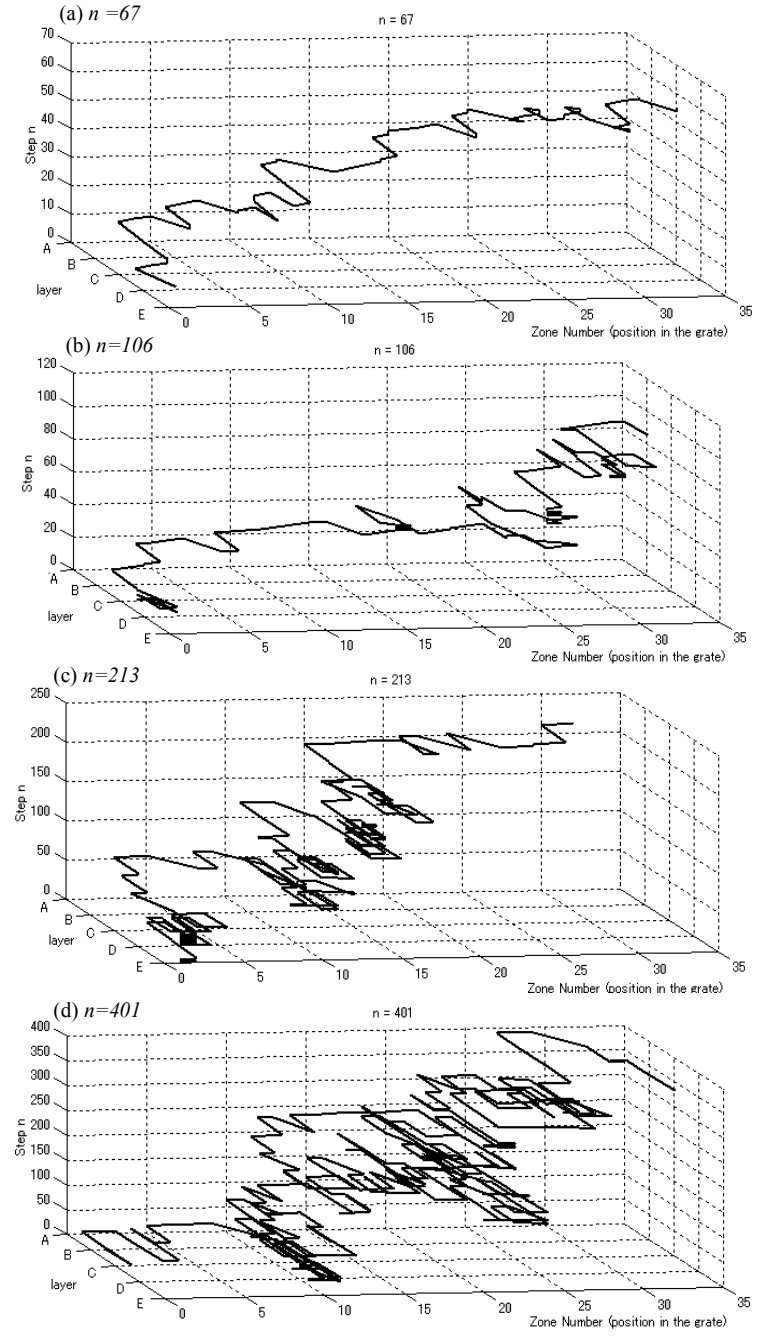


*Figure 5-22: Movements (paths) of MSW particles on the Reverse Acting Grate: (a) n=67, (b) n=106, (c) n=213 and (d) n=401*

In summary, a novel two-dimensional model simulating the mixing of the MSW fuel on the Martin reverse acting grate has been developed using the stochastic simulation. This model can be as a tool for charactering and quantifying the mixing process, although the properties of MSW particles, such as size, shape, and density, was not taken into account. The probabilities in the transition matrix ***P*** were assumed based on the successful results of the one-dimensional model. However, these assumed probabilities were found to be relatively low. Lower probabilities results in longer residence time and more strokes to reach ash bin (for example, as shown in Figure 5-22-d, 401 strokes of reciprocating bars is too high, even though, the particle remained same zones many times in this case). In order to determine these probabilities in transition matrix ***P***, they are measured as shown in section 3-3 and 5-1-2, using full-scale physical section model.

### 5-2-3. Results from mass reduction model

Figure 5-23 shows the simulation results of the gamma distribution discussed in section 4-3-2. Dots represent experimental data and lines are the predicted distribution. As summarized in Table 5-1, the PSD of MSW has an "a" constant value of 2.5 x 100, an $\alpha$ parameter of 4, a $\beta$ parameter of 3.2, a mean $\mu$ of 12.8, a standard deviation, $\sigma$, of 6.4, and a covariance, CV, of 0.5. The PSD of ash resulted in having a constant a value of 0.3 x 100, an $\alpha$ parameter of 12, a $\beta$ parameter of 0.17, a mean $\mu$ of 2.04, a standard deviation, $\sigma$, of 0.5889, and a covariance, CV, of 0.289. Compared with the measured PSDs shown in Figure 5-23, the predicted PDSs have a

similar shape except for the asymptotic tail of the MSW PSD (30-40 cm). This tail group of MSW particles contains a small peak. That is primarily because some of physical phenomena such as compaction and breakage have not been included in this combustion model asyet.

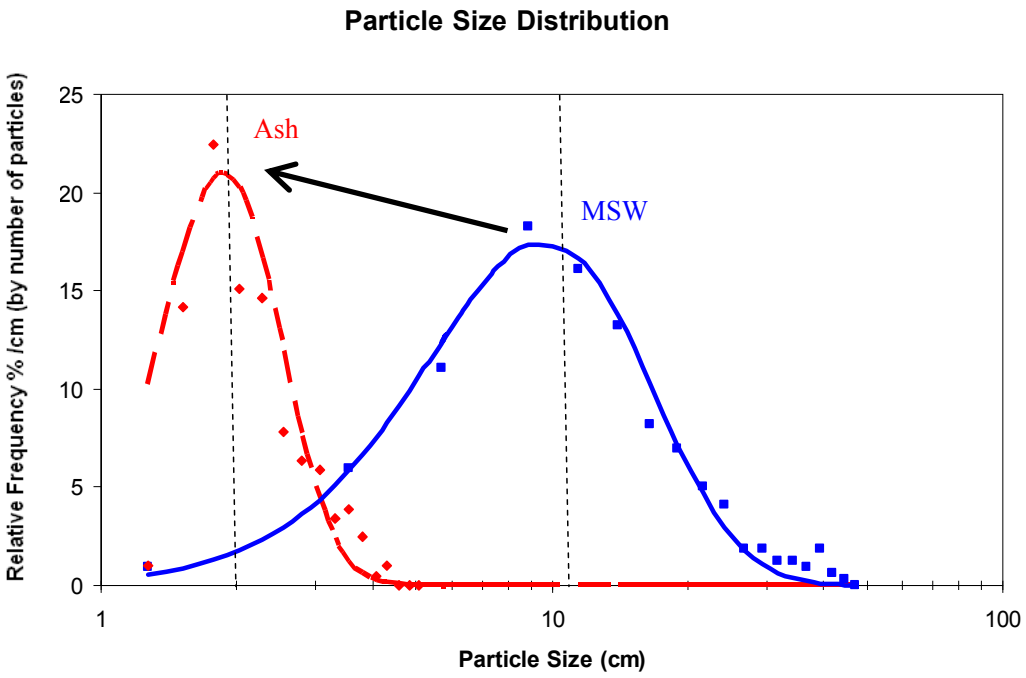


*Figure 5-23: Particle size distributions (PSD) by particle numbers of residential MSW and combined ashes in NYC: (lines: estimated gamma distributions, dots: experimental data)*

| Parameter | *Ash particle size distribution* | | *MSW particle size distribution* | |
|---|---|---|---|---|
| | **Predicted** | **Experimental** | **Predicted** | **Experimental** |
| **Mean μ** | 2.04 | 2.32 | 12.8 | 14.3 |
| **Standard dev. σ** | 0.589 | 0.821 | 6.4 | 8.508 |
| **Covariance CV** | 0.289 | 0.354 | 0.5 | 0.594 |
| **a** | 0.3 X 100 | - | 2.5 X 100 | - |
| **α** | 12 | 7.97 | 4 | 2.83 |
| **β** | 0.17 | 0.29 | 3.2 | 5.045 |

*Table 5-1: Particle size parameters obtained from residential MSW and combined ashes in NYC*

### 5-2-4. Integrating model for flow and mixing with data from the full-scale physical model

Visual representation of the computed particle movement behavior, that is difficult impossible to measure experimentally can be very useful understanding and characterizing the mixing phenomena on the grate. Figure 5-24 shows the calculated movements for 12 particles traveling from section 1 through 32. Each particle travels along different paths in the MSW bed, but trends are consistent for a given size

especially in the vertical (depth) direction. The general trend indicated by the simulation is that small particles tend to migrate downward (toward the grate surface) and large particles tend to migrate upward (toward the free surface) as they move along the bed. This size segregation has been called the Brazil Nut Effect (BNE) (Mohabuth, N., and Miles, N. 2005) and results from the slight differences in vertical probabilities as a function of size. The segregation mechanism we observed in this study is illustrated in Figure 5-25. The moving grates create empty space after one stroke from the top to the bottom position. Immediately, because of the unstable conditions, particles whose size is less than the grate height, can easily drop into the empty space. Larger particles are less likely to drop into this newly created vacancy because their comparatively larger size offers more opposition to easily slipping into this limited empty space. After several reciprocations of moving bars, the size segregation appears as shown in Figure 5-25. This mechanism of size segregation can be observed in rock, sand, powder, and granular movement. Some studies have been carried out employing this vertical selectivity mechanism for electronic waste (Mohabuth, N., and Miles, N. 2005), and for applying separation and recycling technologies to the processing of industrial waste and residential MSW.

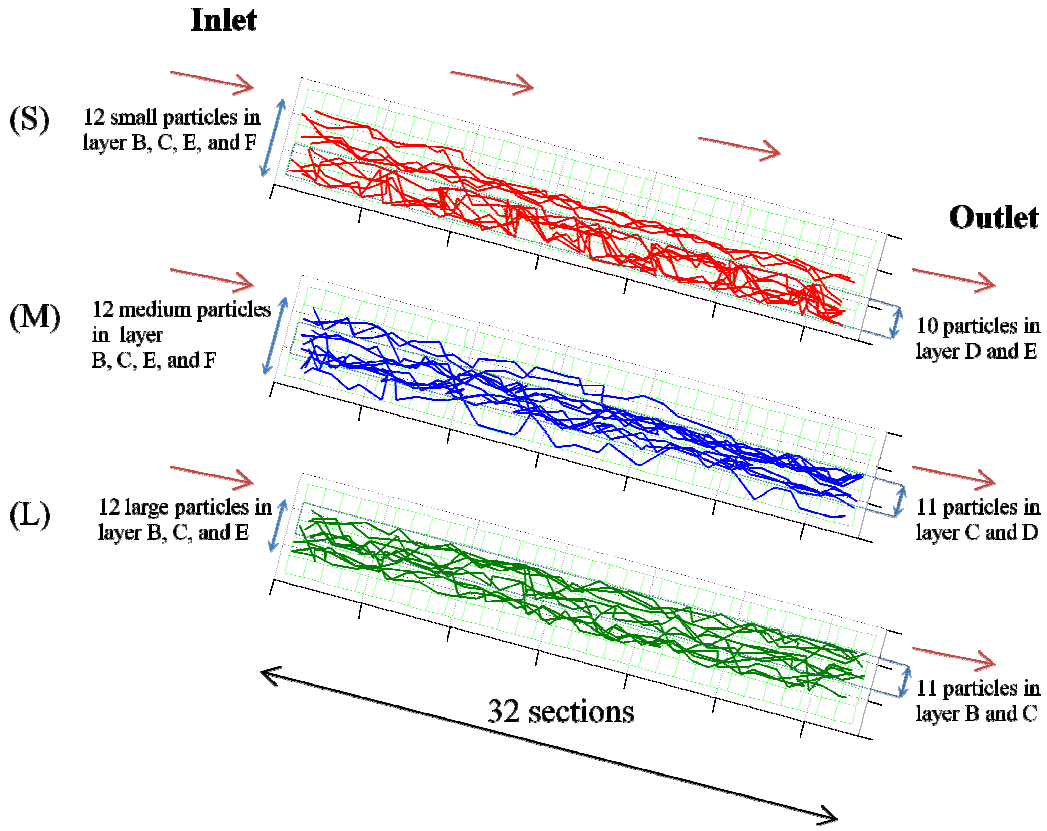


*Figure 5-24: Calculated particle path over the grate as a function of size: small particles (S), medium particles (M), and large (L) particles*

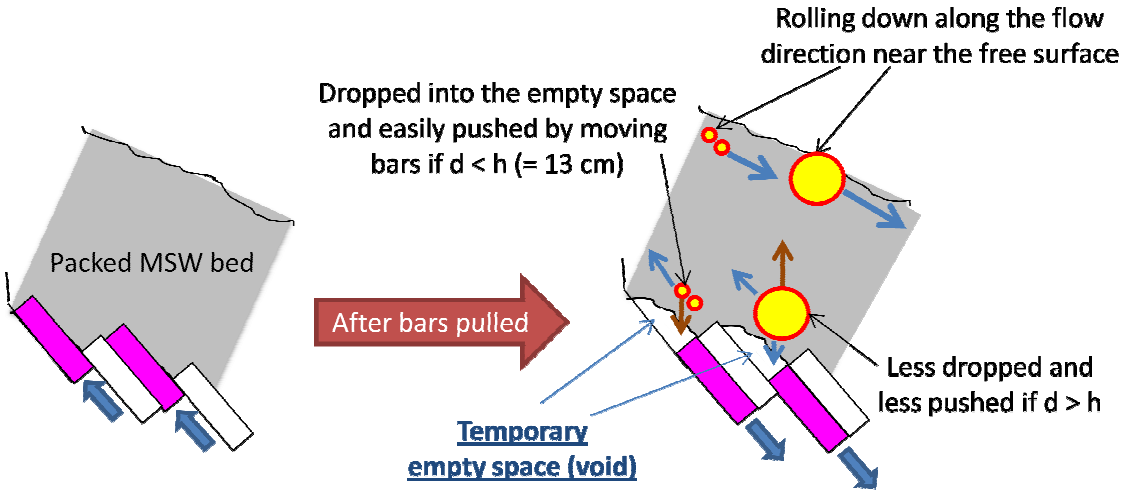


*Figure 5-25: Brazil Nut Effect (BNE) in a packed MSW bed*

Figure 5-26 shows the residence time distributions (RTD, dimensionless concentration versus residence time *t*) for small, medium, and large particles for a grate speed ranging from 15 to 90 reciprocation/hour. Residence time distributions of a flow material were originally defined by Levenspiel (Levenspiel, O. 1999). The motion of the reverse acting grate increases the mean residence time of small and medium particles to 106 min (68%) and 69 min (9%), respectively, while decreasing that of large particles to 51 min (17%). In addition, two peaks of residence time distributions for small particles prominently appeared when the reciprocation speed exceeded 30 recip./hr. As we discussed earlier, it is reasonable that the difference of mean residence times with size comes from the following reasons: (1) Small and medium particles are pushed by the reverse acting grate because their diameters are nearly the same or smaller than the height of the moving bars, *h*. (2) Larger particles are less likely to be caught by the grate so that their motion is less likely to be in

opposition to the flow direction. (3) A special mode of transport, rolling down the top surface along the flow direction, is available exclusively to those particles near the free surface of the bed. These two opposing motions at the bottom and the surface of the bed enhance MSW particle mixing and are responsible for the different residence time distributions. Due to the particle motion behavior (1)-(3), a vertical selectivity mechanism known as the Brasil Nut Effect (BNE) develops that tends to keep small particles in the bottom of the MSW bed. This effect is manifested by the presence of two peaks that appear only in the residence time exit concentration distributions of the small particles. The full data sets of RTDs (C and F diagrams) for grate speed ranging from 15 to 90 recip./hr are shown in Figure 5-27, 5-28, and 5-29.

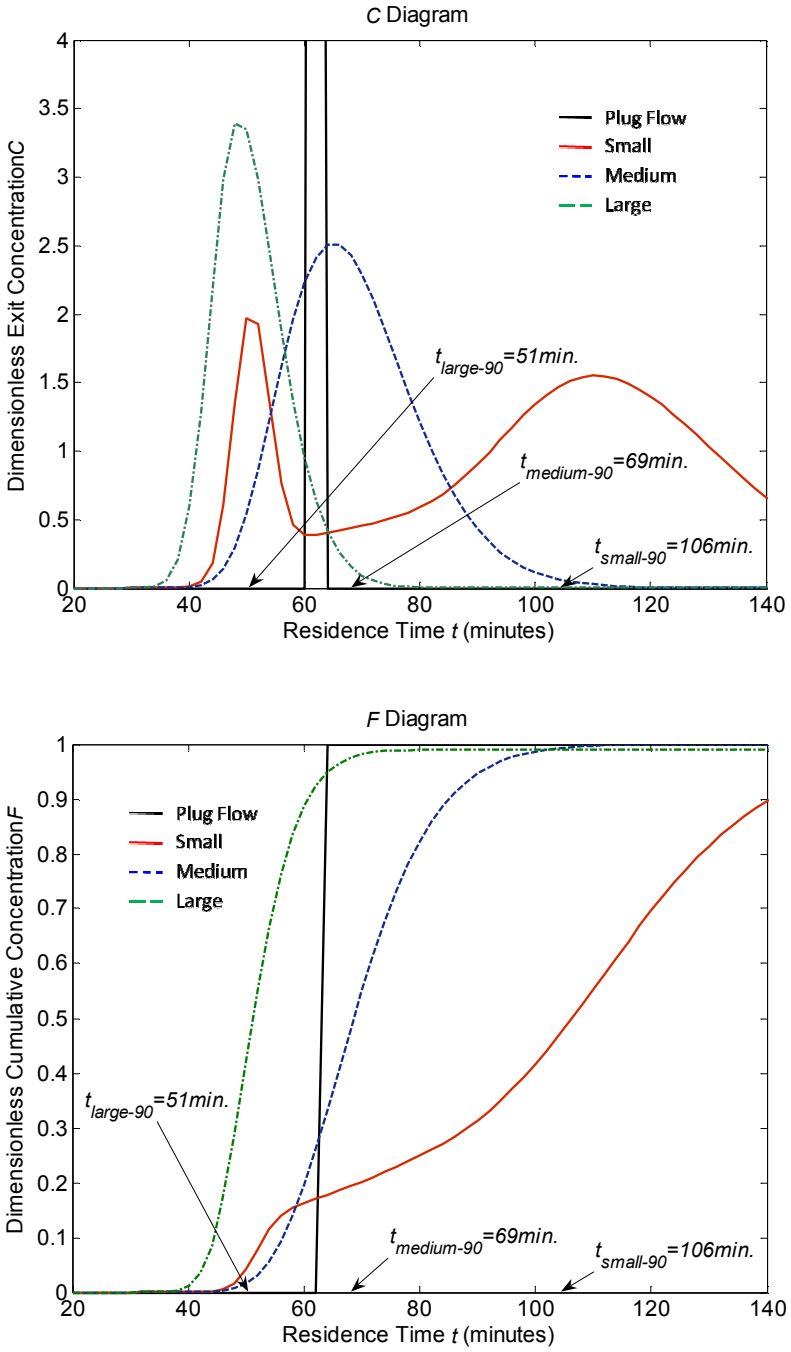


*Figure 5-26: C (top) and F diagrams (bottom) for small, medium, and large particles with a reciprocation speed of 90 recip./hr.*

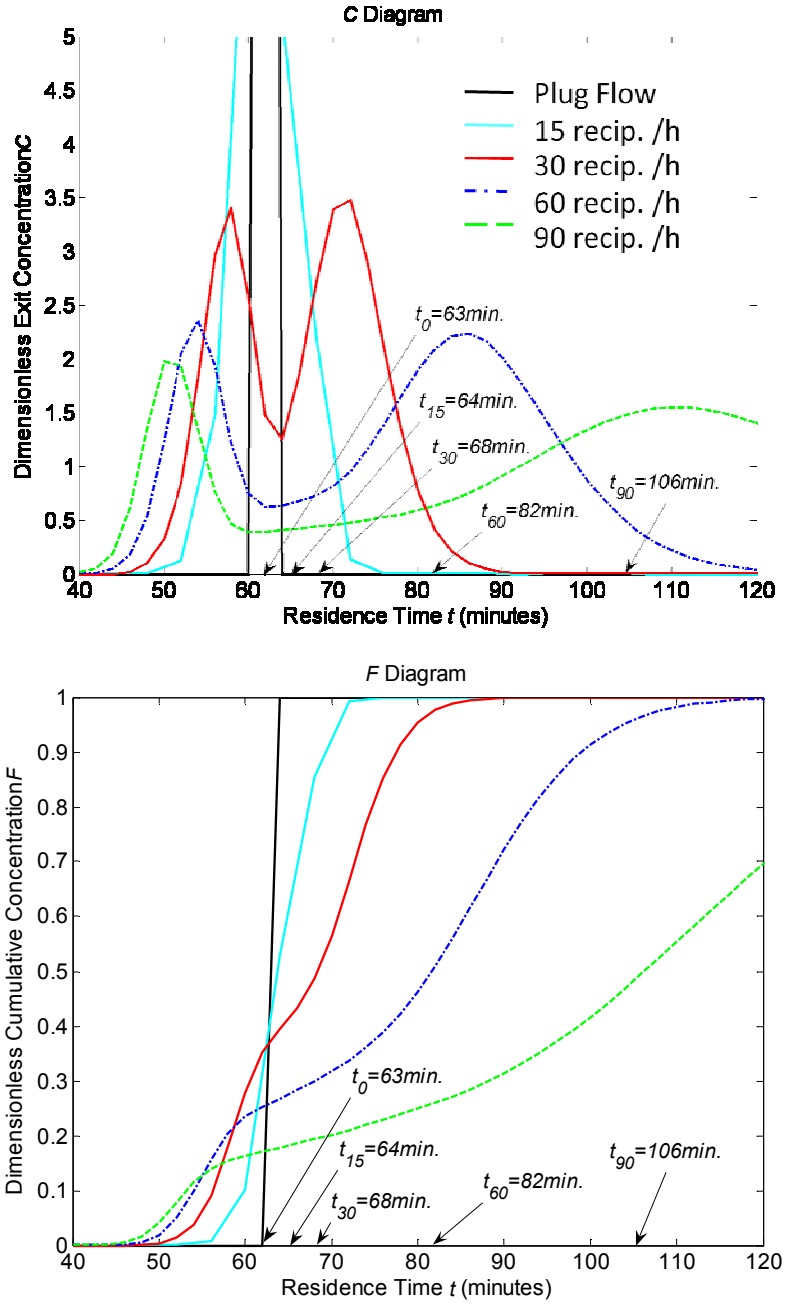


*Figure 5-27: C and F diagrams for small particles: Dimensionless exit concentration C (top) and Dimensionless cumulative concentration F (bottom) versus residence time (min) with different reciprocation speeds ranging from15 to 90 recip./hr*

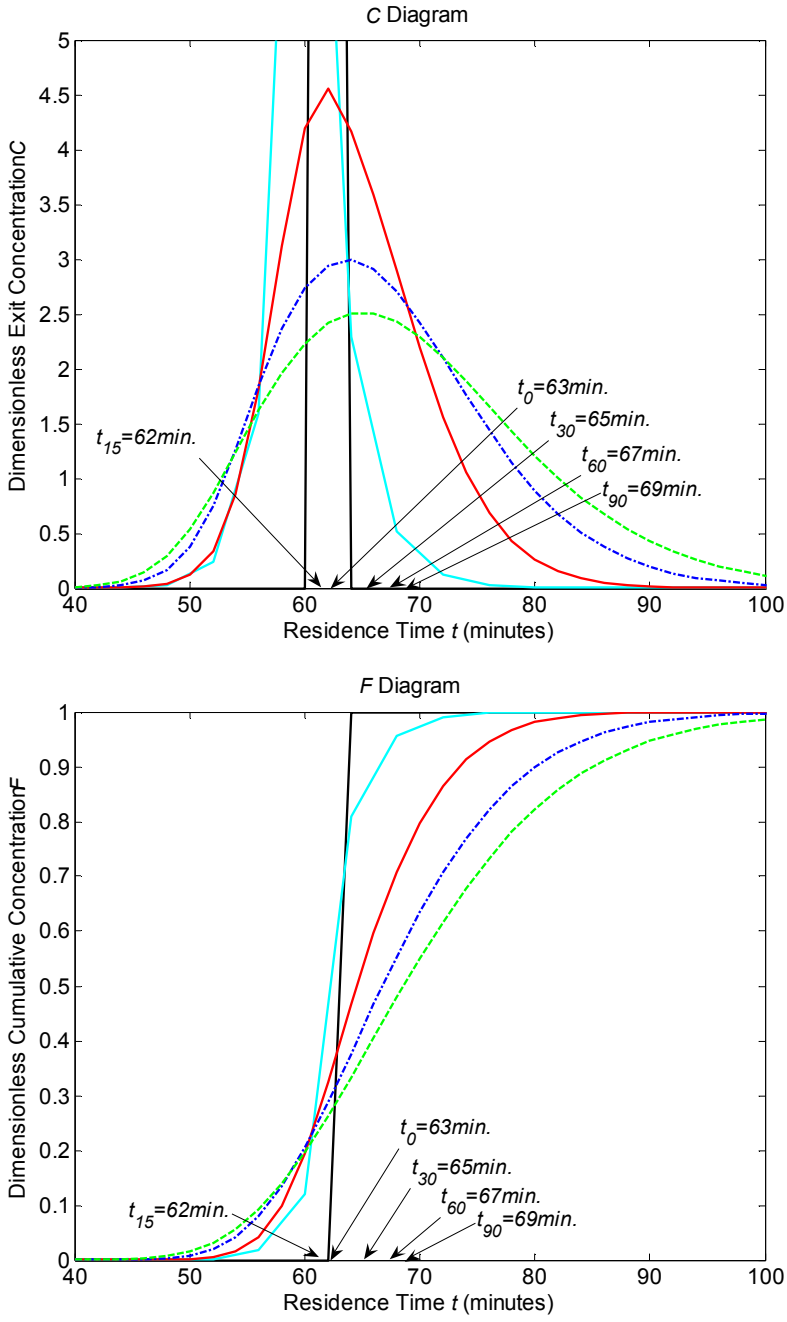


*Figure 5-28: C and F diagrams for medium particles: Dimensionless exit concentration C (top) and Dimensionless cumulative concentration F (bottom) versus residence time (min) with different reciprocation speeds ranging from15 to 90 recip./hr*

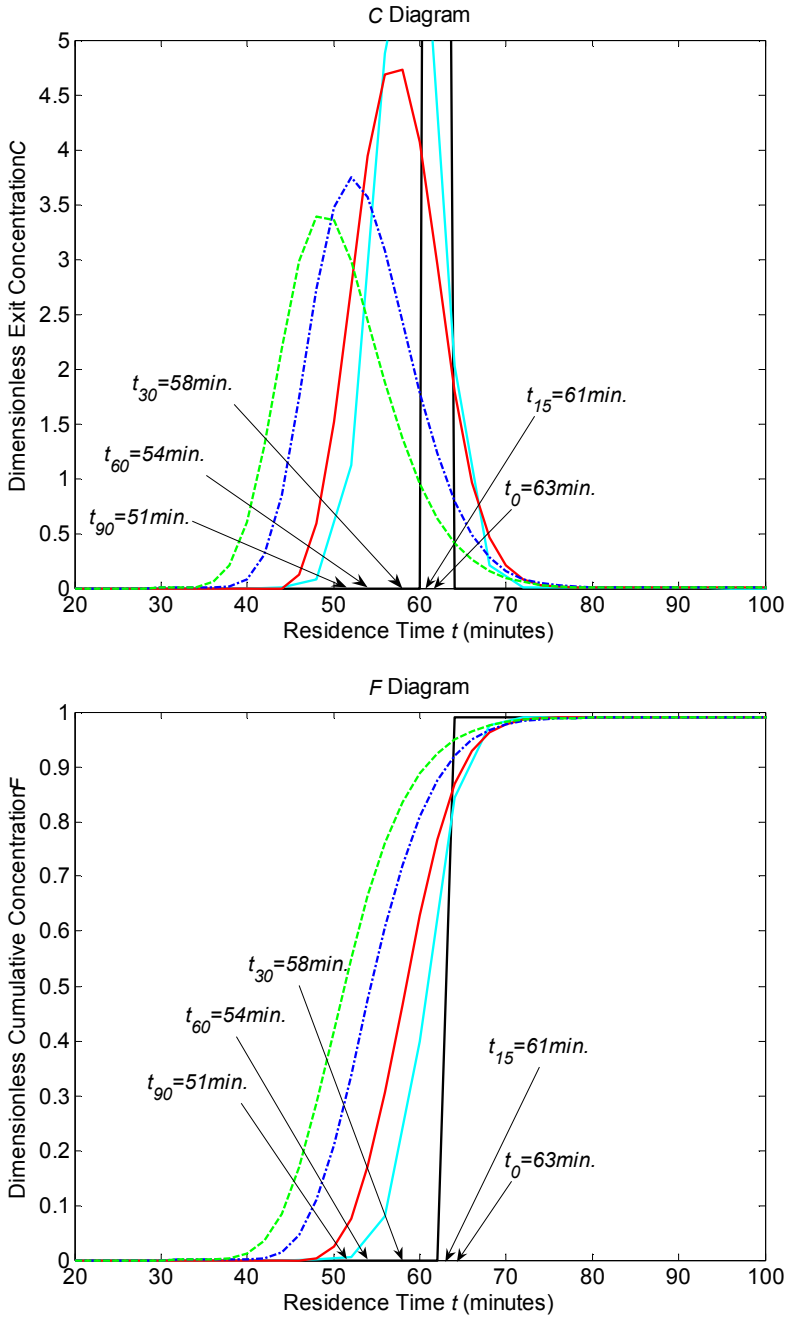


*Figure. 5-29: C and F diagrams for large particles: Dimensionless exit concentration C (top) and Dimensionless cumulative concentration F (bottom) versus residence time (min) with different reciprocation speeds ranging from15 to 90 recip./hr*

**Mixing Diffusion Coefficient**

Figure 5-30 shows the mixing diffusion coefficient $D_e$ for different particle sizes and grate reciprocation speeds $R_r$. The mixing diffusion coefficient $D_e$ for all particle sizes increases linearly for speeds up to 30 recip./hr. The $D_e$ for medium particles has a weak linear relationship with $R_r$, throughout the entire speed range from 15 - 90 recip./hr. In contrast, the coefficient $D_e$ for large particles increases at a much slower rate and reaches a value of about 45 $cm^2$/min when the reciprocation speed reaches 90 recip./hr. For small particles, $D_e$ increases exponentially to 192 $cm^2$/min. For $R_r < 30$ recip./hr, these relationships of grate reciprocation speeds $R_r$ and mixing diffusion coefficient $D_e$ can be described as follows:

$$D_e(R_r, d, h) = \begin{cases} a\left(\frac{d}{h}\right)^2 R_r^{\left(\frac{h}{d+b}\right)} & if\ d < h \\ a\left(\frac{d}{h}\right)^2 R_r^{\left(\frac{h}{d}\right)} & if\ d \geq h \end{cases} \qquad \text{(Eq. 5-1)}$$

where $a$ is a constant ( $\approx 1.1$) and can be considered to be a function of the number of moving bars. The constant $b$ has an approximate value is of 2.8. The parameters $d$ and $h$ are the particle size and height of the moving bars, respectively, whose ratio $d/h$ controls the relationship between $D_e$ and $R_r$. The mixing diffusion coefficients range from 11 to 99 $cm^2$/min and monotonically increase for all particle sizes that with increasing reciprocation speed from 10 to 60 recip./hr. These numbers represent the range at which the reverse acting grate is operated in commercial WTE plants. This range of $D_e$ is in good agreement with the results of full-scale furnace tests in another study (Yang Y.B.et. al., 2005), also shown in Table 5-2. In this full-scale test $D_e$

varies from 27 to 109 $cm^2$/min, though the type and operational conditions of the traveling grate are not specified. Though no mention was made of the tracer size, their densities were given as values 225 and 770 $kg/m^3$. Particle motion along the MSW bed is highly dependent on the experimental conditions such as the tracer size and density as well as physical properties of the bed itself.

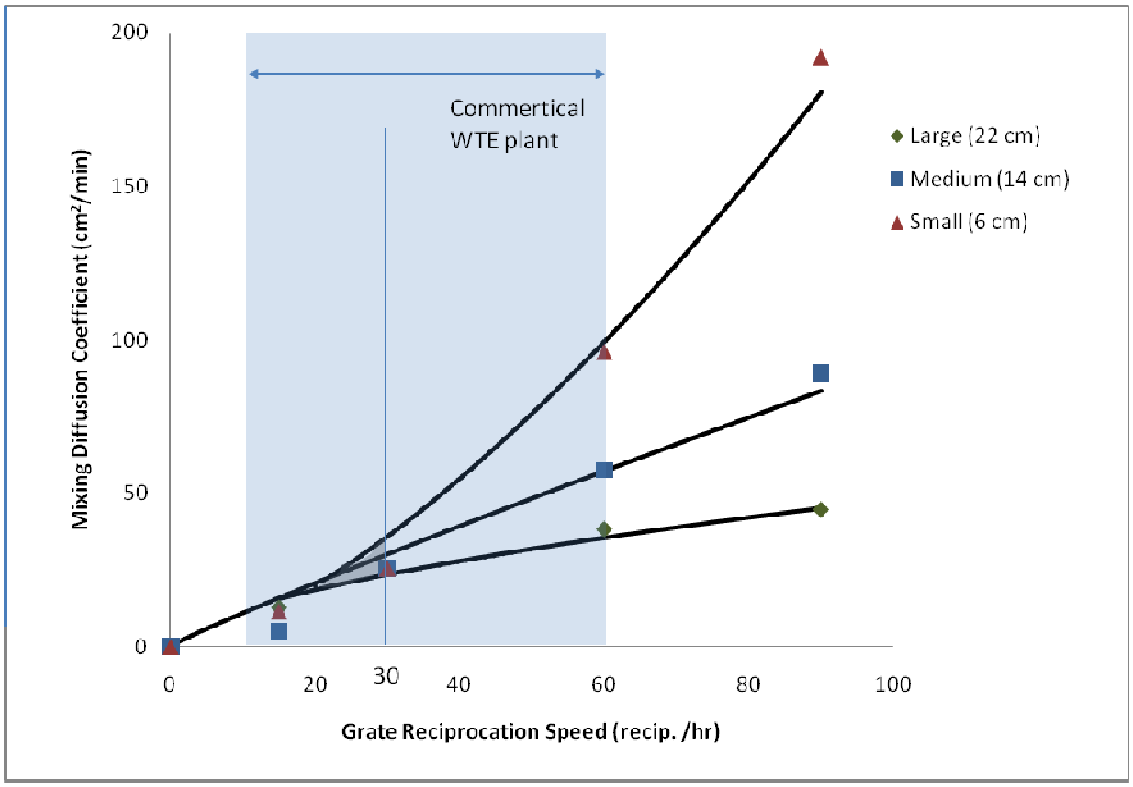


*Figure 5-30: Mixing Diffusion Coefficients versus grate reciprocation speed for different particle sizes*

| Material | Density (kg/m$^3$) | $D_e$ (cm$^2$/min) |
|---|---|---|
| Kaowool boards | 225 | 109 |
| Insulation bricks | 480 | 88 |
| Refractory bricks | 770 | 27 |

*Table 5-2: Mixing Diffusion coefficient with different densities [full-scale test] (Yang et al 2005)*

As noted earlier, in real combustion chambers, the particle size is reduced because of volatilization and combustion processes, and the motion can be characterized as a reacting flow. Pushed by the reverse acting grate, small particles, stay in the combustion chamber longer than medium and large particles, although they require a shorter time for complete combustion. According to a study of wood particle size versus conversion time, the 95% reaction time for small, medium and large sized particles at temperature of 900$^o$C is about 12 min, 46 min, 95 min, respectively (coversion time $\approx d^{1.62}$) (Petek J., 1998) as shown in Figure 5-31. The mixing diffusion coefficient $D_e$ for small particles is higher and they are easily dispersed along the horizontal direction. The advantage of this effect is that small particles that are mostly burned out can transfer their heat to large particles which need more heat and take more time to be thermally processed, especially during the drying and gasification processes. Primary air at room temperature comes from the bottom of the MSW packed bed. Due to the burn-out of the small particles pushed by the reciprocating bars and due to the high residence times at the bottom of the MSW bed, the primary air is warmed up by these small particles. The burn-out particles that

turn into ash have a higher heat capacity than MSW and so they transfer heat to the large particles and the primary air. Operators of the reverse acting grate have observed that, within the range of 15 to 90 recip./hour, "the speed of the reciprocating bars does not look that it affects burnout of the entire MSW bed." This study showed that this is due to the fact that the grate motion effects only small/medium particles of diameters less than the bar height, and whose mass volume is less than 20% of a typical MSW (Nakamura, et al 2008). In the future research, when the stochastic model is combined with particle size change due to combustion, the stochastic model simulation will become much more complicated, because the Markov property will be applicable. In this case, the calculation should be carried out for each single time step (reciprocation), since the initial condition, instead of only the previous step.

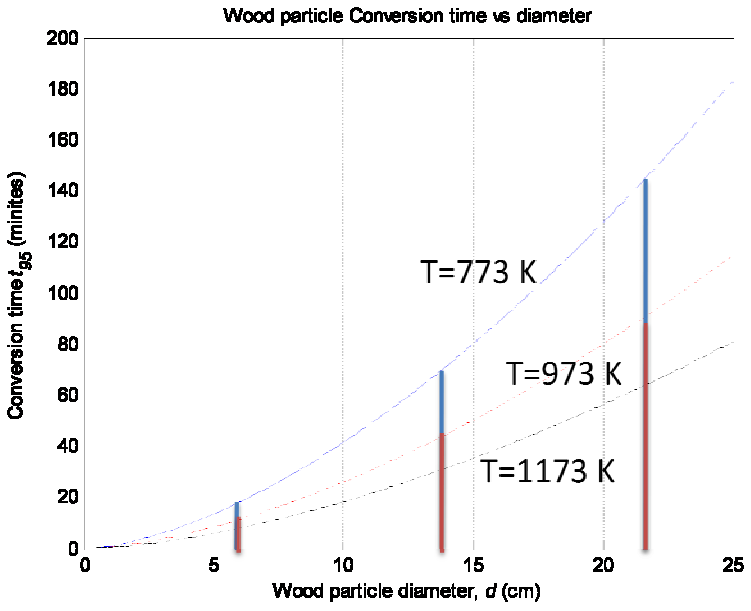


*Figure 5-31: Wood particle conversion time vs particle diameter (Petek J, 1998)*

# Chapter 6: Conclusions

The principal findings of this study can be summarized as follows:

1. In sphericity distributions, the peak of the MSW particles was found to be at 1.5 and of the ash particles at 2. The Aspect Ratio Distributions are 1.2 and 1.4 and the Roundness Distributions 1.3 and 1.4, respectively.

2. The movement and state diagram (transition graph) of three particle sizes (small, medium, and large) at different MSW bed heights (20, 40, 60, and 80 cm) were estimated by means of a full scale physical model of the reverse acting grate. Tracer particles exhibit a different behavior in different cells. For example, a tracer particle located in the bottom of the bed cells (layer E) moves quickly because it is pushed by a reciprocating bar.

3. The probability of particle movement with bed height (layer) of MSW was calculated. All sizes of tracers have the highest probabilities in the bottom layer E; the next highest probability of particle movement is in the top layer B (60-80 cm in the physical model, when the MSW in the physical model was loaded over 80 cm). In the top layer, the tracer particles can slide or roll easily along the surface of the bed because there are no particles resting on them.

4. The percolation model has shown the mechanism of transient phenomena such as channeling and break-up of solid waste. The governing parameters such as void probability $P_v$, channeling probability $P_{ch}$, critical probability $P_c$, and ash probability $P_a$ were determined by using this model.

Also a novel two-dimensional model simulating the flow and mixing of the MSW fuel on the Martin reverse acting grate was developed using the stochastic simulation. This model can be a useful tool in characterizing and quantifying the flow and mixing phenomena on a combustion grate:

5. Different particle sizes result in different residence times according to the Brazil Nut Effect (BNE): Larger particles rise to the surface while smaller particles migrate to lower depths of the bed where the reciprocating bars push them backwards against the main direction of flow due to the gravity force.

6. The motion of the reverse acting grate, at speeds ranging from 15 to 90 recip./hr, resulted in the net effect of increasing the mean residence time of small and medium sized particles by 68 % and 9%, respectively, while decreasing that of large particles by 17%.

7. The calculations of the mixing diffusion coefficient $D_e$ showed that it was affected principally by the ratio of the height of reciprocating bars, $h$, to the diameter of the tracer particle. Although the physical model tests were all

carried out at one $h$ value (13 cm), the results showed conclusively that the diffusion coefficient $D_e$ for a given particle size distribution will increase with grate bar height.

8. A grate speed does not affect burnout of the entire MSW bed. This is due to the fact that the grate motion effects only small/medium particles of diameters less than the bar height, and whose mass volume is only 18% of the total NYC-MSW. Pushed by the reverse acting grate, small particles, stay in the combustion chamber longer than medium and large particles, although they require a shorter time for complete combustion (coversion time $\approx d^{1.62}$). The advantage of this effect is that small particles that mostly burned out can easily transfer their heat to large particles which need more heat and take more time to be thermally processed, especially during the drying and gasification processes.

**Suggestions for Future Work**

This study developed a quantitative analytical tool for examining the mixing of solid waste particles of different sizes during the combustion process in a WTE chamber. The results can be used to assist in the evaluation of operational parameters as well as geometric parameters of a reverse acting grate. The combination of stochastic and full-scale physical modeling can also be used for comparing and

evaluating various types of traveling grate systems and designing the next generation of combustion chambers. Suggestions for future work are as follows:

1. The forward acting and roller grate systems can be investigated by means of full-scale physical models and stochastic simulation, as was done for the reverse acting grate in this study.

2. A combination of traveling grate systems such as the reverse acting grate and roller grate, or of parts of the reverse acting grate moving at different reciprocating speeds can be investigated using full-scale physical models and stochastic simulations, as illustrated in Figure 6-1

3. Analysis of the mixing phenomena for different shapes and densities of MSW particles, along with the size effect investigated in this study, is necessary to more accurately simulate the actual particle motion in the combustion chamber of an MSW packed bed.

4. A combustion model can be combined with this stochastic mixing model. The effect of mixing phenomena for different operation conditions (reciprocation speeds) on the drying, gasification, and combustion stages, can be analyzed. In this case, the stochastic model simulation will become more complicated, because losing its Markov property. The calculation should be carried out in each single time step (reciprocation).

5. The Discrete Element Method (DEM), based on Newtonian equations, may be popularly used for mathematical simulation of MSW mixing and combustion, when much faster computers become available in the future. Currently DEM has started being used for solid fuel conversion on forward acting grate (Simsek et. al. 2008).

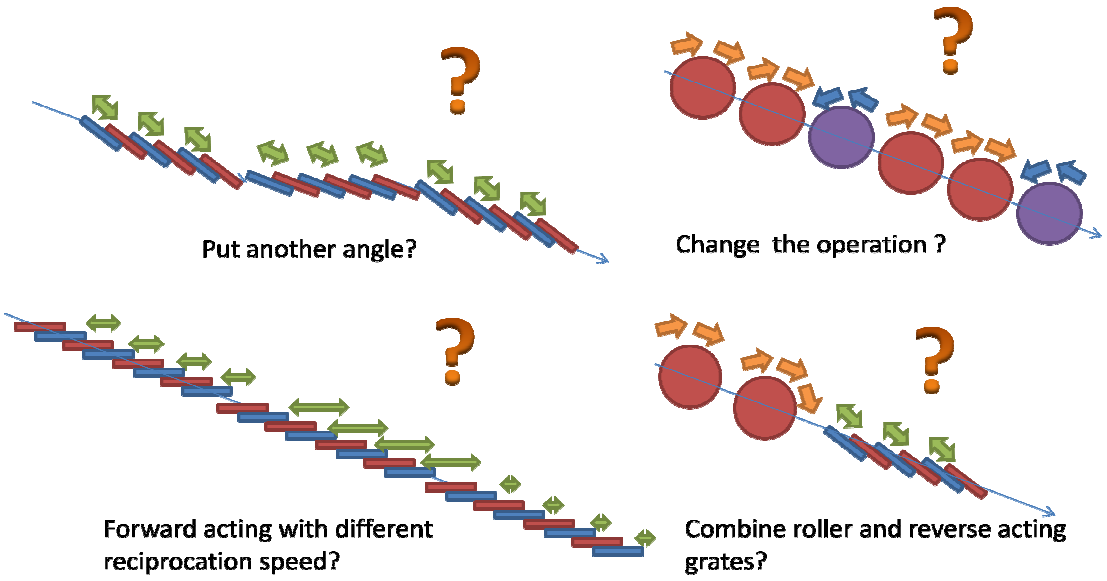


*Figure 6-1: Stochastic models, calibrated by full scale grate tests, can simulate concept design for novel traveling grate systems*

## References

ANSYS, Inc., CFX software for thermal and fluid simulation http://www.ansys.com/default.asp

Allen, Terence, "Particle Size Measurement Volume 1, Powder Sampling and Particle Size Measurement," Fifth Edition, Powder Technology Series, Chapman & Hall (1997)

Aoun-Habbache, M., M. Aoun, H. Berthiaux, and V. Mizonov (2002), "An experimental method and Markov chain model to describe axial and radial mixing in a hoop mixer." *Powder Technology* **128**, pp. 159-167.

Anthony, D. B., Howard, J. B., Hottel, H. C., and Meissner, H. P. (1975). "Rapid devolatilization of pulverized coal." *Fifteenth Symposium (International) on Combustion, The Combustion Institute, Pittsburgh,*.

Beckmann**,** M. Scholz, R. "Residence Time Behaviour of Solid Material in Grate Systems," Proc. INFUB 2000, 5th European Conference on Industrial Furnaces and Boilers, Porto, Portugal, 11.-14. 04. 2000.

Bowen, William A. Digital Atlas of NYC. California Geographical Survey (1997), http://130.166.124.2/ny_3.html (accessed June 6, 2004)

Beckmann, M. and Scholz, R., Simplified mathematical model of combustion in stoker systems. Third European Conference Industrial Furnaces Boilers 18/21 (1995), pp. 61–70.

Beckmann, M., Scholz, R., “Residence Time Behaviour of Solid Material at Grate Systems.” *Proc. INFUB 2000, 5th European Conference on Industrial Furnaces and Boilers*, Porto, Portugal, 11.-14. 04. (2000).

Bremaud, P. (1991): “Markov Chains Gibbs Fields, Monte Carlo Simulation, and Queues.” Springer.

Broaddbent, S. R., Hammersley, J. M. “Percolation Processes I. Crystals and Mazes,” Proceedings of the Cambrigde Philosophical Society 53 (1957), 629-641

Badzioch, S., and Hawksley, P. G. W. (1970). "Kinetics of Thermal Decomposition of Pulverized Coal Particles." *Ind. Eng. Chem*, 9, 521.

Bruch, C., Peters, B., and Nussbaumer, T. (2003). "modelling wood combustion under fixed bed conditions." *Fuel*, 82, 729-738.

Campbell, G., M., Webb, C. (2001). On predicting roller milling performance Part I: the Breakage equation. Powder Technology 115 pp. 234-242

Chejne, F., Hernandez, J. P., Florez, W. F., and Hill, A. F. J. (2000). "Modelling and simulation of time-dependent coal combustion processes in stacks." *Fuel*, 79, 987-997.

Chern, J. S., and Hayhurst, A. N. (2004). "Does large coal particle in a hot fluidised bed lose its volatile content according to the shrinking core model?" *Combustion and Flame*, 139, 208-221.

Clustan Ltd. Clustan software for cluster analysis for solving classification problems http://www.clustan.com/

Cho, K. W., Park, H. S., Kim, K. H., Lee, Y. K., and Lee, K. H. (1995) “Estimation of the heating value of oily mill sludges from steel plant, ” Fuel Vol. 74 No. 12, pp. 1918-1921

Essenhigh, R. H. and Kuo, T. J. (1970): “Combustion and Emission Phenomena in Incinerators: Development of Physical and Mathematical Models of Incinerators, Part1: Statement of the problem.” Proceedings of the National Incinerator Conference, ASME, New York, pp. 261-271.

ECOMB AB, The Ecotube system for optimizing combustion processes and principally, http://www.ecomb.se/

Everson, R., Heomagus, H., and Kaitano, R. (2005). "The modeling of the combustion of high-ash coal-char particles suitable for pressurised fluidized bed combustion: shrinking reacted core model." *Fuel*, 84, 1136-1143.

Fluent Inc., Fluent software, commercial computational fluid dynamics (CFD) http://www.fluent.com/

Gaur, S., and Reed, T. B. (1998). *Thermal Data for Natural and Synthetic Fuels*, Marcel Deeker, Inc.IWSA (International Solid Wastes Association), Energy from Waste, State-of-the Art Report, www.wte.org.

Gohlke, O., and Busch, M., “Reduction of combustion by-products in WTE plants: O2 enrichment of underfire air in the MARTIN SYNCOM process,” Chemosphere 42 (2001) 545-550

Gbor, P. K. Jia, C. Q. (2004). Critical evaluation of coupling particle size distribution with the shrinking core model, Chemical Engineering Science 59 pp. 1979-1987

Grimmett G., “Percolation” Springer (1991)

Heidenreich, C. A., Yan, H. M., and Zhang, D. K. (1998). "Mathematical modelling of pyrolysis of large coal particles - estimation of kinetic." *Fuel*, 78, 557-566.

Homma, S., Ogata, S., Koga, J., and Matsumoto, S. (2005). "Gas-solid reaction model for a shrinking spherical particle with unreacted shrinking core." *Chemical Engineering Science*, 60, 4971-4980.

Hwang, C. L., and Hogg, R. (1980). "Diffusive mixing in flowing powders." *Powder Technology*, 26(1), 93-101.

Japanese Advanced Environment Equipment: Mitsuhishi Martin Refuse Incinerator: *http://nett21.gec.jp/JSIM_DATA/WASTE/WASTE_3/html/Doc_435.html*

Jentsch, T., Beckmann, M., Davidovic, M., and Biollaz, S. (2003). "Investigation of Heavy Metal Release during Thermal Waste Treatment on a Forward-Acting Grate by Means of Radiotracers." *Chemical Engineering & Technology*, 26(6), 691 - 696.

Kaufman, S. M., Glodstein, N., Millarth K., Themelis, N.J., “The State of Garbage in America,” BIOCYCLE, January (2004), 31-41

Kira et al., Development of New Stoker Incinerator for Municipal Solid Wastes Using Oxygen enrichment, Mitsubishi Heavy Industiries Technical Review, Vol.38 No.2 (2001) p.78

Klasen, T. and Goerner, K. “Numerical Calculation and Optimization of a Large Municipal Solid Waste Incinerator Plant,” IFRF Combustion Journal, February (2002) ISSN 1562-479X

Kobayashi, H., J. B. Howard, and Sarofim, A. F. (1977). "Coal Devolatilization at High Temperature." *Int. Symp. on Combust., Combustion Institute, Pittsburgh*, 411

Kunii, D., and Levenspiel, O. (1991). *Fluidization Engineering*, John Wiley & Sons, Inc., Butterworth, Boston, MA.

Levenspiel, O. (1999). *Chemical reaction engineering*, John Wiley & Sons, Inc.

LECO Co. Ultimate analysis of the elements C, H, N, S and O Downloadable literature http://www.leco.com/organic/elementalanalyzers/chns.htm

Lim, C. N., Goh, Y. R., Nasserzadeh, V., Swithenbank, J., Riccius, O, “The modelling of solid mixing in municipal solid incinerators,” Powder Technology 114 (2001) 89-95

Martin GmbH: The MARTIN reverse-acting grate *http://martingmbh.de/englisch/index2.htm*

Mohabuth, N., and Miles, N. The recovery of recyclable materials from Waste Electrical and Electronic Equipment (WEEE) by using vertical vibration separation, Resources Conservation & Recycling 45, 60-69 (2005)

Nakamura, M., Zhang, H., Millrath, K., and Themelis, N. J. ( 2003). "Modeling of Waste-to-Energy Combustion with Continuous Variation of the Solid Waste Fuel." *2003 ASME ICMEE, Washington, D.C.*

Nakamura, M., and N. J. Themelis, "Modeling of Solid Waste Flow and Mixing on the Traveling Grate of Waste- to-energy Combustion Chambers," *Proc. 12th annual North American Waste To Energy Conference (NAWTEC12)*, Georgia. (2004)

Nakamura, M., Castaldi, M.J., and Themelis, N.J. (2005). Measurement of Particle Size and Shape of New York City Municipal Solid Waste and Combustion Residues Using Image Analysis," Proc. 16th Japan Society of Waste Management Experts (JSMWE) Fall Conference, pp. 1-3, Sendai, Japan

Nakamura, M., Castaldi, M.J., and Themelis, N.J., (2008)"A 2-dimensional stochastic modeling for Municipal Solid Waste (MSW) particle mixing within a waste-to-energy (WTE) combustion bed" submitted to International Journal of Thermal Sciences

Petek J., Experimentelle Untersuchung der Pyrolyse in inerter und reaktiver Atmosphare unter den Bedingungen der Wurfbeschickung, PhD thesis, TU Graz, (1998)

Peters, B., Dziugys, A., Hans Hunsinger, and Krebs, L. (2005). "An approach to qualify the intensity of mixing on a forward acting grate." *Chemical Engineering Science*, 60(6), 1649-1659.

Peters, B. (1994). "A model for numerical simulation of devolatilization and combustion of waste material in packed beds." *KERNFORSCHUNGSZENTRUM KARLSRUHE, KARLSRUHE (GERMANY).*

Peters, B., Schroder, E., Bruch, C., and Nussbaumer, T. (2002). "Meaturements and particle resolved modelling of heat-up and drying of a packed bed." *Biomass and Bioenergy*, 23, 291-306.

Reindorf, T., and Vodegel, S., "Dynamic Grate-Model as a Tool for the Optimization of Thermal Waste Treatment Plants," CUTEC-Institut GmbH, Germany

Ruf, John Adam, "Particle Size Spectrum and Compressibility of Raw and Shredded Municipal Solid Waste," The University of Florida, Ph.D. Thesis (1974)

Simsek, E., Brosch, B., Wirtz S., Scherer, V., Krüll, F., "Numerical Simulation of Solid Fuel Conversion on a Forward Acting Grate with a Coupled CFD / Discrete Element Method (DEM)" INFUB-8th European Conference on Industrial Burners and Furnaces, Vilamoura, Portugal, March 25-28, 2008-03-27

Smoot, L. Douglas, and Smith, Philip J., "Coal combustion and gasification," The Plenum Chemical Engineering Series, Plenum (1985)

Sohn, H. Y. (1973). "On the maximum temperature rise in gas-solid reactions." *AIChE Journal*, 19(1), 191

Tchobanoglous, G., Theisen, H. and Vigil, S. "Integrated Solid Waste Management," McGraw-Hill, New York (1993)

Themelis, N. J., Kim, Y. H. and Brady, M. H. "Energy Recovery from New York City Solid Wastes." ISWA Journal of Waste Management and Research (2002): 20: 223-233

Takatsudo, Y., Nakamura, N., Ono, H., Mitsuhashi, M., Kira, M. "Advanced Automatic Combustion Control System for Refuse Incineration Plant." MHI Technique Vol. 39, No. 2 (1999-5) in Japanese

Tchobanoglous, G., H. Theisen, and S. Vigil, S (1993): "Integrated Solid Waste Management." McGraw-Hill, New York, NY.

Von Roll, Inc., Brochure of Waste-to-energy Combustion System, http://www.vonrollinc.com/

Wolf, C., "Erstellung eines Modells der Vermischung von Abfall auf Rostsystemen unter besonderer Berucksichtigung der Vermischung - ein Beitrag zur Simulation von Abfallverbrennungsanlagen", Doctoral Dissertation, the Fraunhofer Institute for Environmental, Safety and Energy Technology (UMSICHT) (2005)

Yagi, S., Kunii, D., Studies on combustion of carbon particles in flames and fluidized beds. In: Fifth Symposium (International) on Combustion Reinhold, New York, pp. 231-244 (1955).

Yang, Y. B., Goh, Y.R., Zakaria, R., Nasserzadeh, V., Swithenbank, J. "Mathematical modelling of MSW incineration on a travelling bed." Waste Management 22 (2002) 369-380

Yang, Y.B.; Nasserzadeh, V.; Goodfellow, J.; Swithenbank, J. Simulation of channel growth in a burning bed of solids. Chemical Engineering Research and Design, v 81, n 2, p 221-232, 2003.

Yang Y.B., Lim C.N., Goodfellow J., Sharifi V.N., Swithenbank J., A diffusion model for particle mixing in a packed bed of burning solids, Fuel, 84, 213-225. (2005).

Yang, Y. B., Sharifi, V. N., Goh, Y. R., and Swithenbank, J. (1999). "User's Manual, The Fluid Dynamic Incinerator Code (FLIC) For Modelling Incinerator Bed Combustion."

# Appendices

## Appendix A: Bed calculation by FLIC*

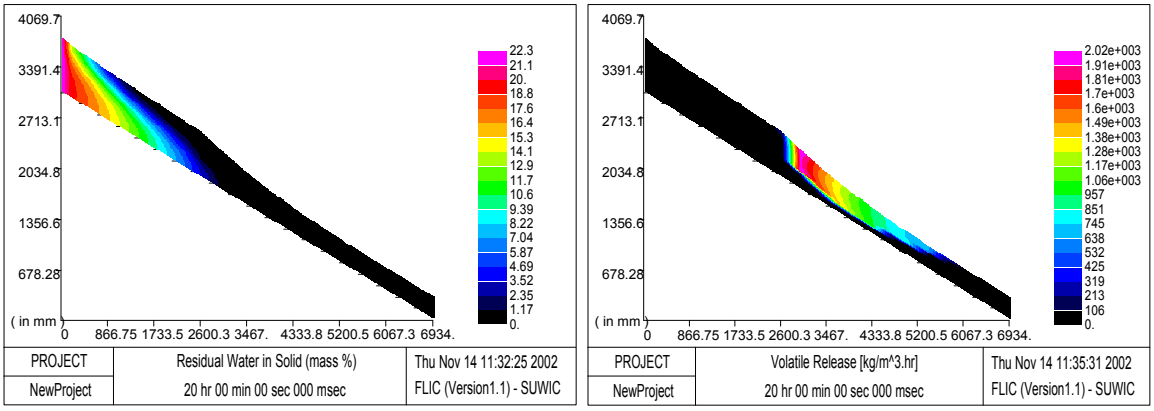


a) Water evaporation

b) Volatilization

c) Combustion

d) Temperature

*Figure A-1: Calculation results of Bed modeling (Nakamura et al.2002)*

** Data from a commercial reverse acting grate indicates the peak temperature is located in the beginning of grate more than FILC calculation results, because of the effect of mixing agitated by the motion of the reverse acting grate.*

## Appendix B: Chamber Calculation by CFD

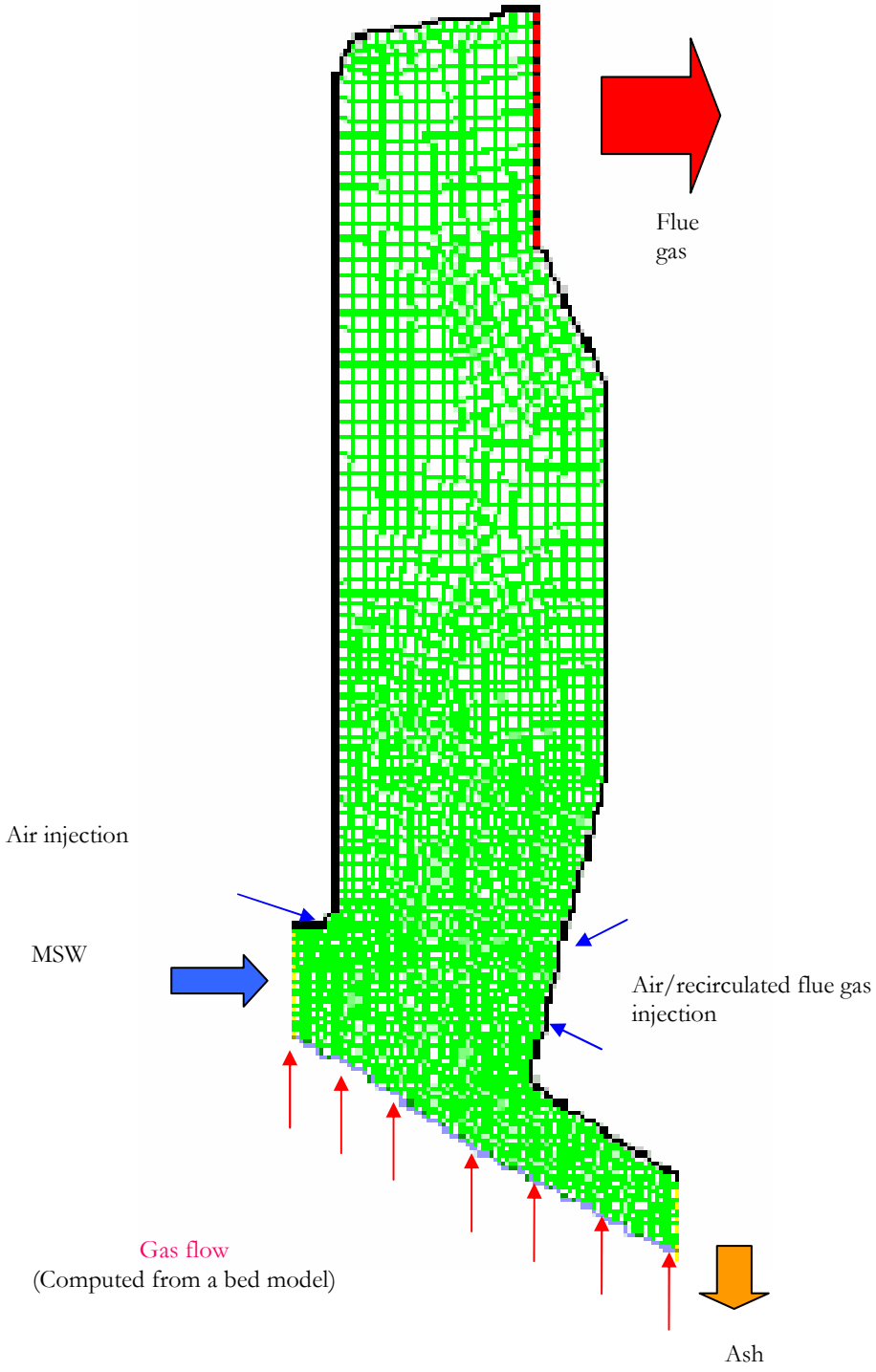


*Figure B-1: A grid structure of CFD modeling (Nakamura et al.2002)*

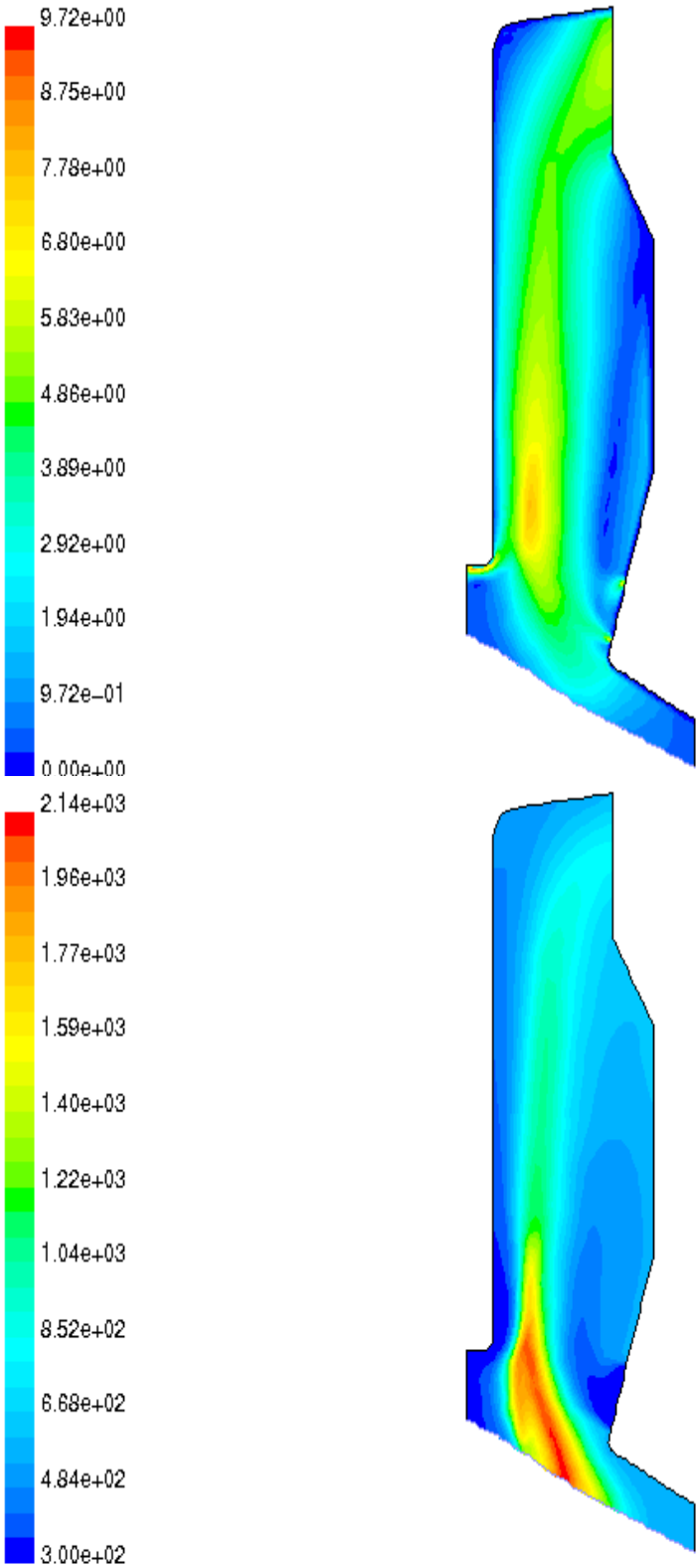


*Figure B-2: Calculated contours of Velocity (m/s) (top) and Total temperature (K) (bottom)*

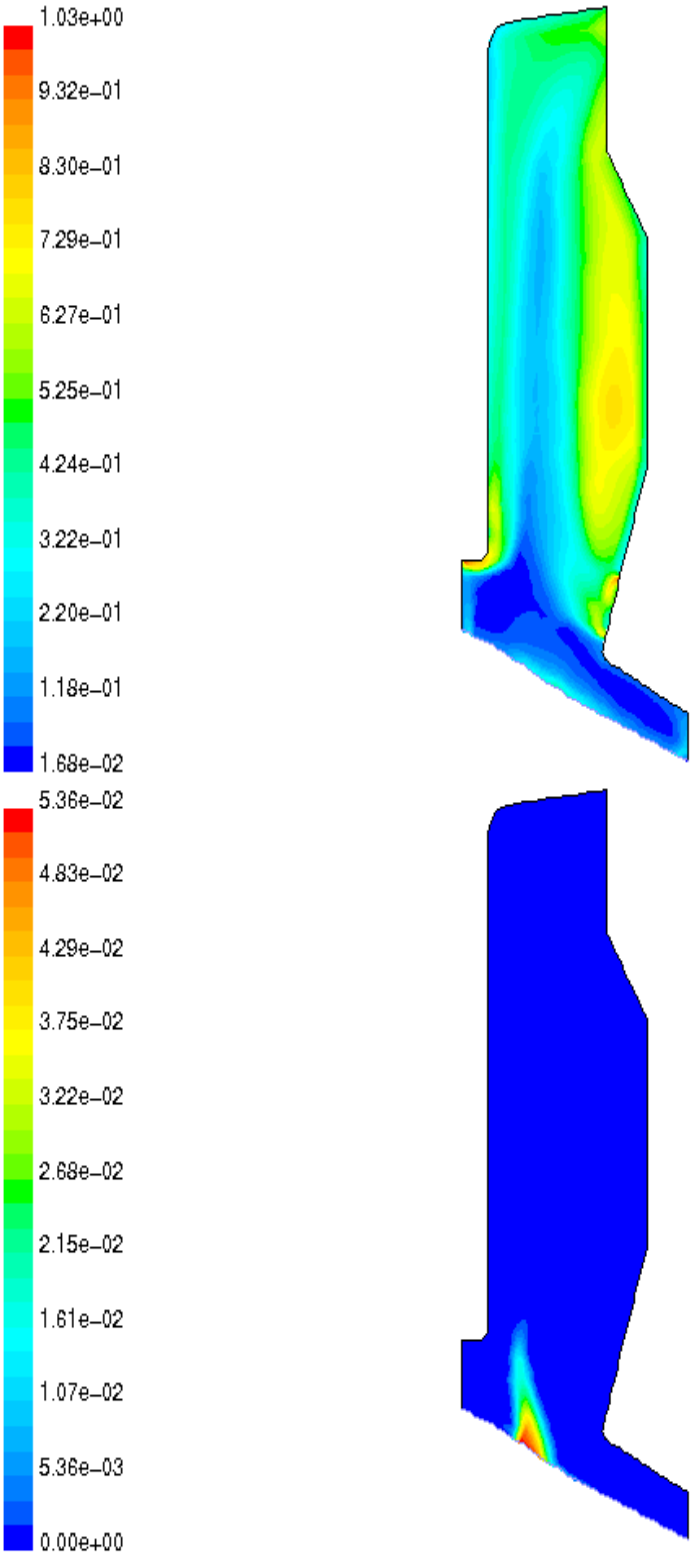


*Figure B-3: Calculated contours of Turbulence intensity (top) and mass fraction of hydrocarbon concentration (bottom)*

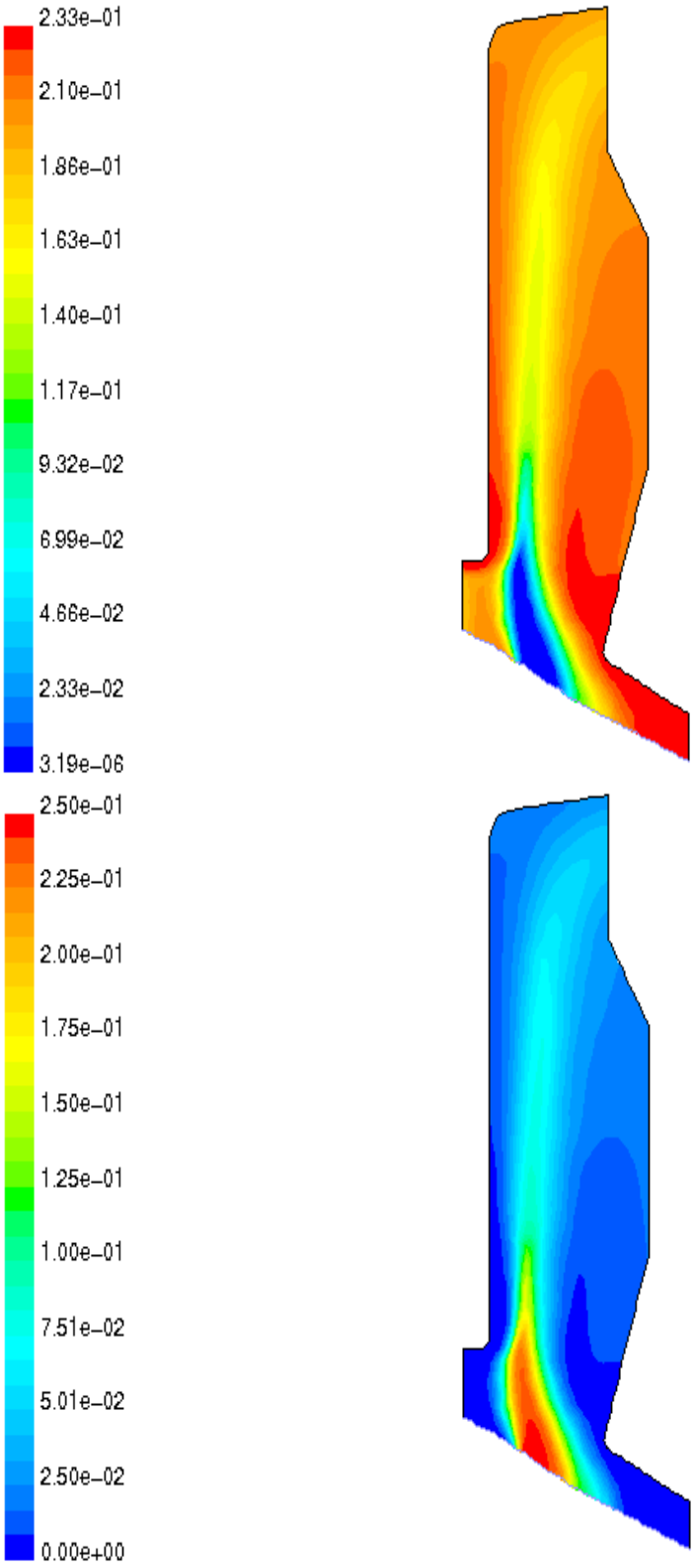


*Figure B-4: Calculated mass fraction of oxygen concentration (top) and of CO2 concentration (bottom)*

## Appendix C: Comparison of combustion models

| Developer's Name | Model Name | Fuel Type (MSW, Coal, Wood) | Solid Reaction, (Drying, Devolatlization, Char oxidation ) | Gas Reaction Volatile combustion | Heat /Mass Transfer | Remarks | References |
|---|---|---|---|---|---|---|---|
| Ahmed et al. | | Cellulose | pyrolysis<br>[Cellulose → volatiles] | | Heat (convection, radiation ) transfer | 1-demension | (Ahmed et al. 1989) |
| Beckmann et al. | | MSW | General Gas-solid reaction | | Heat and Mass transfer | Combination of several continuously stirred reactors | (Beckmann et al. 1995) |
| Shin et al | | Wood, Coke | Drying, pyrolysis, oxidation<br>[Wood → char + volatiles] | | Heat (radiation) and Mass transfer | Fuel shrinkage sub-model and a two-flux radiation sub-model | (Shin et al 2000) |
| Yang et al. | FLIC | MSW | Gaussian distribution of activation energies for waste devolatilization, | mixing effect between volatile matter and oxidant in the volatile combustion rates | Heat (convection, radiation) and Mass transfer (diffusion) | The governing equations for mass, momentum, and heat transfer for both gases and solids. | (Yang et al. 1999, 2002) |
| Peters, Peters et al. | | Wood | During drying and devolatilization the diameter is assumed to remain constant.<br>$\dot{r} = k_o \exp(-\frac{E_a}{RT})\prod_{k=1}^{3} c_{i,k}$ | N/A | Heat transfer (convection, radiation, conduction)<br>Mass transfer (diffusion) | Single-particle model<br>Packed-bed model (including shape factor)<br>SIMPLER algorithm<br>Connectivity with other particles, Thiele modulus | (Peters 1994, Peters et al. 2005) |
| Sohn | | General | General Gas-solid reaction | | Heat transfer | | (Sohn 1973) |
| Chern and Hayhurst | | Coal | Devolatlization<br>[Coal → char + volatiles] | N/A | Heat transfer (Examined from 750 to 950 C) | Shrinking-core Model | (Chern and Hayhurst 2004) |
| Cheijne et al. | | Coal | Drying<br>[Wet coal → coal + $H_2O$]<br>Devolatilization<br>[Volatiles → $B_1CO_2 + B_2CO + B_3O_2 + B_4N_2 + B_5H_2O + B_6H_2 + B_7CH_4 + B_8SO_2 + B_9NO + B_{10}C_2H_6 + B_{11}H_2S + B_{12}NH_3 + B_{13}$tar]<br>Char Oxidation<br>[Coal +$\alpha O_2$ → $(2\beta\text{-}1)CO_2 + (2\text{-}2\beta)CO + a_1H_2O + a_2NO + a_3SO_2$] | $CO + H_2O \rightarrow CO_2 + H_2O$<br>$2CO + O_2 \rightarrow 2CO_2$<br>$2H_2 + O_2 \rightarrow 2CO_2$<br>$CH_4 + 2O_2 \rightarrow 4CO_2 + 6H_2O$<br>$4NH_3 + 5O_2 \rightarrow 4NO + 6H_2O$ | Heat and Mass transfer | Packed bed model and Shrinking-core Model (only for char oxidation) | (Chejne et al. 2000) |
| Heidenreich et al. | Distributed Activation Energy Model (DEAM) | Coal (large particle) | Volatiles generation by DEAM<br>$\left(\frac{V_i^* - V}{V_i^*}\right)_{avge} = \frac{3}{R_0^3}\sum_{j=1}^{n} \times \left(X_j \int_0^{R_0}\left[\int_0^{\infty} \exp\left(-\int_0^t k_{0j}\exp(-E/RT(r,t))dt\right) f(E)dE\right] r^2 dr\right.$<br>where<br>$f(E) = \frac{\exp(-(E-E_{0j})2/2\sigma_j^2)}{\sigma\sqrt{2\pi}}$ | N/A | Heat transfer (convection, radiation, conduction) from 400 to 1000C | Shrinking-core Model (only for devolatilization) | (Heidenreich et al. 1998) |
| Everson et al. | | Coal (high ash particle) | Char Oxidation<br>Coal + O2→ Ash | N/A | N/A(Estimated at 750, 800, 850, 900, and 950 C) | Shrinking-core Model (only for char oxidation) Thiele modulus | (Everson et al. 2005) |

*Table C-1: Comparison of combustion models*

**Appendix D: Movie files on CD-ROM**

On the attached CD-ROM, there are 5 movie files: comb_chamber2_mpeg1, sideview80_mpeg1, plugflow, large8bars, and small8bar. comb_chamber2_mpeg1 shows the view from the end of a commercial WTE combustion chamber. sideview80_mpeg1 is the movie taken from the side of the full-scale physical section model. plugflow shows the simulated plugflow using the stochastic model. large8bar is the result of simulated particle density profile for large particles. small8bar is the movie file that shows simulated particle density profile for small particles.